EXPERIMENTAL INVESTIGATIONS INTO PULSED MAGNETORHEOLOGICAL FINISHING OF HARD METAL

A THESIS SUBMITTED IN FULFILMENT OF

THE REQUIREMENT FOR THE AWARD OF THE DEGREE

OF

DOCTOR OF PHILOSOPHY

IN

MECHANICAL ENGINEERING

BY

HIMMAT SINGH

(ROLL NO- 2K16/Ph.D./ME/12)

GUIDED BY

Dr. M. S. NIRANJAN — **(Associate Professor)**

Prof. REETA WATTAL — **(Professor)**

Mechanical Engineering Department
Delhi Technological University
Main Bawana Road, Shahabad Daulatpur, Delhi- 110042, India

CERTIFICATE

This is to certify that the work embodied in the thesis entitled **"Experimental Investigations into Pulsed Magnetorheological Finishing of Hard Metal"** being submitted by **Himmat Singh (Roll No- 2K16/PhD/ME/12)** for the award of Doctor of Philosophy Degree (Ph.D.) in Mechanical Engineering at Delhi Technological University, Delhi is an authentic work carried out by him under our guidance and supervision. It is further certified that the work is based on original research and the matter embodied in this thesis has not been submitted to any other university/institute for award of any degree to the best of our knowledge and belief.

Dr. M. S. Niranjan

Associate Professor

Department of Mechanical Engineering

Delhi Technological University

Delhi- 110042

Prof. Reeta Wattal

Professor

Department of Mechanical Engineering

Delhi Technological University

Delhi-11042

ACKNOWLEDGEMENT

I came across a number of persons who contributed in various ways to my field of research while bringing this thesis to its final shape, and they deserve special recognition. I take this opportunity to express my gratitude to each one of them. I would like to express my deep sense of gratitude and indebtedness to my supervisors Dr. M. S. Niranjan and Prof. Reeta Wattal for providing valuable guidance, motivation and constructive criticism throughout the course of my research work. I would also like to express my deep sense of gratitude and indebtedness to my Head, Department of Mechanical Engineering, Prof S. K. Garg for his motivation and support during my research work. I want to express my gratitude to all faculty members of the department especially Prof. Ranganath M. S. and Prof. Qasim Murtaza for their invaluable advice and support. I would also like to thank all technical staff especially Mr. Sunil Kumar of Metal cutting lab, DTU for all the help received during the experimentation. I would like to express my sincere gratitude to my parents for their blessings.

I am also thankful to my friends, Dr. Parvesh Ali, Sanjay Sundriyal, Kapil Pandey and Anant for their invaluable encouragement, suggestions and support for this research and providing me extraordinary experiences throughout the work.

Himmat Singh

Roll No- 2K16/PhD/ME/12

PREFACE

In this thesis a newly developed Pulsed Ball End Magnetorheological Finishing Process has been described and it would help the researchers to understand the technique how to get better surface texture by utilizing pulse DC power supply. The contents of the thesis are as follows:

Chapter 1 In this chapter, nontraditional finishing processes have been described along with its different types of classification. The mechanism of material removal from the processed parts by BEMRF process has been elaborated. Later in this chapter, various hybrid forms of BEMRF process based on MR fluid have been discussed along with benefits and application of BEMRF process.

Chapter 2 A comprehensive review of the literature has been discussed with BEMRF process and magnetic field assisted finishing processes. Studies related to the various process parameters affecting material removal rate, surface finish, residual stress have been reviewed. In the last section, the gaps in the research work in BEMRF process were identified and based on that present research objectives have been drawn. In order to fulfill these objectives, a research methodology has been discussed and sequence of activities to be performed to complete the research objectives are planned.

Chapter 3 In this chapter, a newly developed setup of Pulsed ball end magnetorheological finishing has been discussed along with various devices required to make complete PBEMRF setup.

Chapter 4 In this chapter comparative study on EN-31 work-piece surface using BEMRF process with pulse DC power supply and without pulse DC power supply on same process parameters has been carried out. The preliminary experiments were conducted on flat EN-31 steel work-piece surface with MR polishing fluid on BEMRF

process with and without pulse DC power supply and the response percentage reduction in surface roughness has been compared.

Chapter 5 This chapter introduces the Design of experiment to develop the proper plan of experiments using Response Surface Methodology (RSM). The statistical analysis has been done along with analysis of variance (ANOVA) to elaborate the process and optimum process parameters were obtained for the response percentage reduction in surface roughness. Optimization was performed for the response percentage reduction in surface roughness.

Chapter 6 This chapter includes results and discussion part of the investigations in this thesis. The effect of various process parameters such as magnetizing current (*MC*), working gap (*WG*), feed rate (F) and rotational speed of tool (*RST*) on the response percentage reduction in surface roughness (%ΔRa) is studied.

Chapter 7 This chapter elaborates atomic force micrographs (AFM) and scanning electron micrographs (SEM) obtained with pulse BEMRF process at optimum process parameters (3.5 A, 30 m/min, 0.5 mm and 700 rpm) have been studied.

Chapter 8 In this chapter, the residual stress of grinded surface before BEMRF process and after conducting experiments on BEMRF setup with pulse DC power supply and without pulse DC power supply using x- ray residual stress analyzer is studied. Thereafter percent reduction in residual stress (%ΔRS) was calculated. The statistical analysis with response surface methodology has been done to elaborate the process. Optimum process parameters have been obtained for the response percentage reduction in residual stress.

Chapter 9 This chapter elaborate the conclusions of the research work. The results obtained were discussed thoroughly. Further the scope of future improvement and work that can be done is discussed.

TABLE OF CONTENTS

S.N.	Title			Page No.
	Certificate			**ii**
	Acknowledgement			**iii**
	Preface			**iv-v**
	List of Figures			**x-xv**
	List of Tables			**xvi**
	Acronyms			**xvii**
	Abstract			**xviii-xix**
1	**CHAPTER 1-INTRODUCTION**			**1-15**
	1.1	Background		1
	1.2	Non-Conventional Manufacturing Processes		1
	1.3	MR fluid assisting finishing process		6
		1.3.1	Magnetorheological finishing (MRF)	7
		1.3.2	Magnetorheological abrasive flow finishing process (MRAFF)	7
		1.3.3	Magnetorhelogical abrasive honing (MRAH)	9
		1.3.4	Rotational magnetorhelogical abrasive flow finishing (R-MRAFF)	9
		1.3.5	Magnetorheological finishing (MRJF)	10
		1.3.6	Chemo-mechanical magneto-rheological finishing (CMMRF)	11
		1.3.7	Ball end magnetic rheological finishing (BEMRF)	12
	1.4	Magnetorheological fluid		13
	1.5	Benefits of ball end magnetorheological finishing process		15
	1.6	Applications of BEMRF Process		15

2	**CHAPTER 2 – LITERATURE REVIEW**			**16-42**
	2.1	Major area of BEMRF Research		16
		2.1.1	Experimental research	16
		2.1.2	Hybrid form of BEMRF Process	17
		2.1.3	Analytical Research	17
	2.2	Literature Review		17
	2.3	Research gap		41
	2.4	Research objectives		42
3	**CHAPTER 3 – DEVELOPMENT OF MAGNETORHEOLOGICAL FINISHING SETUP**			**43-53**
	3.1	Design of PBEMRF setup		43
		3.1.1	Magnetic field intensity at tool tip	46
		3.1.2	Design of dies with work-piece	47
		3.1.3	Chiller	49
		3.1.4	Thermocouple	49
		3.1.5	Pulse DC power supply	50
		3.1.6	CNC part programming	51
		3.1.7	Preparation of work-piece samples	52
4	**CHAPTER 4 – COMPARATIVE STUDY WITH PULSE DC POWER SUPPLY AND WITHOUT PULSE DC POWER SUPPLY**			**54-67**
	4.1	Mechanism of material removal		54
	4.2	Preliminary Experimentations		58
5	**CHAPTER 5 – DESIGN OF EXPERIMENT FOR PROCESS PARAMETERS**			**68-76**
		5.1	Response Surface Methodology (RSM)	68
		5.2	First order design	70
		5.3	Second order design	70
		5.4	Non Central composite design	71
		5.5	Rotatable Second order design	71

		5.6	Analysis of Variance	71
6	**CHAPTER 6 – RESULTS AND DISCUSSIONS**			**77-88**
	6.1	Effect of magnetizing current on %ΔRa		77
	6.2	Effect of feed rate on %ΔRa		78
	6.3	Effect of working gap on %ΔRa		79
	6.4	Effect of rotational speed of tool on %ΔRa		80
	6.5	Validation of results through confirmatory experiment		86
	6.6	Numerical Optimization		87
7	**CHAPTER 7 – SURFACE TEXTURE ANALYSIS THROUGH SEM AND AFM**			**89-91**
	7.1	SEM analysis		89
	7.2	AFM analysis		90
8	**CHAPTER 8 – STUDY OF RESIDUAL STRESS**			**92-123**
	8.1	Study of residual stress		92
	8.2	Destructive and nondestructive technique		92
	8.3	Residual stress analyzer		93
	8.4	X-Ray diffraction		94
	8.5	Preliminary Experimentation for residual stress		96
		8.5.1	Residual stress analysis of finished surface with BEMRF process using DC power supply without pulse	97
		8.5.2	Residual stress analysis of finished surface with BEMRF process with pulse DC power supply	101
	8.6	Residual stress analysis through design of experiment for process parameters		105
		8.6.1	Effect of magnetizing current on %ΔRS	110
		8.6.2	Effect of feed rate on %ΔRS	111
		8.6.3	Effect of working gap on %ΔRS	112
		8.6.4	Effect of rotational speed on %ΔRS	112
		8.6.5	Residual stress at optimum process parameters	118

9	**CHAPTER 9 - CONCLUSIONS AND SCOPE OF FUTURE WORK**		**123-126**
	9.1	Conclusions	123
	9.2	Scope of future work	126
	REFERENCES		**127-143**
	RESEARCH PUBLICATIONS		**144**

List of Figures

Figure No.	Figure Caption	Page No.
1	MR fluid assisted finishing processes	6
2	Mechanism of MRAFF	8
3	Schematic diagram of CMMRF set-up	12
4	Material removal mechanism in Ball end magnetorheological finishing process	13
5	Fluid flow pattern (a) At no magnetic field (b) In presence of magnetic field	15
6	Schematic of Magnetorheological finishing tool	45
7	Steps followed in design of finishing tool through ANSYS 15.0	45
8	3-D design of Ball End magnetorheological finishing tool	46
9	Magnetic flux density on finishing tool tip at magnetizing current 3.5A, number of turns 2100 and 1 mm working gap	47
10	Schematic dimension of dies and work-piece	47
11	The work-piece position and its die	48
12	PBEMRF experimental setup	48
13	Chiller for cooling the electromagnetic coil	49
14	Thermocouple connected to display temperature reading	50
15	(a) Pulse DC power supply (b) HMI unit for adjusting pulse ON/pulse OFF value	50
16	CNC part program	51
17	Finishing tool moves over the EN-31 work-piece surface	51
18	EN-31 samples before grinding	52

19	EN-31 work-piece samples during finishing on Surface grinder	53
20	a) Semi solid ball is formed at finishing tool tip (b) Mechanism of material removal during finishing of EN-31 work-piece surface with force acting on single abrasive	55
21	(a) Initial stage of EN-31 work-piece surface (b, c) Gradual removal of roughness peaks	55
22	(a) Formation of semi solid ball at pulse ON condition (b) Destruction of semi solid ball at pulse OFF condition	57
23	Schematic diagram (a) Formation of semi solid ball at pulse ON condition(b) Destruction of semi solid ball at pulse OFF condition	57
24	Finished EN-31 work-piece using pulse DC power supply at 2.5A, 50 mm/min, 1.5 mm and 500 rpm	59
25	Finished EN-31 work-piece using DC power supply without pulse at 2.5A, 50 mm/min, 1.5 mm and 500 rpm	59
26	Graph between percent reductions in surface roughness with duty cycle	61
27	Taylor Hobson instrument during measurement of surface roughness	62
28	Surface roughness profile of EN-31 (a) Before finish (b) After finish using DC power supply without pulse	62
29	Surface rroughness profile of EN-31(a) Before finish b) After finish with pulse DC power supply at 0.16 duty cycle	63
30	Surface roughness profile of EN-31(a) Before finish (b) After finish with pulse DC power supply at 0.27 duty cycle	64
31	Zeta instrument for measurement of optical microscopic view	65

32	Optical microscopic views of finished surface (a) With DC power supply without pulse (b) With pulse DC power supply at 0.27 duty cycle (c) With pulse DC power supply at 0.16 duty cycle		65
33	Images of work-piece surface (a) Before finish, (b) After finish at 0.27 duty cycle, (c) After finish at 0.16 duty cycle, (d) After finish with DC power supply without pulse		66
34	SEM images of work-piece surface at ×600 magnification) (a) Before finish, (b) After finish at 0.27 duty cycle, (c) After finish at 0.16 duty cycle, (d) After finish with DC power supply without pulse		67
35	35.1	Effect of magnetizing current (MC) on %ΔRa	78
	35.2	Effect of feed rate (F) on %ΔRa	79
	35.3	Effect of working gap (WG) on %ΔRa	80
	35.4	Effect of rotational speed of tool (RST) on %ΔRa	81
	35.5	a) Perturbation diagram for %Δ*Ra* with (A – Magnetization current, B – Feed rate, C- working gap, D – Rotational speed of tool) b) Actual vs. Predicted graph c) 3-D surface graph between feed rate and MC on %ΔRa d) 3-D surface graph between WG and MC on %ΔRa e) 3-D surface graph between WG and F for %ΔRa f) 3-D surface graph between RST and WG on %ΔRa	82
	35.6	Contour surface graph between (a) Feed rate and Magnetizing Current (b) Working Gap and Magnetizing Current (c) Working	83

		Gap and feed rate (d) Rotational Speed of Tool and Working Gap on %ΔRa	
	35.7	Interaction graph between Magnetizing Current and Feed rate on %ΔRa	84
	35.8	Interaction graph between Magnetizing Current and Working Gap on %ΔRa	85
	35.9	Interaction graph between Feed rate and Working Gap on %ΔRa	85
	35.10	Interaction graph between Feed rate and Rotation Speed of Tool on %ΔRa	86
36	Surface Roughness profile (a) Before finishing (b) After finishing with PBEMRF process at optimum process parameters (3.5A, 30 mm/min, 0.5 mm and 700 rpm).		87
37	Scanning electron micrograph a) Before finish at 300x b) After finish at 300x c) After finish at 600 x d) After finish at 1200x		90
38	Atomic force micrograph of (a) Grinded work-piece surface (b) Finished work-piece surface with PBEMRF process at optimum process parameters		91
39	Residual stress analyzer with position of EN-31 work-piece		93
40	Diffraction of X-ray from work-piece surface		95
41	Formation of Debye-Scheerer ring		95
42	Debye ring (3D) and Distortion ring of (a) Initial grinded work-piece at 122 MPa, FWHM= 3.35 (b) Finished work-piece surface at 78MPa, FWHM= 3.52 without pulse DC power supply in BEMRF process..		98
43	FWHM graph with peak strength of initial grinded work-piece surface		99

44	FWHM graph with peak strength of finished work-piece surface using DC power supply without pulse		100
45	Residual stress graph of (a) Initial grinded surface at 122 MPa (b) Finished surface by BEMRF without pulse at 78 MPa.		101
46	Debye ring (3D) and Distortion ring of (a) Initial grind surface at 102 MPa, FWHM= 3.32º(b) Finished surface at 55 MPa, FWHM=3.43º with PBEMRF.		102
47	FWHM graph with peak strength of initial grinded work-piece surface		103
48	FWHM graph with peak strength of finished surface with PBEMRF Process		104
49	Residual stress graph of (a) Initial grinded surface at 102 MPa (b) Finished surface by PBEMRF at 55 MPa		105
50	50.1	Effect of Magnetizing Current on %ΔRS	111
	50.2	Effect of Feed rate on %ΔRS	111
	50.3	Effect of Working Gap on %ΔRS	112
	50.4	Effect of Rotational Speed of Tool on %ΔRS	113
	50.5	(a) Perturbation diagram for %Δ*RS* with (A – Magnetization current, B – Feed rate, C- working gap, D – Rotational speed of tool) (b) Actual vs. Predicted graph (c) 3-D surface graph between feed rate and MC on %ΔRS (d) 3-D surface graph between RST and MC on %ΔRS (e) 3-D surface graph between WG and F for %ΔRS	114
	50.6	Contour surface graph between (a) Feed rate and Magnetizing Current (b) Rotation Speed of Tool	116

		and Magnetizing Current (c) Rotation Speed of Tool and Working Gap for %ΔRS	
	50.7	Interaction graph between Magnetizing Current and Feed rate on %ΔRS	117
	50.8	Interaction graph between Magnetizing Current and Rotation Speed of Tool on %ΔRS	117
	50.9	Interaction graph between Working Gap and Rotation Speed of Tool on %ΔRS	118
51	Debye ring (3D) and Distortion ring of (a) Initial grinded work-piece surface at 119MPa, FWHM= 3.31 (b) Finished surface at 42 MPa, FWHM= 3.50 by PBEMRF process		119
52	FWHM graph with peak strength of initial grinded work-piece surface		120
53	FWHM graph with peak strength of finished surface with PBEMRF process at optimum process parameters (3.5A, 30 mm/min, 0.5 mm, 700 rpm)		121
54	(a) Residual stress graph of initial Grinding surface is 119MPa (b) Residual graph of finished surface with PBEMRF process is 42 MPa at 3.5 A, 30 mm/min, 700 rpm, 0.5 mm		122

List of Tables

Table No.	Table Caption	Page No.
1	Preliminary experimentation with pulse DC power supply	60
2	Preliminary experimentation using DC power supply without pulse	60
3	Level and ranges of process parameter	72
4	Plan of experiments and output response in surface roughness (%Δ*Ra*)	73
5	ANOVA for Quadratic model	74
6	ANOVA for Reduced Quadratic model	75
7	Confirmatory experiment after finishing of work-piece using PBEMRF	86
8	Best solutions through numerical optimization	88
9	Experimental results for residual stress by DC power supply without pulse	96
10	Experimental results for residual stresses with pulse DC power supply	97
11	Level and ranges of process parameter	106
12	Design and result of output response in surface roughness (%Δ*RS*)	106
13	ANOVA for Quadratic model	108
14	ANOVA for Reduced Quadratic model	109
15	Fit statics of reduced quadratic model	109
16	Confirmatory experiment after finishing work-piece using PBEMRF	122

ACRONYMS

d	Density, [gm/cm^3]
MC	Magnetizing current, [A]
WG	Working gap, [mm]
Ra	Surface roughness, [µm]
RST	Rotational speed of tool, [rpm]
$\%\Delta Ra$	Response parameter percentage reduction in surface roughness, [%]
r	Duty cycle, [-]
T_{ON}	ON-time of pulse DC power [µs]
T_{OFF}	OFF-time of pulse DC power [µs]
$\%\Delta RS$	*P*ercentage reduction in residual stress [MPa]
RS	Residual stress [MPa]

ABSTRACT

Ball end magnetorheological finishing (BEMRF) is a high level nanofinishing process used to finish different kinds of surfaces include flat, two dimensional and three dimensional and curved surfaces. The preliminary experiments have been conducted on EN-31 flat work-piece surface using DC power supply with and without pulse at magnetizing current (MC) 2.5 A, feed rate 50 mm/min, working gap (WG) of 1.5 mm and rotational speed of the tool (RST) 500 rpm. The preliminary study has been carried out to analyze the effect of Duty cycle on the response percentage reduction in surface roughness (%ΔRa). It has been observed that an improved %ΔRa has been found with the use of pulsating DC power supply as compared to %ΔRa obtained with DC power supply without pulse at same process parameters. Taylor Hobson surface analyzer instrument was used with cut-off length 0.8 mm and data length of 4 mm to measure the surface roughness before and after pulsed ball end magnetorheological finishing (PBEMRF) process. The surface roughness has been measured initially after grinding of work-piece samples and then after finishing of work-piece through BEMRF process.

After conducting the preliminary experiments, the detailed experimental study has been conducted with PBEMRF at 0.16 duty cycle. The statistical analysis was done to analyze the effect of various process parameters on %ΔRa using response surface methodology (RSM). The maximum predicted *%ΔRa* has been found as 55.52% through actual regression equation at optimum process parameters 3.5A magnetizing current, 30 mm/min feed rate, 0.5mm working gap and 700 rpm rotational speed of finishing tool. The experiment was conducted on PBEMRF process at optimum process parameters. The value of %ΔRa obtained through experimentation was found to be 51.23% which is close to the predicted value of %ΔRa with error of 4.29%.

The residual stress plays an important role on finished components. The performance of the machine component can be improved with reduction of residual stress. The residual stress and surface finish play an important role in overall efficiency and durability of the components. The present work is aimed to relieve the residual stress of work-piece surface with the improvement in surface finish using pulse DC power supply in BEMRF process. The preliminary experiments have been conducted at magnetizing current (MC) of 2.5A, Feed rate (F) 50 mm/min, tool rotational speed (RST) 500 rpm, and working gap (WG) 1.5 mm on flat EN-31 steel in finishing time 30 minutes with and without pulse DC power supply. The residual stress of grinded EN-31 surface before experimentation and of finished surface after experimentation on BEMRF process has been measured with X-ray residual stress analyzer using Cosα method. It has been observed that the residual stress was found reduced from 122 to 78 MPa after finishing with BEMRF process using DC power supply without pulse while residual stress was reduced from 102 to 55 MPa after finishing with BEMRF process using pulse DC power supply at 0.16 duty cycle. After preliminary experimentation, the statistical analysis with design of experiment has been conducted with pulse DC power supply using 0.16 duty cycle to visualize the effect of various process parameters on residual stress. The maximum predicted %ΔRS of 70.35% was found at optimum process parameters 3.5A current, 30 mm/min feed rate, 700 rpm tool rotational speed and 0.5 mm working gap while maximum experimental %ΔRS was found as 64.70% which is very close to predicted %ΔRa with error of 5.65%. The residual stress was found reduced from 119 to 42 MPa after finishing with BEMRF process at optimum process parameters using pulse DC power supply

CHAPTER 1

INTRODUCTION

This chapter explains about non-conventional finishing processes and its classifications based on magnetic field. The details about nonconventional Ball end magnetorheological finishing process, advantages, and applications of this process and Residual stresses are discussed. Later the details of the MR fluid and its compositions, design of finishing tool and PBEMRF setup are described.

1.1 Background

There is a requirement of more demanding technology in current competitive environment for finishing components very accurate with high part quality. In order to have qualities on component like corrosion resistance, residual stresses, and wear resistance, it must have a better surface finish. The finishing operation is often the last stage of the manufacturing process for any product, and it can be quite expensive and difficult to complete complex geometric designs. A lot of effort and money are needed to produce a product with improved surface quality. Technology has improved recently, necessitating the usage of cutting-edge materials including ceramics, nonferrous metals, and stainless steel. However, finishing these sophisticated materials affordably with traditional finishing methods is not simple.

1.2 Non-conventional finishing process

In non-traditional finishing processes, the application of magnetic field has become very important for nano level finishing on variety of surfaces. Nano finishing of critical shapes is always difficult to control despite the high demand for nano finishing. The traditional finishing processes such as honing, grinding etc. produce finished surfaces but these finishing processes produce some thermal and residual stresses on the surface

of work-piece. It is therefore becoming a challenge to finish such kind of components with minimum residual stresses [1].

With the development of advanced new materials having complex shapes and geometry of work-piece, there are some advanced finishing techniques employed to resolve these problems. Surface finish on these types of components plays very crucial role for high quality product. These processes are helpful for polishing any type of materials [2-3].

Magnetorheological (MR) finishing process has more flexibility in process control and used for getting high level of surface finish along with close dimensional tolerances without leaving any kind of defect on the surfaces or sub surfaces. A finishing spot is developed at MR finishing tool tip which acts as semi-solid finishing tool and finishing spot has relative motion over the work-piece surface during finishing of any kind of work-piece surface [4].

MR fluid has more flexibility during finishing action and these fluid changes from liquid to semi solid in a very short duration with due effect of the magnetic field. MR fluid is prepared with ferromagnetic particles and abrasive particles mixed with base fluid like paraffin oil heavy and grease. In advancement of MR fluid for getting better finish, bidisperse MR polishing fluid has been used with different percentage of carbonyl iron powder (CIP) of HS and CS grade along with abrasives and response has been compared with monodisperse MR polishing fluid based finished surface at same process parameters. The magnetorheological characterization of bidisperse and monodisperse MR polishing fluid samples have been studied at various level of magnetic fields on magnetorheometer [5].

In MR finishing process, variety of process parameters such as central core rotation of tool, working gap, current and feed rate are studied for improvement of surface roughness. The MR polishing fluid composition has also been analyzed and found that

the CIP concentration is the most influential parameter than other parameters for improvement of surface roughness of hardened AISI 52100 steel [6].

Variety of magnetic field assisted finishing techniques are available in the literature. Some of these magnetic field assisted finishing technique are magnetorheological finishing (MRF) [4], magnetic abrasive finishing (MAF) [7], magnetorheological jet finishing (MRJF) [8], magnetic float polishing (MFP) [9], rotational magnetorheological abrasive flow finishing (R-MRAFF) [10], and ball end magnetorheological finishing (BEMRF) [11]. In MR finishing techniques, MR fluid behaves like semi solid finishing spot in the presence of applied magnetic field which is used for finishing action on the work-piece surface during relative motion. MAF is one kind of process which has been used to finish flat surface, two dimensional (2D) surface and any complex shape of work-piece with high dimensional accuracy. An efficient way to deburr, polish, or remove the recast layers created by electrical discharge machining is with the use of magnetic abrasive finishing (MAF) [12–14]. This approach not only cause chatter or vibration during the operation but also has no restrictions on the shape of the work-piece. In addition, the surface roughness of the work-piece can be quickly reduced to nanoscale in MAF [15-16]. Additionally, magnetically produced flexible magnetic abrasive brush can easily suit irregular surfaces when polishing. As a result, complicated surfaces can also be polished by MAF technique [17-19]. A better-quality product is achieved by MAF process with high level of surface finish without any defect on surface or sub-surface [20].

In MAF process, direct current (DC) power supply was used to energize electromagnet of finishing tool to finish variety of surfaces. As per more demand for improvement in surface roughness along with better productivity, Pulse DC power supply has been used in MAF process instead of DC power supply without pulse. Experiments were conducted on MAF by using DC power supply and pulsating DC power supply. It is observed that the better surface finish is achieved with the use of pulse DC power supply as compared to DC power supply without pulse at same process

parameters. It is also observed during continuous DC power supply that the active abrasive particles are not so effective to finish the work-piece surface after certain time because the cutting edges of active abrasive particles lose their finishing capability in finishing zone. On the use of pulsating DC power supply, the orientation of active abrasive particles may get changed or new effective grains of active abrasive particles come in contact with the work-piece surface during finishing which enhances finishing capability at same process parameters [21].

Many magnetic field assisted finishing processes are available in the literature which are not suitable for finishing of three dimensional (3D) complex shaped work-piece like narrow cut in work-piece. In advancement of MR finishing process with some modification, a novel BEMRF process is developed for finishing of variety of work-piece surfaces such as flat, curved surface, 2D, 3D and stepped surfaces etc. Electromagnetic coil of finishing tool is energized with the use of DC power supply and MR fluid used at the tip of finishing tool formed a semi solid hemisphere or ball due to applied magnetic field. The semi-solid ball shaped MR fluid at finishing tool tip is now responsible for finishing action on the surface of work-piece irrespective of any kind of work-piece materials. BEMRF process can finish variety of work-piece surfaces as achieved by finishing in computer navigated controlled (CNC) milling machine for three dimensional surfaces [3]. BEMRF process has major applications in aerospace, optics industry and automotive component, etc. Remaining stresses in a solid material after machining are known as residual stresses, and they play a significant impact in how well machined components perform in real life application. Residual stresses are generally undesirable in the machined components. The functional behavior and efficiency of machined components can be enhanced by reduction of residual stresses [22]. The study of residual stress becomes important for overall part quality and functional durability. The parametric study on residual stress (RS) has been done by performing the experiments on stainless steel (AISI 304) [23]. Measurement of residual stress on the machined work-piece was done on X-ray

diffraction technique and observed that the sharpness of tool influences the surface residual stress significantly [24]. Finite element model was developed to study the residual stress due to moving heat source and predicted that the residual stresses in grinding process are generated by thermal and mechanical abrasion [25]. Conventional finishing processes like grinding, lapping, honing etc. produce burrs, residual stresses, and damage of subsurface of the components. It becomes essential to achieve good surface finish in nano level or beyond to get desired quality product with enhanced overall performance. In the available literature, many unconventional finishing process assisted by externally applied magnetic field have been reported which control the finishing forces and hence final surface finish.

In Magnetorheological Finishing (MRF) process, the finishing forces are controlled by externally applied magnetic field and hence better surface finish is achieved. The wear occurs on work-piece surface during finishing by selective mechanical abrasion in MR finishing while in grinding, the wear occurs due to thermal and mechanical abrasion. This mechanical abrasion is responsible for finishing of work-piece. The material is removed from the work-piece surface with the use of abrasives which produces higher residual stresses, and damage of surface or subsurface in grinding or lapping processes. The sub surface damage is linked with a layer of material in residual stress. The damage of surface or subsurface and residual stresses present in the work-piece was reduced effectively by MRF process [27]**.** MR fluid at finishing tool tip behaves like a semi solid hemisphere when continuous DC power supply is used to energies electromagnetic coil. The magnetic field is produced and focused at the tip of finishing tool due to which semisolid hemi spherical ball of MR fluid is formed. This hemi spherical ball acts as a finishing tool and has the capability for finishing variety of typical work-piece surfaces at various process parameters i.e. magnetizing current, working gap, rotational speed of tool and feed rate etc. The effect of magnetization current on %ΔRa has been studied and found increased with increase in magnetizing current. This is happened because of magnetized flux density at tip of the finishing tool

increases as the magnetizing current is increased. The effect of working gap (WG) on %ΔRa has also been studied. It has been observed that the %ΔRa decreases as the working gap increases. The flux density is inversely related to the working gap. It is found that rotational speed of tool was increased, % ΔRa is found to be slightly increasing [26].

1.3 MR fluid assisted finishing process

The MR fluid and its compositions are crucial in magnetorheological finishing process. The MR fluid consist of CIP and abrasive particles along with base fluid. The MR fluid becomes stiffer due to applied magnetic field and semi solid behavior of MR fluid is responsible for finishing of work-piece surface. Some MR fluid based finishing techniques are evolved as given in Fig.1.

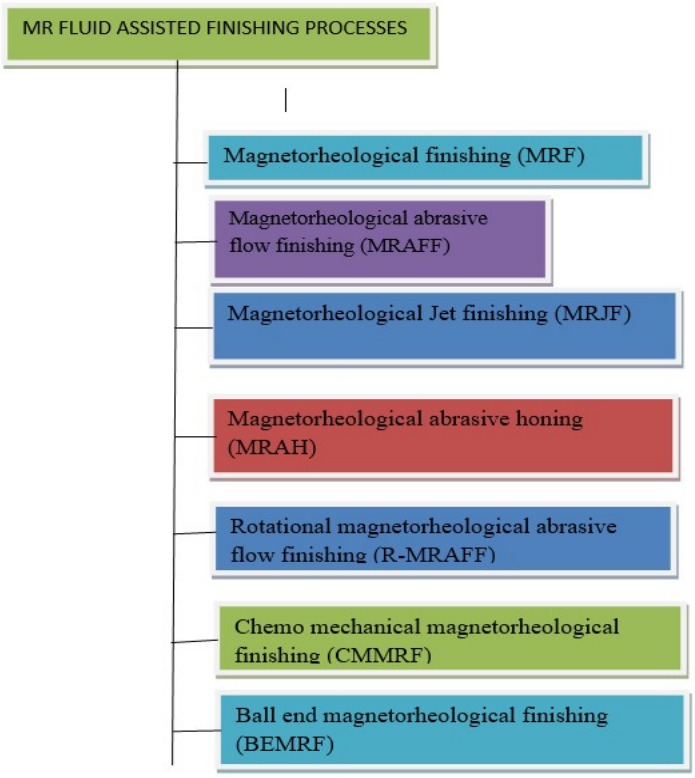

Fig.1: MR fluid assisted finishing processes

1.3.1 Magnetorheological finishing (MRF)

MRF can be used for variety of materials raging from optical components to hard crystals. MRF was initiated in Minsk, Belarus by Kordonski, Prokhorov, Gorodkin, and coworkers in 1988 [1]. In MRF, the MR polishing fluid is deposited by a nozzle on the rim of a rotating wheel, which transports the fluid to the work-piece surface. A converging gap formed by the wheel rim and the surface to be polished is exposed to a magnetic field. Through the converging gap, the moving wall, which is in the rim surface, creates a flow of magnetically stiffened MR polishing fluid. The unsheared fluid that is attached to the moving wall and is associated with the magnetically stiffened MR fluid creates a distinct pressure distribution in the gap [28–29]. The formation of a quasi-solid moving boundary extremely close to the work-piece surface really causes high shear stress in the contact zone and material removal across a portion of the work-piece surface [30–31]. This space has been set aside as a polishing area. Nonmagnetic abrasive particles that are part of the MR fluid and are pushed to the polishing contact by a magnetic field gradient improve material removal [32]. Material is removed when an MR fluid mixture including abrasives runs over a specimen surface because the fluid's shear stress causes the abrasives to migrate.

1.3.2 Magnetorheological abrasive flow finishing (MRAFF) process

MRAFF is the hybrid process of MRF and abrasive flow machining (AFM) process. Extrusion of a magnetically stiffened MRP fluid back and forth through or across the passage created by the work-piece surface and fixture is the foundation of the MRAFF process [2]. In Fig. 2, the process's mechanism was depicted. The finishing action in MRAFF is carried out by the abrasive particles [33]. The yielding stress of MRP fluid was increased in the presence of magnetic field. There were two force involved during finishing named as normal force due to magnetic field and tangential force due to reciprocating motion of MRP fluid as shown in Fig.2. The normal force is responsible for packing of CI particles causing due to indentation into the work-piece

surface and tangential force is responsible for micro-chipping. The material removal from the work-piece surface takes place due to these forces during finishing. Abrasive Flow Finishing technique is similar to MRAFF process. Any geometry can be finished using the abrasive flow machining technique by letting an abrasive-loaded polymeric medium to flow over it. The abrading forces in the abrasive flow machining process are mostly dependent on the polymeric medium, and the rheological behaviour of the media is not predetermined by external forces. Keeping the above in mind, a brand-new hybrid technique called the "Magnetorheological abrasive flow finishing process" was created. The abrasive medium's rheological properties should be made more predictable and controllable. The studies were conducted to investigate the impact of surface roughness variation on extrusion pressure, magnetic flux density, and number of finishing cycles. According to their analysis, the key factor increasing surface quality was magnetic flux density [34]. The faster finishing action and improved abrasive retention provided by CIP chains takes place as the magnetic flux density rises. When the number of finishing cycles increases, the surface roughness gradually decreases until the necessary level of surface finish is reached. MRAFF can use boron carbide, silicon carbide, and diamond abrasives to super polish hard materials like silicon nitride (Si_3N_4) [35]. In the MRAFF process, a magnetic field is developed to a cylindrical fixture with two electromagnet cores that are positioned across from one another. The magnetic field is consequently relatively weak on either side and quite strong in front of the core material [36].

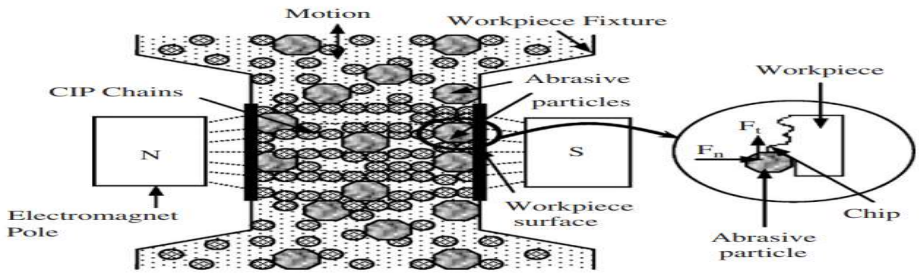

Fig.2: Mechanism of MRAFF [2]

1.3.3 Magnetorheological abrasive honing (MRAH)

The Magneto-rheological Abrasive Honing (MRAH) procedure, which is an improvement on traditional honing, is one of the unorthodox nanofinishing techniques that may effectively finish non-magnetic freeform surfaces [37]. The finishing action in MRAH is guided by the magneto-rheological effect provided by the magnetic carbonyl iron particles and the abrasives delivered through the carrier liquid. The finishing fluid and the work-piece in the MRAH process were given an up and down motion with rotational motion, respectively. With the exception of rotating the work-piece rather than rotating the stone as in traditional honing, a finishing technique was created that is identical to conventional honing. While the work-piece is rotating inside the medium, the medium is also given a reciprocating motion. The trial experiments were conducted on work-pieces made of aluminum and stainless steel. According to the results of the trials, the surface finish can be improved by boosting the magnetic field density as the fluid gains more yield strength to smooth out surface defects. Additionally, they discovered that the work-piece surface finish improved with increased rotational speed. In order to quantify the axial stress caused by the flow of MR fluid, understand the nature of the magnetic field that would likely be produced, and forecast the final surface roughness value (Ra), finite element analysis was also carried out [38]. The results comparison shows only mildly satisfactory agreement. Radial stresses that have evolved in the medium were not taken into account in this research.

1.3.4 Rotational magnetorheological abrasive flow finishing (R-MRAFF)

To improve the finishing performance of the MRAFF process, a brand-new finishing technique called "rotational- magnetorheological abrasive flow finishing (R-MRAFF)" has been developed [39]. In this method, a spinning magnetic field and hydraulic apparatus rotate and reciprocate the polishing media. A homogeneous

surface is produced with better material removal and finishing rates by the intelligent management of these two processes.

MRP medium is extruded through the work-piece surface using tooling system in R-MRAFF process, and it is provided up-and-down motion by driving two opposing pistons. At the same time the polishing medium is rotated. By superimposing these two motions, a relatively high velocity is obtained and better surface finish is achieved [40]. The additional forces, other than the axial force, acting on the abrasive particles due to the rotational motion of the polishing fluid enhances the abrading capabilities of the abrasives to remove surface undulations from hard work-pieces like stainless steel.

1.3.5 Magnetorheological Jet finishing (MRJF)

A technique that has been proposed, created, and tested involves using an axial magnetic field to magnetise the circular jet of magnetorheological (MR) fluid as it exits from the nozzle. A local magnetic field within the MR fluid results in longitudinal fibrillation and high effective viscosity [41]. The worst first disturbances are therefore suppressed. As a result, the MR fluid that is released from the nozzle creates a highly collimated, coherent jet. The stabilising structure that the magnetic field built inside the jet eventually starts to collapse as the jet goes beyond the magnetic field. The MR jet can stabilise and move up to several metres (depending on the jet diameter) without suffering from severe spreading and structural loss since the remnant structure is still suppressing disturbances. The jet is only stable for two nozzle diameters in water (transparent section of the jet at the outlet). The MR fluid has a higher viscosity than water, hence the coherent section of the jet has a diameter of 7-8. The early disturbances, which are initially visible as ripples on the surface of the coherent component of the jet, eventually lead to the breakdown and rapid spread of the jet. When magnetised at the output, the MR fluid jet is coherent for more than 200 diameters. The MR fluid jets have the same fluid viscosity and jet velocity. As a result, when the magnet is turned off, the viscosity is too low and the velocity is too high,

making it impossible to form a stable jet of fluid. When the magnet is turned on, the same high-velocity, low-viscosity jet of MR fluid is stabilised by the application of the magnetic field.

1.3.6 Chemo-mechanical magneto-rheological finishing (CMMRF)

Chemo-mechanical magneto-rheological finishing (CMMRF), a new process, combines the advantageous aspects of CMP and MRF without the drawbacks of either procedure as shown in Fig.3. Chemical reaction and mechanical abrasion happen simultaneously while removing material in the CMMRF process. Soft silicon dioxide is created chemically when silicon reacts with cerium oxide, deionized water, and oxygen [42]. The mechanical action of relatively soft abrasive and magnetic particles then readily sweeps the chemically softened layers. After attacking Si-Si bonds to create Si-H and Si-OH, water molecules made up of H+ and [OH]_ ions replace all four Si-Si bonds. The silicon atom will not be released as a soluble silicate if all four bonds are not broken; rather, it will remain attached to the surface as an oxide. Si-OH bonds gradually take the place of the Si-H bonds. It has been found that removing the protective oxide from the silicon surface does, in fact, favour the development of soluble silicates. Thus, chemical processes soften the surface of the Si work-piece and remove the peak from surface.

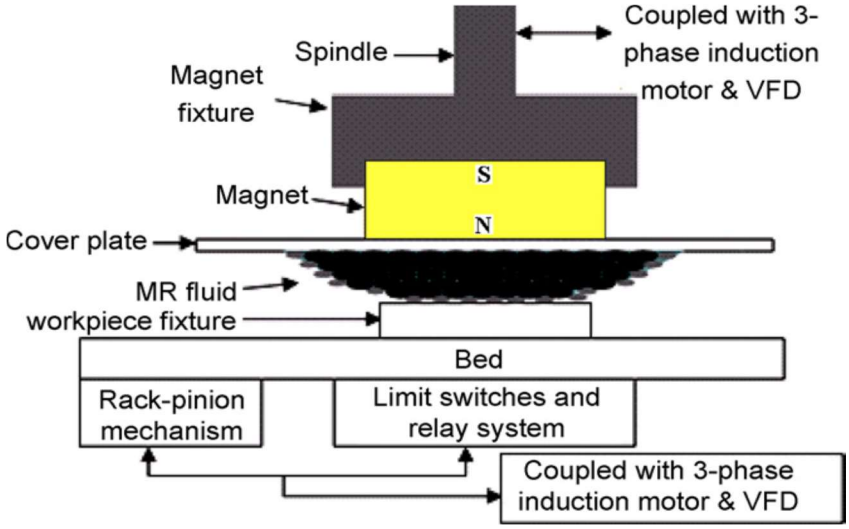

Fig.3: Schematic diagram of CMMRF set-up [42]

1.3.7 Ball end magnetic rheological finishing (BEMRF)

Precision optics are made using the sub-aperture polishing method known as magnetorheological finishing (MRF). A magnetorheological (MR) fluid contains magnetic carbonyl iron particles (CIP), nonmagnetic polishing abrasives, water or other non-aqueous carrier fluids serves as the foundation for the MRF's removal function [3]. For fine finishing with tight tolerances and without destroying surface topography, the exact control of finishing forces is crucial. These are unable to finish complicated three-dimensional curved surfaces. The ball end MR finishing tool is designed to get beyond the aforementioned limitations of the aforementioned finishing processes as shown in Fig.4.

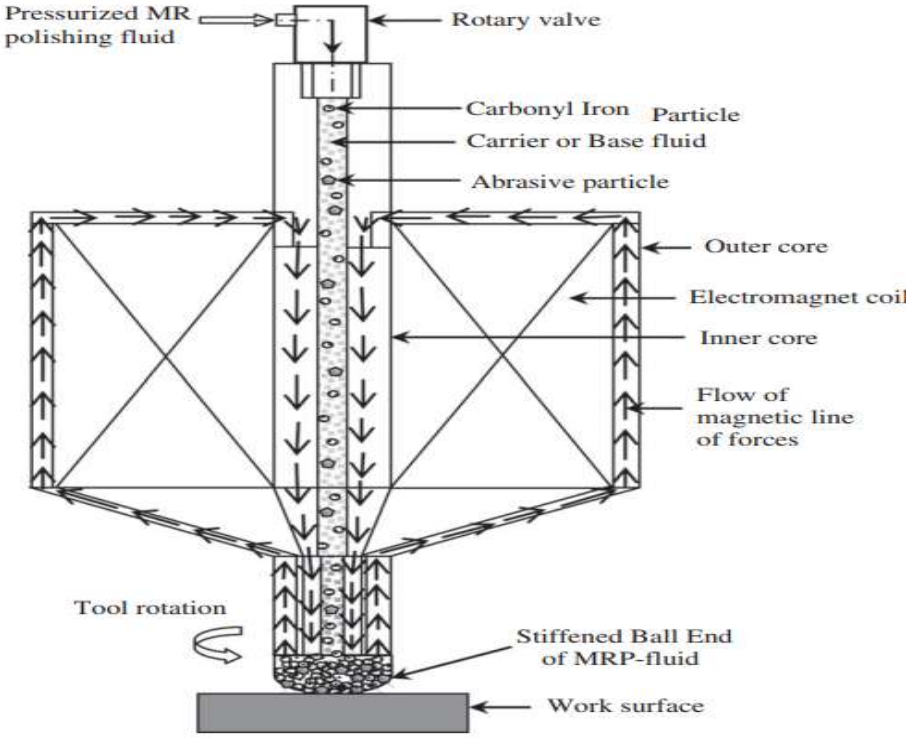

Fig. 4: Material removal mechanisms in Ball end magnetorheological finishing process [3]

1.4 Magnetorheological fluid

MRF processes depend mainly on the composition of the magnetorheological fluid. Rainbow discovered magnetorheological fluids in 1948 [43], which are intelligent fluids that change their rheological behaviour in response to an applied magnetic field. MR fluids are viscoelastic base media with certain additives suspended in micron-sized magnetic particles. These fluids have weak Bingham behaviour, which is non-Newtonian behaviour, in the absence of a magnetic field. These fluids stiffen up when a magnetic field is applied, and it takes a lot of shear force to get them to flow. Hydrocarbon oil has some benefits due to its low viscosity, despite silicone oil being the most widely utilized carrier liquid [44]. In concentrated MR fluids, unwanted particle aggregation develops as a result of the particles' residual magnetization. As a result, the development of hard sediments that are challenging to disperse is aided. Add

thixotropic agents (such as carbon fibers, silica nanoparticles, surfactants, and magnetic nanoparticles [47–48]) to minimize particle aggregation and settling. The utilization of water-in-oil emulsions as carrier liquids and viscoplastic media as a continuous phase [49]. In water-based fluid, surfactants and glycerol are utilized as stabilizers. Alkaline also aids in enhancing stability and corrosion resistance [50]. In order to specifically account for the effects of magnetic nonlinearity and saturation, a numerical and analytical model of a magnetorheological fluid phenomenon was created [51–52]. Analysis was done on the shear stress and the inter-particle magnetostatic force. According to their findings, the maximum shear stress of the particles rises in direct proportion to their saturation magnetization. [53]

On the characterization of MR Polishing fluid, very few researches have concentrated. Three models are employed to evaluate the rheological behaviour of MR Polishing fluid. The newly constructed hydraulically powered capillary rheometer, to characterize the polishing fluid [54]. Their research shows that the MRP fluid cannot be classified as a Bingham plastic fluid because of nonlinearity in the flow curve. Due to the CIP chains breaking more quickly under high shear rates, the behaviour of all MRP fluids is viscoplastic in character and exhibits shear thinning. It is challenging to predict the nature of these fluids due to abrasive particle. Since the particles are ferromagnetic in nature and magnetization occurs unevenly in various sections of the particles, the strength of the MR fluid grows nonlinearly as the applied magnetic field increases as shown in Fig.5. For the water-based MR polishing fluid, a characterization investigation was also carried out utilizing a parallel plate magnetorheometer. Their research also demonstrates that MRP fluid exhibits shear thinning property [55].

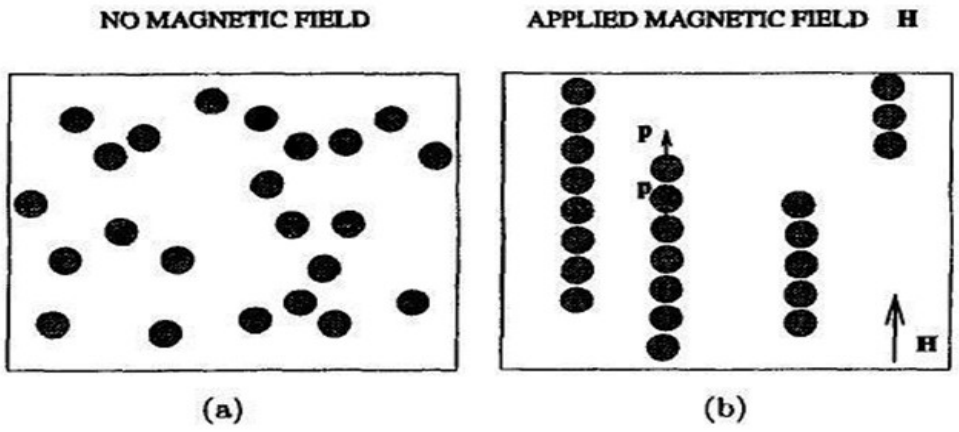

Fig.5: Fluid flow pattern (a) At no magnetic field (b) In presence of magnetic field [54]

1.5. Benefits of ball end magnetorhelogical finishing

- A brand-new, precise finishing procedure for 3D surfaces produced by CNC milling.
- In-process tool geometry control for precise finishing operations.
- Cutting tool edges don't wear since the polishing fluid is constantly refilled at the tip.
- Heat and debris are removed from the polishing zone using MRP-fluid.
- This technique can be used to finish both ferromagnetic and non-ferromagnetic materials.

1.6 Applications of BEMRF process

- Automotive parts
- Mould manufacturing industries
- Aerospace industry
- Optics finishing
- Semiconductor finishing
- FDM fabricated components

Chapter 2

LITERATURE REVIEW

This chapter starts with a thorough analysis of the non-conventional literature that is currently available. Research pertaining to magnetic field density, finishing forces, and other variable elements impacting surface finish and residual stress have also been evaluated. In the last section hybrid forms of ball end magnetorheological finishing process are discussed followed by research gaps.

The finishing operations take up the most time and money in the modern metalworking business. Additionally, labor-intensive manual handling is required for sophisticated finishing operations, which can be harmful to worker's health in some cases. Modern manufacturing processes has been discussed for finishing of intricate profile of surface and the objects which are difficult to machine. The aforementioned issues can be overcome using BEMRF process. Many manual finishing procedures have been replaced by the BEMRF process, improving the standardization of manufactured parts. Due to the extensive research that has been done on BEMRF and its hybrid forms with other machining techniques are discussed.

2.1 Major area of BEMRF research

The following three fundamental research trends in the field of BEMRF process can be readily identified:

2.1.1 **Experimental Research:** There are many variable parameters affecting the performance of BEMRF process such as Magnetizing current, Feed rate, Working gap, Rotational speed of tool, CIP concentrations, EIP concentrations, MR fluid composition, Base fluid, abrasive particle and work piece material. In the present research, effect of the vital process parameters over the material removal, percentage improvement in surface roughness, residual stress was analysed and an attempt was

made to optimize the process parameters.

2.1.2 **Hybrid forms of BEMRF Process:** There is a lot of research being done to hybridise the fundamental BEMRF technique with other machining methods in order to increase its efficiency.

2.1.3 **Analytical Research:** Analytical research includes mathematical modelling, design of experiment and other optimizing technique of variable parameters.

2.2. Literature Review

A thorough literature analysis is conducted in order to understand the state of the art, the impact of process parameters on the percentage decrease in surface roughness, and the study of residual stresses as a measurement tool. Amazing research has been done to examine how magnetorheological fluid affect the process performance. In addition to these process parameters, the finishing operation is significantly impacted by the properties of the MR fluid, specifically the base fluid, SiC particles, CI particles, and rheological parameters. The selection of the process parameters for improved process performance is made possible by having information of all these variable parameters. The following research has been described as improving understanding of the impact of various parameters on quality attributes for finishing requirements:

Golini (1997) [56] has conducted experiments to finish different kind of surfaces with two different machine configurations through MRF process and it was observed that this process is highly capable for finishing of optical materials.

A. B. Shorey, (2000) [57] Studies on MRF's macroscopic features. A magnetorheometer's construction and operation are described. The dynamic yield stress of an MR fluid can be precisely measured using this novel device in the same field orientation as polishing. It is demonstrated that taking into account the field direction is crucial for determining the magnitude of yield stress. In order to calculate

the shear stress at the glass component's surface using experimentally discovered pressure distributions, the result is utilised to describe the bulk flow of the MR fluid underneath a glass part during polishing. It is demonstrated that these shear stress distributions correspond with the removal profile.

R. A. Steven [2001] [27] used technique known as magnetorheological finishing (MRF) shown to be efficient for controlling fine structure and polishing a variety of optical glassware and crystals. The stress of the surfaces of single crystal silicon wafers are relieved. The MRF is used in the semiconductor industry to create integrated circuits. By measuring the bending of the wafer using interferometry, the stress produced in the wafer surface was identified. Dimpling was used with a fixture created to define the thickness of the subsurface damage (SSD) layer. The subsurface damage and related residual stress created in the wafer surface during loose abrasive lapping were successfully removed by MRF's subsequent polishing.

A. B. Shorey, et.al. [2001][58] have done the characterization of dynamic yield stress of the magnetorheological (MR) fluid. In MRF process with nonaqueous MR fluids and no nonmagnetic abrasives, material removal experiments demonstrate that the nanohardness of CI is significant, but it is very minor in aqueous MR fluids. It was predicted that the hydrated layer created by water's chemical interactions influences how material is removed by hard CI when the MR fluid transitions from a nonaqueous to an aqueous state. Drag force measurements and atomic force microscope scans show that nonmagnetic abrasives (cerium oxide, aluminum oxide, and diamond) are forced toward the work-piece surface when an MR fluid is applied, and this causes material removal. Material removal rate rises when these are included.

S. Gorodkin, et.al. [2002][59] investigated experimentally MR fluid deformation between two magnetic plates. The static yield stress for radially grooved plates was found to be 2.8 times higher than for smooth ones. Strong magnetic fields and small iron particle volume fractions produced the most noticeable effects. Grooves are

thought to produce a magneto mechanical barrier that inhibits particle aggregates from sliding against the wall.

A.J. Bombard, et. al. [2002][60]have chosen three grades to prepare magnetorheological suspensions (MRS). We measured the yield stress in the absence of a magnetic field and at 100 and 200 Gauss magnetic field. In the following order, the yield stress rise in the field: CC, SM, and OX. This finding implies that the performance of MRSs is influenced by particle size distribution at least as much as magnetic susceptibility. Also evaluated in an MTS 850 test system was a damper (Lord RD-1005-3) that had been slightly modified and filled with an alternate MRS made using one of these powders.

W. Kordonski & D. Golini [2002][61] have used a suction cup for MR polishing fluid to extract the fluid from the wheel surface once it has left the polishing zone. A dynamic magnetorheological fluid seal is created between the cup and the wheel surface by the magnetic system inside the cup. Magnetic systems, flow design and optimization have been accomplished using finite element analysis software.

H. See & R. Tanner [2003][62] have done experimental study for the normal force in a magnetorheological suspension. It was found that normal force is increased with magnetic flux density as in the absence of deformation, and acted to separate the rheometer plates. The normal force first dropped with strain when shearing began at a constant shear rate, reaching a plateau value that shrank as the shear rate was increased. This behaviour can be explained by the aggregate model of magnetorheological suspensions, in which the elongated aggregates that span the space between the plates provide the normal force and are sheared into smaller particle clusters.

W-B. Kim, et.al. [2004] [63] have proposed a method for three-dimensional microchannel structures. As a polishing tool, the technique uses magnetorheological fluid that has been combined with abrasives. Investigated were the effects of the process variables on the removal of the material, and contrasted were the surface

topographies before and after completing. The bottom and side silicon channel surfaces' roughness was reduced by a factor of 5–10 when a micro channel was finished using the suggested procedure. The results of the experiments showed that the suggested method finished microstructures well.

M. Tricard, et.al. [2004][64] have studied MRF applications. MRF is a deterministic, sub-aperture finishing process with system stability. It worked effectively for many industrial and optical applications.

S. C. Jayaswal et. al. [2005] [65] investigated the MAF process. A finite element model was developed to evaluate distribution of magnetic forces on work surface with magnetic flux, number of turns 3000, Work-piece SUS304 stainless steel, abrasive Al_2O_3 (dia. 5μm), and iron particles 70%. Due to the edge effect, the normal magnetic force is greater close to the magnetic pole's edge. After completing for 4 minutes, the simulated results compare favourably with the experimental outcome.

D. K. Singh et.al. [2005] [66] have studied on magnetic abrasive finishing (MAF) of alloy steel work-pieces using unbonded magnetic abrasive particles (UMAPs). It was found that the magnetic flux density rises as magnetising current rises.

D. K. Singh, et.al. [2006] [67] have done experimental investigations into forces acting during a magnetic abrasive finishing process. They discussed a correlation between the surface polished and the forces as well as experimental results about the forces acting during MAF. It was concluded that increasing magnetizing current and decreasing working gap, forces and changes in surface roughness (Ra) rise.

V. K. Jain., et.al. [2008] [21] have used pulsating DC power supply in MAF process. DC power supply has been used to electromagnetic coil for MAF process with process parameters such as duty cycle, On-time (ms) Off-time (ms). It has been found that under continuous DC power supply, the abrasive particles lose their capacity to finish the work-piece surface at the cutting edge of the particle after a given amount of time.

While finishing a work piece with a pulsing DC power source, the orientation of the abrasive particles may shift or fresh, efficient abrasive grains may come into contact with the surface, which encourages a superior surface finish.

V.K. Jain et.al. [2005] [42] developed chemo-mechanical magneto-rheological finishing (CMMRF) setup for polishing silicon blanks. In this finishing process, variables like finishing time, working gap, rotational speed, and abrasives (aluminium oxide and cerium oxide) were used. Superior surface polish was attained with the use of very fine abrasives during finishing. The use of the four distinct finishing phases produced an ultra-finished surface free of scratches.

S. Jha and V.K. Jain [2006] [68] have done worked in magnetorheological abrasive flow finishing (MRAFF), surface roughness is modelled and simulated. Process under the influences of finishing cycle, magnetic flux density, MRP fluid, mess size 800 to 2000 and carbonyl iron powder CS and HS grade. The highest improvement was achieved with CIP-CS.

A. G. Olabi, et.al. [2007][69] have studied MRF-based solution may be more cost-effective and functional for any system. The MRF technology's major characteristics are simplicity and increased intelligence in the functioning. MRF is the next technology of choice for many applications due to its excellent characteristics and controllability.

J. E. De Groote, et.al. [2007] [70] have focused on material removal of glass. The glass composition, MR fluid pH, polishing abrasive size and concentration are all included in this model. To the best of our knowledge, we are the first to incorporate quantitative chemical predictors into an MRF removal rate model. We independently evaluate each term in our model before combining all the terms. Using a set of six optical glasses and nano diamond MR fluids, we collected all of our experimental data for material removal.

C. Miao, et.al. [2008] [71] discussed the magnetorheological finishing (MRF) procedure and measures drag force as well as normal force for spots taken on optical glasses and hard ceramics in real time. For these materials, removal rate rises nonlinearly with shear stress.

D. W. Kim, et.al. [2008] [72] have focused onto the material removal at different slurry conditions. In order to find the best slurries and process variables such as wheel rotation speed and electric current for polishing glass, a number of fundamental tests were initially carried out. Groove polishing was then carried out using the results acquired, and the outcomes are examined. On the glass specimen, an exceptional surface roughness of Ra=3.8nm was attained. The current findings emphasize the potential for using this polishing technique to produce ultra-precision micro components, particularly in MEMS applications.

A. Sidpara., et.al. [2009][5] have studied the rheology of the fluid (yield stress and viscosity) under the influence of the magnetic field. It was found that the yield stress is most affected by the magnetic field.

J. Seok, et al. [2009] [73] have developed a finishing process, a magnetorheological (MR) fluid's tribological characteristics are examined in this article. The tribological behaviour of the MR fluid in the finishing process is described by a semi-empirical material removal model.

F.F. Fang et.al. [2009][74] have focused on novel PS/ Fe3O4 particles. Shear stresses and yield behaviours were slightly higher in the MR fluid that had magnetic CI nanoparticles added to it.

A. Sadiq and M. S. Shunmugam [2009][75] have studied on magnetic field analysis. The duration of the process and the work-piece's rotation speed are affected by magnetic flux. Researchers have found that the MR fluid acquires more yield strength

as increasing with magnetic field density to remove the surface imperfections, the surface quality was enhanced.

C. Miao, et.al. [2009][76] have done measurements of both drag and normal forces in MRF. Using a dual force sensor, measurements are made across the full region of material removal, or the anticipated area of the MRF removal function or point on the component surface.

Sim [2010][77] have focused on quality of product. Millions of Euros are spent year trying to improve the quality of parts or components, particularly in the aerospace sectors, by removing or avoiding such distortions, according to the description

C. Miao, et.al. [2010] [78] have studied the process parameters of MRF process. The impact of process variables on material removal for borosilicate glass were examined here. A typical aqueous magnetorheological (MR) fluid is used to gather data on a magnetorheological finishing (MRF) spot taking machine (STM).

Jang et. al. [2010][79] developed electrochemical polishing process using MR fluid. The parameters were used in this process for finishing of hard materials. In comparison to the usual technique, this process increases the surface roughness by 14 times.

A. Kumar et.al. [2011] [3] designed and developed a BEMRF tool for finishing variety of work-piece surfaces. Using parameters magnetic field (0.2T), completing time (60–100 min), rotation speed (100–600 rpm), and working gap (2mm), and DC power supply. The experiment was conducted on EN-31 and grooved surface (30 V, 2.6 A). Surface roughness on the ferromagnetic work-piece steadily decreases from 414.1 nm to 70 nm with 100 minutes of finishing, while surface roughness on the groove surface decreases from 336.8 nm to 102 nm with 60 minutes of finishing.

A. K. Singh, et. al. [2012] [80] have studied to see the effect of finishing process on surface roughness using process parameters such as work-piece position, rotational speed, magnetizing current and feed rate. On the flat, 30°, 45°, and curve surfaces of

the 3D work-piece, surface finish as 16.6nm, 30.4nm, 71nm, and 123nm, respectively, were attained. It was discovered that the ground surface performed better during finishing than the milled surface. The impacts of variations on typical 3D finished work-piece surfaces were achieved in terms of the final surface roughness. The fluctuation in magnetic normal forces can be reduced by giving the MR finishing tool a tilting motion. This can be accomplished by including a rotational axis in the current finishing setup, ensuring that the tool tip surface is constantly parallel to the surfaces of the three-dimensional work-piece.

A. Sidpara and V.K. Jain [2012] [81] have proposed a theoretical model of forces using process parameters such as working gap, CIPs vol% (30 -40), abrasive vol % (0 to10) and wheel speed 150 to 350 rpm. Normal and tangential forces rise when CIP concentration rises, while they fall as working gap and abrasive particle concentration rise. Additionally, it was observed that the theoretical normal force, tangential force, and squeezing force models show better agreement with experimental results than the model that does not take squeeze force into account.

A. Katiyar et. al. [2012][82] concerned with the preparation of paraffin oil based nanofluid and studied their magnetorheological behaviour using magnetic rheological fluid, magnetic flux density and Fe-Ni nanoparticles. The findings demonstrate the significant impact on the yield stress and viscosity. According to research, the impact of nano particle concentration on MRNF viscosity has been studied under applied magnetics flux intensity. MRNF having more than 8.0 weight percent of Fe-Ni nanoparticles exhibits a striking rise in viscosity. When the applied magnetics flux density increases from 0 to 1 T, the MRNF with 10 weight percent Fe-Ni nanoparticles likewise exhibits an impressive increase in yield stress. Therefore, in a 1 T magnetic field, a magnetorheological nanofluid containing 10 wt.% Fe-Ni nanoparticles exhibit a 24 times increase in Bingham property.

Yamaguchi et.al. [2012][83] analyzed the finishing of uncoated carbide tool surfaces using magnetic abrasive finishing with selected process parameters such as abrasive and iron particles abrasive 0.1 μm and lubricant compound (pH 9.5) to improve the tool characteristics.

H. Hezaveh. et.al. [2012][84] have studied on Synthesis and rheological behaviour of $Fe_2O_3$with concentration of nano particles. The experiment demonstrates that ferro fluids behave almost Newtonian at low concentrations. But, by adding more nanoparticles, they stop being Newtonian.

Amineh et. al. [2013][85] have proposed a study to remove the WECDM-produced recast layer. By increasing abrasive particle size using the MAF technique, the removal of the recast layer and surface roughness were both improved.

Y.R.Su, et.al. [2014] [86] developed permanent magnet ball-end tool. To investigate the processing features of this polishing technique, a prototype apparatus is developed. MRF spots are taken on stationary work-pieces to the response on material removal. After polishing a 3x3mm square of fused quartz (FS) for 100 minutes, the surface roughness was decreased.

Judal & Yadava [2013][87] have proposed a FEM for magnetic field distribution.The electromagnetic current (0.5-2.5A) with electrolyte current (05-25T) were used. Around the margins of magnetic poles, the magnetic field is stronger.

A. K. Singh., et.al. [2013][88]have proposed a model for surface finishing. The developed mathematical model was used to anticipate the magnetic normal finishing force and the results from the experiments were compared. Close agreement was observed between the two. Additionally, the % change in surface roughness during finishing was used as an experimental measure of the influence of variations in magnetic normal force. Magnetic normal force experimental and projected values were found to differ by 11.20% to 2.02%. In presence of magnetic field, the normal force

was raised on decreased in the working gap. It is because of more active abrasives contact with the work-piece surface for a longer time. Two-body wear mechanisms were used to polish the surface by abrasion. Higher magnetic normal forces were shown to result in greater material removal as measured by the % change in surface roughness. When the magnetic field produced normal force was reduced with an increase in working gap, less active abrasives contact with the work-piece surface was seen during surface finishing. Abrasion action was used to polish the surface with a three-body wear mechanism. Lower magnetic normal forces were shown to result in less material removal in terms of % change in surface roughness.

A. Sidpara and V.K.Jain [2013][89] have measured the normal, tangential and axial forces. Increases in the work-piece surface's angle of curvature result in a significant reduction in the normal and tangential forces. The optimal value for tool rotation speed and work-piece feed rate obtained when both forces are high due weak structure of the CIP chains.

W.L.Song, et.al. [2013] [90] have investigated the finishing effect of magnetorheological fluid on specimen. According to test results, a magnetorheological fluid can effectively reduce surface roughness of a steel but brass and aluminum specimens' finishing surfaces become noticeably harsher as a result. With an increasing magnetic field, the steel's surface roughness decreased. Additionally, the proposed empirical model could suit the surface roughness and reflect how the experimental conditions affected it.

A. K. Singh, et. al. [2014][11] have done studied on smart behavior of MRP fluid and magnetostatic simulation. The creation of the ball-end finishing spot is indicated by the magnetostatic simulation. For the same magnetizing current, it was discovered that, depending on the working gap, the form and size of the finishing spot in contact with the work-piece surface varied.

M.S. Niranjan et.al. [2014] [91] have studied on bi-disperse magnetorheological polishing fluid with different compositions. The MR polishing fluid compositions (Sample 3) 16 vol% CIP of CS grade, 4 vol% CIP of HS grade, 25 vol% SiC abrasive and 55 vol% base fluid have shown maximum yield shear stress and better surface finish among all samples.

Mishra et. al. [2014][92] have studied on transient thermal analysis of work-piece. The temperature increased the most at 450 rpm of electromagnet rotation and 0.23 T of magnetic flux.

A. K. Singh et. al. [2015] [8] have focused on the reduction in roughness using Silicon carbide abrasive composition. Finishing time, magnetizing current, rotational speed, working gap, and fluid composition on response are some of the process characteristics that have been considered. For finishing the work-piece, it was discovered that the MR polishing fluid compositions of 5 vol% SiC800 and 15 vol% SiC1200 were somewhat less effective. With 15% of SiC400 in the MRP fluid, the process was found to function better in terms of the percentage change in Ra value. The process mechanism showed that the majority of the abrasives were discovered near the work-piece surface due to gradient of magnetic field. During the finishing process, these active abrasives are held on the work-piece surface by the chain of CIPs.

M.S. Niranjan and S. Jha [2015] [93] have studied sintered magnetic abrasives based MRP fluid. In this study, process variables including sintered magnetic abrasive (SMA), tool rotational speed, working gap, and total finishing time (minute) were used. After conducting tests, it was determined that finishing the work-piece's surface using SMA was superior than using unbonded magnetic abrasives (UMA) based in terms of %ΔRa. By running trials at higher speeds with SMA based MR polishing fluid, it has been possible to determine the impact of tool rotating speed on %Ra and tool ageing effect. It was found that %ΔRa increases as tool rotational speed increases, and then

declines later owing to the aging impact of the tool. Therefore, 600 RPM was determined to be the ideal tool rotating speed.

M. S. Niranjan et.al. [2015][94] have done comparative study on mild steel surface with synthesized and UMA based fluid. Then it was estimated and compared how much the surface roughness had decreased (%Ra). When using synthesized MRP fluid to finish, the response %Ra was discovered to be superior. To create the experimental strategy, a thorough research using a central composite design of experiments (DOEs) with three factor and five levels was conducted. It was decided to use Response Surface Methodology (RSM) which containing useful features and their interactions was created. The percentage Ra was then computed following an experiment using the optimal machining conditions and compared to the highest percentage Ra determined by a regression model.

D. A. khan et.al. [2016][95] have studied for finishing of copper (diamagnetic) by using this process and process variables including core rotating speed, working gap, and magnetizing current are used in magnetic simulation. The outcomes of the simulation of ferromagnetic materials reveal a region of high flux density below the tool tip and a very low flux density at the copper surface. Mild steel bases show a slight improvement in magnetic flux density over copper work-pieces, but permanent magnets placed beneath the copper work-pieces are the only way to see a considerable improvement. Using a gauss meter, it is experimentally proven that inserting a permanent magnet beneath a copper work-piece improves the magnetic flux density. The surface roughness of the copper work-piece is decreased using a permanent magnet base.

M. S. Niranjan., et.al. [2016][96] have studied the flow behaviour of MAPs based MR polishing fluid. At various current values, magnetorheological characterization was done, and steady state rheograms were drawn. In comparison to MR polishing fluid based on unbounded magnetic abrasives, the results reveal that MAPs-based MR polishing fluid exhibits better yield behaviour and viscosity.

F. Iqbal, et.al. [2016][97] observed that some amount of MR fluid remains at work-piece surface after the finishing process. For feedback control of the BEMRF process, the measurement of surface roughness necessitates the use of an automatic cleaning system. In the current work, a revolutionary technique that uses kerosene to clean the work-piece surface has been devised. In this study, an electro-pneumatic control system is used to automate the entire cleaning system. For cleaning using air spray, water jets, and surfactant solutions, various studies were carried out. Kerosene, when sprayed at a high enough pressure, was found to eliminate any remaining MR fluid without altering the surface roughness. The BEMRF system's feedback control mechanism is therefore supported by a potent automatic cleaning system.

D. A. Khan, et.al. [2016] [98] have used cerium oxide, alumina, and diamond are used as the abrasives in the BEMRF process to polish polycarbonate up to nanoscale. Alumina and diamond polishing have essentially the same results. For alumina, analysis of variance (ANOVA) is used to assess the influence of the variables and their respective contributions. It is observed that acetone mixed with a water-based MR polishing solution works well for polishing polycarbonate. Alumina can be used to polish polycarbonate since its polishing results are essentially identical to those of diamond abrasives and because it is less expensive.

F. Iqbal, et.al. [2016] [99] have researched completed component surface quality. The degree of surface finish identifies a superior quality surface. The degree of surface polish that results from a surface's manufacturing process. Better surfaces can be created by some procedures than by others. Grinding, honing, lapping, buffing, super finishing, and polishing are the traditional techniques recognized for good surface finish.

S. Maan, et.al. [2017] [100] have concentrated on two distinct MR fluid-based finishing techniques. The external circular surface of the mould die punch is finished using a turning type MR finishing technique, and the flat surface is finished using an

MR ball end with a solid rotating tool core. The current permanent mould punch is made of P20 tool steel, which has a 431 VHN hardness rating. The enhancement of the die punch surface at the microscopic level and the decrease in surface roughness at the nanoscale have shown that the smooth surface of plastic bottle caps may be produced using the current finishing procedures.

P. Skalski & K. Kalita [2017] [101] have outlined the function of elastomers and magnetorheological fluids in the modern environment. Review of elastomer and magnetorheological fluid applications in equipment and machinery. Elastomers and magnetorheological fluids are examples of smart materials. A magnetic field can influence the characteristics of elastomers and magnetorheological fluids. Magnetorheological elastomers, as opposed to magnetorheological fluids, circumvent the challenges associated with MR fluid applications, such as sedimentation, sealing concerns, and environmental pollution. Due to their capacity to attenuate vibrations in the presence of a regulated magnetic field, magnetorheological fluids and elastomers offer significant potential for current and future uses in transportation. Magnetorheological dampers and shock absorbers are used in a variety of applications, including high-tension wire damping, building and bridge operation, and damping control. New magnetorheological elastomer-based solutions are increasingly being patented in the automobile sector, including an adaptive energy absorption system, a system of magnetically dissociable and a drive shaft vibration reduction system.

Z. Alam & S. Jha [2017][102] have developed model for force acting on abrasive particle. It is suggested to use the yield stress of MRP fluid as a function of flow density in a shear force model. Understanding the wear mechanism associated with the BEMRF process is based on the idea of resistive force, normal and shear force. The mathematical model that is utilized to find the surface roughness in the BEMRF process has undergone experimental validation at various magnetizing current values.

A. Khurana et.al. [2017] [103] have studied revolving core with a central hole allows polishing fluid to flow at the tool end surface in the current ball end magnetorheological finishing (BEMRF) technique. At the end surface of the solid rotating core tool, the uniform magnetic flux density was plainly discernible. The magnetostatic finite element analysis compared to the present BEMRF tool core with a central hole. In order to evaluate the variance in surface roughness values, the experiment was done on a ferromagnetic work-piece surface using spot finishing.

D. A. Khan, and S. Jha [2017] [104] have discussed about CIP and EIP based fluid for finishing of copper work-piece surface. EIP is recommended for copper finishing instead of CIP since it has larger particle size than CIP, which is typically utilized in MR polishing fluids. Moreover, compared to CIP-based fluid with EIP based which have the normal finishing force is higher for EIP-based fluid. Studies have also been done on the impact of MR polishing fluid composition parameters on finishing of copper surface. Abrasive mesh size is discovered to be the most crucial factor. Less cutting occurs during finishing as the abrasive mesh size is raised, and vice versa, as the abrasive particle size is decreased. The finishing effect, as measured by an increase in %ΔRa, increases with an increase in iron powder concentration. The percentage Ra rises with an increase in abrasive concentration in MRP fluid, however beyond a given volume of abrasive, the percentage Ra falls off due to the weakening of the iron particle chain.

P. Kala, et.al. [2017] [6] have focused on simulation of mathematical model on surface roughness. The relationship between the work-piece's surface roughness and process variables like working gap and rotational speed has been modelled. The simulation of the mathematical model demonstrated that the effect of decreased feed rate becomes more pronounced with smaller working gaps.

A. Barman et.al. [2017][105] have proposed a modelling and simulation of magnetic field assisted finishing process (MFAF). Magnetorheological (MR) fluid was

employed to regulate the MFAF process using the magnetic field. A permanent magnet was utilized to produce the magnetic field in the finishing area. The MR fluid was used as a polishing bush to remove material from the work-piece surface. A FEM of the process was built in this research to describe the magnetic field's direction and distribution on the work-piece's surface.

A. kumar et.al. [2018] [106] focused on conducting an experimental and analytical investigation to complete the production of poly lactic acid materials utilizing the FDM technique and BEMRF. The process parameters such as core rotational speed, working gap, abrasive, Electrolytic Iron particles (EIPs) size concentration and magnetizing current are selected in this study. The BEMRF process operation used for nanofinishing FDM parts has a considerable impact on the percentage change in surface roughness. On increase the concentration of the abrasive, %ΔRa, rises to a certain point and then falls as the concentration of EIP rises. The best MRP fluid composition for finishing FDM parts utilizing the BEMRF method was determined through experimental analysis.

L. Nagdeve, et.al. [2018] [107] have prepared the MR fluids by varying fluid compositions. The fluid's composition consists of 25% CIPs, 10% abrasive (by volume), and the remaining base medium. At 0.33 Tesla of magnetic flux density, the yield stress was assessed. In comparison to other combinations, it has been found that it MR fluid with CIP and abrasive particle sizes of the same size produces increased yield stress. The example with 9 μm abrasive particle size is observed to have the lowest yield stress. To comprehend the impact of the relative sizes of magnetic and abrasive particles on surface roughness, a series of finishing tests were conducted.

Z. Alam et.al. [2018] [108] have investigated the relationship between polishing fluid volume and finishing spot size, corresponding to surface finish. The fluctuation in flux density is determined through magnetostatic simulation in a given working gap. The area of the threshold magnetic flux density region on the work-piece surface the

minimal value necessary for finishing is used to determine the upper limit of the polishing fluid volume. By adjusting the fluid volume, the surface properties and finishing spot diameter are examined. Due to the extra fluid flowing out of the working gap and forming a thick ring at the tool tip's outer periphery, the surface produced by using a large fluid volume is imperfectly completed and has scratch marks. In contrast, if the fluid volume is too small, the work-piece's surface is simply rotated around without any finishing activity taking place. An ideal fluid volume range results in a consistent finished spot size and an excellent grade surface finish.

D. A. Khan, et.al. [2018] [109] have focused on finishing of copper through BEMRF. Due to its mechanical softness and chemical reactivity, copper is difficult to finish using conventional method and the majority of cutting-edge finishing techniques upto nanometer level. A unique technique involving two magnetic poles that are opposed to one another has enhanced the magnetic flux density distribution between the tool tip and the surface of the copper work-piece. The statistical model created by response surface has been used to study the impact of fluid composition characteristics. Upon completion, a nano-finished surface with only a few light scratches was visible.

Z. Alam et.al. [2019] [110] outlined the use of the five-axis CNC BEMRF method for finishing 3D surfaces. As a result, the rate at which completed products are produced is increased while eliminating the labor-intensive processes and subjectivity associated in manual finishing procedures. The BEMRF machine's motion and process parameters can be sequentially and precisely controlled using a five-axis CNC controller that is specifically designed for this purpose. Through a CNC part programme, real-time management is used to control the magnetizing current that directs the forces involved in finishing in the BEMRF process. An automated finishing process for a freeform mild steel work-piece is carried out using the five-axis CNC controller. The finishing with automated five-axis BEMRF process results for the mild steel test specimen indicate an evenly completed surface profile (upto order of nanometer).

I. Faiz, et.al. [2019] [26] carried out a time-based experimental study for the BEMRF procedure for finishing EN31 steel. A transitory surface roughness reduction event in the BEMRF process was identified. It was done to optimize the machining parameters for EN-31 steel using the BEMRF technique. For the purpose of conducting time-based experimentation, four sets of machining parameters were constructed. The transitory surface roughness phenomenon is established based on the findings of time-based tests, indicating that the BEMRF process tendency to gradually reduce surface roughness over time.

H. Liu, [2019] [111] have succeeded in nanofinishing a complex small-bore component with an irregular form and concave surfaces with a radius of curvature under 3 mm. The complex component's processing strategy is introduced. The full finishing path is magnetostatically simulated to examine the material removal properties. The created device is used to polish a typical shaped small-bore complicated component, and the resulting spherical surfaces have a surface accuracy of 0.3320 m and a surface roughness Ra of 0.0107 m. The results show that a type of small-bore complicated shapes can be nanofinished using the proposed MRF technique.

G. Ghosh [2021] [112] has studied magnetorheological finishing (MRF) of WC-Co coated products. It has been noted that the shear force, magnetic force, and squeezing force all contribute significantly to the creation of overall finishing forces. A surface roughness model is created by taking into consideration of abrasive. A rise in surface temperature is caused by the micro-cutting operations. The one-dimensional heat conduction theory is used to model the temperature rise of the finishing zone. Good correlations with the experimental results are seen for all of the proposed models, which have all been empirically validated. MRF using diamond abrasives reduces the coating's actual surface roughness to 130 nm.

F. Iqbal., et.al. [2022] [113] have studied on surface roughness that was assessed using stylus-based devices, and some optical techniques. When utilized for BEMRF, these

traditional techniques have a tendency to introduce flaws into the part, which must be taken from its fixture for measurement and cannot be mounted in the exact same orientation again. Applications that need the work-piece to be held in the same orientation throughout, like insular finishing make it necessary to measure roughness in situ while using BEMRF. Because of its compact shape and light weight, a confocal sensor meets the criterion. In order to assess roughness in situ, a confocal sensor was integrated into the BEMRF system

A. Aggarwal, et.al. [2022] [114] have done study to attain the fine-finishing requirement over the interior blind hole type ball cup (BHBC) work part surface. The MRHF tool surface is subjected to a magnetostatic finite element analysis in order to produce a stronger and more consistent magnetic field. Additionally, the ideal conditions are forecast for efficient fine-finishing over the inside surface of the BHBC work part. After 80 minutes, the internal surface area of the blind hole type ball cup work-piece has a roughness value that has decreased from 0.310 to 0.070 μm. additionally, improvements in surface qualities and dimensional accuracy are made. The functional capability and service life of the ball transfer units can therefore be improved by fine-finishing the ball cup surface.

J. Tian., et.al. [2022] [115] have studied the impact of temperature on the magnetorheological fluid's flow characteristics. It has been found that the polishing relative velocity increases together with the temperature of the magnetorheological fluid. This can help to improve the pace at which materials are removed from surfaces. However, as the shear stress reduces, the rate of material removal does not improve. As a result, raising the magnetorheological fluid temperature can significantly increase the efficacy of polishing with a small ball-end permanent magnet magnetorheologically and produce highly polished surfaces.

K. Arora, et.al. [2022] [116] have estimated the surface roughness reduction of the hemispherical cups utilizing the current MRF technique, a novel theoretical

mathematical model was constructed. Both theoretical and empirical research has been done on how the magnetic flux density (MFD) affects the fine finishing of the hemispherical acetabular cup work-piece because the magnetic field controls forces in the MRF process. Next, a hemispherical cup work-piece surface is used to experimentally test the mathematical model for lowering surface roughness. With errors ranging from 1.17% to 6.15%, the predicted roughness results closely match the experimental values. SEM, micro-hardness tester, and coordinate measuring tools are also being used to test the work-piece for surface morphology. Micro-hardness and dimensional accuracy respond to assess the effectiveness of the current procedure. The current mathematical model for the MRF process forecasts improved surface quality.

P. O. Horo, et.al. [2022] [117] have used flexible belt that spins with the help of two pulleys for setup. A base plate that is magnetically held in place by three electromagnets. When a magnetized field is applied, the fluid used in magnetorheological polishing (MRP) changes its rheological characteristics and assumes a viscoelastic texture. The work-piece is secured in a fixture and is totally tiltable and rotatable over its whole surface. Large flat work-pieces with externally curved surfaces can be applied with this configuration successfully. Based on the magnetic simulation investigations, a unique belt and pulley type MR finishing arrangement has been developed in this research project.

M. Kumar, et.al. [2022] [118] have worked on a magnetorheological finishing procedure that uses chemical pretreatment to nanofinish electroless nickel-plated surfaces.$H_2O_2$and hydrofluoric acid are the substances that were employed in this project. To comprehend the surface chemistry following chemical treatment, the impact of exposure time and concentration on micro-hardness and roughness is examined. The hydrogen peroxide creates a passivated layer that makes material removal simple. In addition to enhancing surface quality, hydrofluoric acid aids in the elimination of pollutants. To comprehend how chemical treatment affects surface topography and finishing rate, the finished surface is characterized. After chemical

treatment, the hardness and surface condition mostly influence normal and tangential forces. The chemical treatment with 1% HF for 30 min that produced the best combination of characteristics was used to finish the surface, reducing the areal surface roughness to 10 nm.

Z. Alam, et.al. [2022] [119] conducted an experimental study on the finishing forces. The trials are carried out using mild steel as the work-piece on a three-axis CNC BEMRF machine. A dynamometer is used to continuously record the normal and shear forces exerted on the work-piece surface throughout the finishing process while varying the chosen process parameters during the experiment. The results demonstrate good agreement between the theoretical values predicted by the model and the empirically recorded data at lower finishing current values.

Anand.et.al. [2023] [120] focused on a novel finishing method called chemical assisted ball end magnetorheological finishing (CA-BEMRF) used to further increase percent reduction in surface roughness of aluminium 7075 alloy. A comparison of the percentage reduction in surface roughness obtained after ball end magnetorheological finishing (BEMRF) and attained after CA-BEMRF procedure is carried out. The CA-BEMRF process resulted in a 1.84 percent reduction in surface roughness as compared to BEMRF without chemical.

Derakhshan-Samani, M.,et.al [2023] [121] have done the study to provide an enhanced Ball-End Magnetorheological Finishing (BEMRF) tool that can be used to polish borosilicate glass (Bk7) lenses and can be put on a CNC milling machine. To determine the optimal result of the abrasive and carbonyl iron particles in the magnetorheological fluid used for finishing operations on flat Bk7 glass. The response surface method experimental examination was carried out.

Taira.et.al. [1978] [122] have proposed firstly cosα method. This has gained interest from business as a novel approach to measuring X-ray stress that makes use of the

entire Debye-Scherrer (D-S) ring. Taira and Tanka were the ones who first put forth the idea of the cos approach for in-plane biaxial stress analysis [123].

A. Mishra et.al. [1985] [124] have proposed an analytical model based on finite element method. This is provided for calculating the residual stresses caused by surface grinding that are of thermal and mechanical origin. According to the investigation's findings, grinding beneath the surface under specific conditions causes high tensile residual stress. The models anticipated distribution nature is equivalent to the empirically obtained distributions nature.

Sugano [1987] [125] experimentally demonstrated that during the diamond turning of an aluminium alloy, an unintended compressive residual stress of 60 MPa was created, causing subsurface damage. Generally residual stresses are undesired stresses that form in a work-piece after machining. When such undesired stresses are reduced, the performance and behaviour of components can be improved.

D.Y. Jang et.al. [1996] [126] measured the residual stress of turning component. X-ray diffraction method was used to calculate residual stress tensors. The impacts of the turning conditions were examined in relation to mechanically and thermally deformation of the work-piece surface on residual stresses. Experimental measurements of residual stresses were made in order to quantify the surface integrity of the machined components because measurements were taken on a free surface.

Noyan, et.al. [2006] [127] referred to the X-ray diffraction technique as one of the most effective non-destructive methods for determining the residual stress in polycrystalline materials both in real-world settings and in research labs.

Brinksmeier et.al. [2007][128] have explained the causes of the various stages of residual stresses while employing boron nitride and aluminium oxide wheels. The surface finish of highly loaded objects can be achieved by the crucial machining

operation of grinding. The chosen grinding wheel's properties and the machining parameters influence the residual surface stresses that are introduced.

Sakshi.et.al. [2009] [129] have estimated X-rays from various incident angles are used in the many D-S rings taken using the suggested method to measure tri-axial stresses.

A. Paul and A. P. Savio [2015] [130] predicted residual stresses in milling and drilling process. The process parameters included the cutter's teeth (Zc), the depth of cut (t) for milling, the feed (S), and the drill bit diameter (d) for drilling. The residual stresses are brought by the thermo-mechanical impact of machining processes and the ideal value discovered for minimal residual stress. The milling and drilling operation's parameter is optimized. The machining parameters used were feed (S) and drill bit diameter (d) for drilling, and the number of cutter teeth (Zc) and depth of cut (t) for milling. The cutting force is greatly influenced by these factors. These are input parameters, while residual stress is the response parameter. To determine the residual stress for drilling and milling, experiments were carried out. The results were analyzed using ANSYS software, and these responses underwent experimental validation. We have identified the ideal set of milling and drilling parameters from the analytical results that produces the least amount of residual stress.

Tanka.et.al. [2018] [131] have estimated the tri-axial residual stress of carbon steel surfaces that had been milled, planned, and ground was measured using the cos method. Under normal incidence, the Debye-Scherer (D-S) rings were measured, and the full width at half-maximum (FWHM) was averaged throughout the whole circle of the D-S rings. The coarse grains in the specimen cause a significant intensity irregularity in the D-S ring of the annealed specimen. In D-S rings made from machined surfaces, the intensity distribution's irregularity is diminished. Additionally, the planed surface's D-S ring exhibits textural development. The FWHM is smallest for an annealed specimen and increases with increasing levels of machining-induced plastic deformation [132].

Sanjay, et. al. [2018] [133] have done study for the purpose of improving surface integrity and extending the service life of high carbon steel, the impact of residual stresses on a machined surface together with surface roughness and erosion rate was examined. With the goal of optimizing residual stresses and erosion rate, the process parameters chosen for this experiment include vibration type continuous/discontinuous, vibration amplitude, work-piece dimension, duty cycle, peak current, and wire feed rate. The portable X-ray residual stress analyzer is used to measure residual stress effectively by detecting the entire Debye ring data from a single incidence X-ray angle. The surface characteristics of a shaping tool and the substance of the ejection die were related to these frictional forces. Working hardness and specific surface shape of forming tool/die material were frequently mentioned as frictional forces in normal shaping practice [134]. The residual stresses produced by pervious material or the machining process have an impact on the surface morphology of forming tools.

Ghosh [2021][135] have focused on residual stress generation during polishing. Because even occasionally, while polishing a work-piece, a small amount of residual stresses is created on the work-piece surfaces, directly affecting the polished product's refraction index.

Anand et.al. [2022] [136] examined how the BEMRF polishing method can reduce residual tensions left over from the grinding operation on the surface of an Al 7075 work-piece. Through variations in the percentage reduction in residual stresses, the impacts of input limitations such as magnetizing current, tool rotation, and working gap were investigated. The results showed that as the magnetizing current was raised from 1.5 to 3.5 A, the percentage reduction in residual stress value rose. It was found that the percentage reduction in residual stress value increased from 68.24% to 83.54% when tool rotation was increased from 300 to 700 rpm.

2.2 RESEARCH GAP

The following gaps are identified after conducting a literature survey:

- Literature survey reveals that the conventional DC power supply has been used to energize the electromagnet of magnetorheological finishing tool in most of the magnetorheological polishing fluid based finishing processes. It has been observed that the enhanced surface finish has been found with the use of pulse DC power supply as compared to surface finish achieved by the use of conventional DC Power supply without pulse at same process parameters in magnetic abrasive finishing. Hence Pulse DC power supply has not been explored in Ball end magnetorheological finishing process. It was thought of using a pulse DC power supply to energize the electromagnet which makes fluctuating magnetic field at the tip of finishing tool due to which new abrasive grains may come outward or orientation of abrasive particles may change and contact the work-piece surface during finishing action which may further improve the percentage reduction in surface roughness.

- The study of residual stress of the components becomes more important due to high capital and machining costs, so that these machines can be used as effectively as possible to achieve the desired payback. The performance of machined parts is significantly impacted by relative stresses. Residual stresses have a significant impact on how well machined parts work. The study of residual stress of the work-piece surface finished by BEMRF process is not available in the literature.

2.4. RESEARCH OBJECTIVES

Following are the objectives of the present study:

1. Development of Magnetorheological finishing setup for finishing of hard work-piece surface with and without pulse DC power supply.
2. Comparative study with Magnetorheological polishing fluid based finishing with DC power supply and with Pulse DC power supply and to obtain optimum Pulse frequency for the response percentage reduction in surface roughness.
3. Study of various process parameters such as rotational speed of tool core, feed rate, magnetizing current, working gap on the response percentage reduction in surface roughness using response surface methodology.
4. Study of Residual stress of work-piece surface before and after finishing using Residual stress analyser.
5. Study of Surface Texture after finishing using scanning electron microscope and atomic force microscope.

CHAPTER 3

DEVELOPMENT OF MAGNETORHEOLOGICALFINISHING SETUP

The design and construction of the developed pulse ball end magnetorheological finishing (PBEMRF) process are covered in this chapter. The components and configurations used in PBEMRF technique are fully described.

3.1 Design of PBEMRF setup.

The Ball end magnetorheological finishing tool is designed and developed with pulse DC power supply to improve the finishing of EN-31 work-piece surface. The two dimensional design of developed finishing tool is shown in Fig.6. The experimental setup consists of vertically oriented finishing tool for finishing of work-piece surface. The electromagnetic coil wrapped over the hollow aluminum tube consisting rotatory inner core has 2100 turns with 19.6 SWG copper wire. The electromagnet coil has an inner diameter of 20 mm and an outside diameter of 100 mm. Between the inner and outer cores is where the electromagnet coil is located. The magnetic flux generated by electromagnetic coil concentrated at the tool tip and passes through the EN-31 work-piece surface. The rotary inner core made of bright bar has a diameter of 10 mm and 130 mm in length. The tip of finishing tool approximately 8 mm diameter is used for finishing of EN-31 work-piece. The thermocouple PT100 has been used inside the coil to observe temperature. To overcome the heating problem, a chiller is installed to control the constantly rising temperature of the electromagnetic coil due to the continuous supply of current. The Pulse DC power supply has been given to electromagnet coil to energize the finishing tool which have 0-30 volt/ 10 A with digital panel meter. The holding of work-piece includes a platform on X-Y linear movement slides. Through CNC programming, a finishing tool's X, Y, and Z movements can be managed.

The magnetorheological fluid has been prepared for finishing of EN-31 work-piece. A homogenous mixture of MR polishing fluid was synthesized with silicon carbide abrasive particles of 800 mesh size (25 vol %) with density *d* 3.33 gm/cm^3, ferro magnetic iron particles (CIP CS grade, 20 vol %) with density *d* 7.8 gm/cm^3 and 55vol% of base fluid.

Ball End Magnetorheological finishing tool consist of following parts:

Electromagnet coil: 2100 turns (copper wire), 19.6 SWG

Thermocouple: PT 100

Copper tube for cooling: 6 mm diameter

Tool shaft length: 130 mm (Bright bar)

Bearing: ID 10 OD 16

Disk (Aluminum): 5 mm thick

Regulated DC power supply: 0-30 volt/ 10 A with digital panel meter, Timer mili second, PLC, SSR (12 A), HMI

Chiller:

The Magnetorheological finishing tool is designed through ANSYS15.0 version. The dimensions of tool shaft are 130×10 mm and diameter of two aluminum Disk is 100 mm with thickness of 5mm as shown in Fig.6. The steps followed in design of finishing tool through Ansys is shown in Fig.7& Fig.8 respectively.

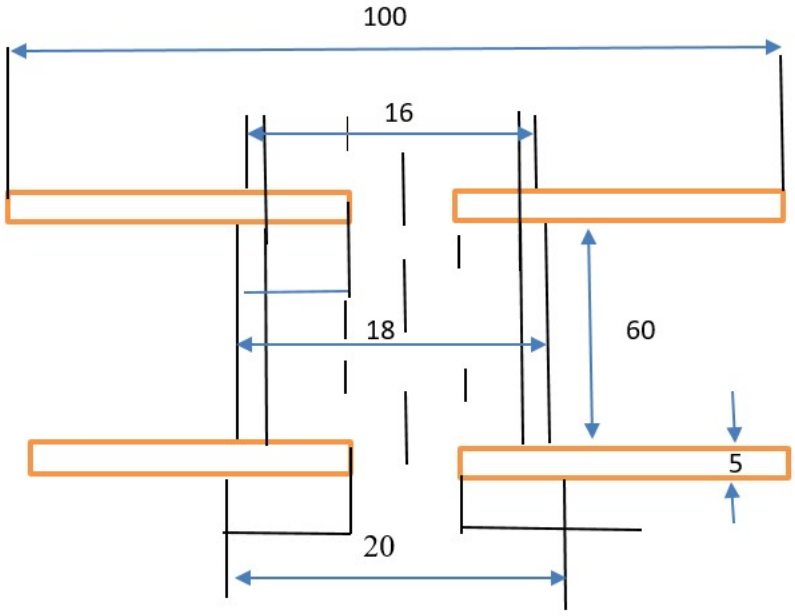

Fig.6: Schematic of Magnetorheological finishing tool

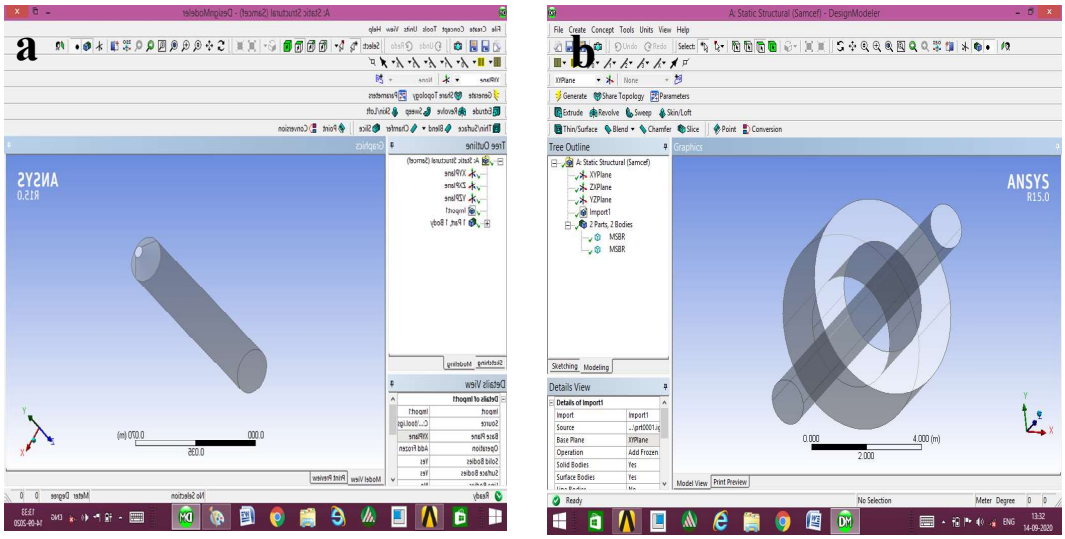

Fig.7: Steps followed in design of finishing tool through ANSYS R 15.0

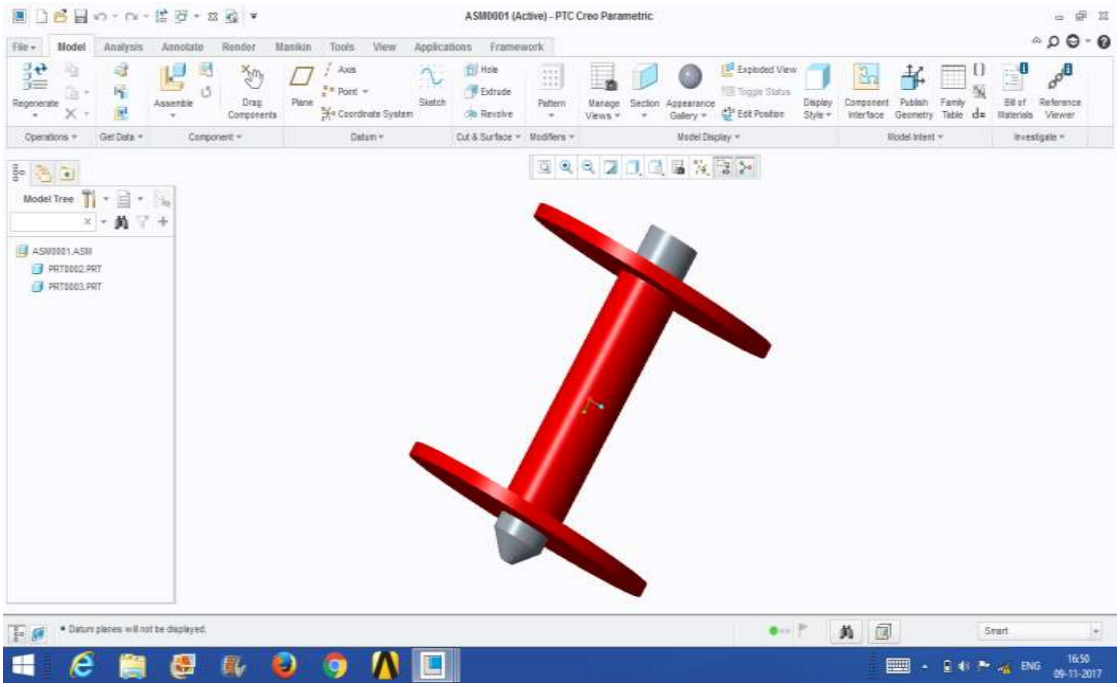

Fig. 8: 3-D design of Ball end magnetorheological finishing tool

3.1.1 Magnetic field intensity at tool tip

Ball end magnetorheological finishing tool has been designed. Here Ansys Maxwell software 15.0 is used to perform the magnetostatic simulation. The mesh is prepared for each rod separately with the same parameters. The total number of nodes for the assembly was 2,180,493, and the total number of elements was 2,159,633. In this simulation mesh size is $6e^{-3}$ and boundary condition is that electromagnetic coil (copper) is insulated because it assist in confining and guiding the electromagnetic field to avoid the losses. Outer core of aluminum is stationary wall. EN-31 work-piece is stationary wall. Magnetorheological rheological fluid is moving wall that consist of CI particle and SiC particle.

The XZ section is generated in electromagnetic coil and current excitation has been done. The magnetic field has been obtained 1.75 tesla at tool tip at magnetizing current 3.5A, number of turns 2100 and 1 mm working gap. Magnetostatic simulation of ball end magnetorheological finishing tool is shown in Fig.9.

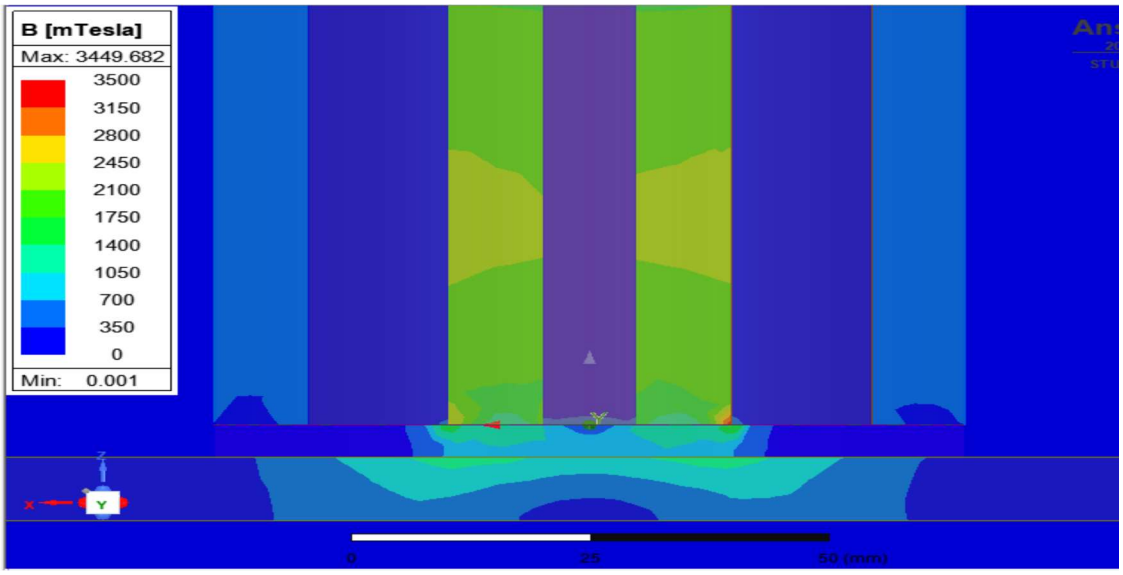

Fig.9: Magnetic flux density on finishing tool tip at magnetizing current 3.5A, number of turns 2100 and 1 mm working gap

3.1.2 Design of dies with work-piece

The work-piece position and its die are given in Fig.10. The total height of work-piece is 10 mm, 70 mm length depth of slot is 8 mm and during finishing operation the work-piece is kept slightly above 2 mm from slot depth as shown in Fig.11.

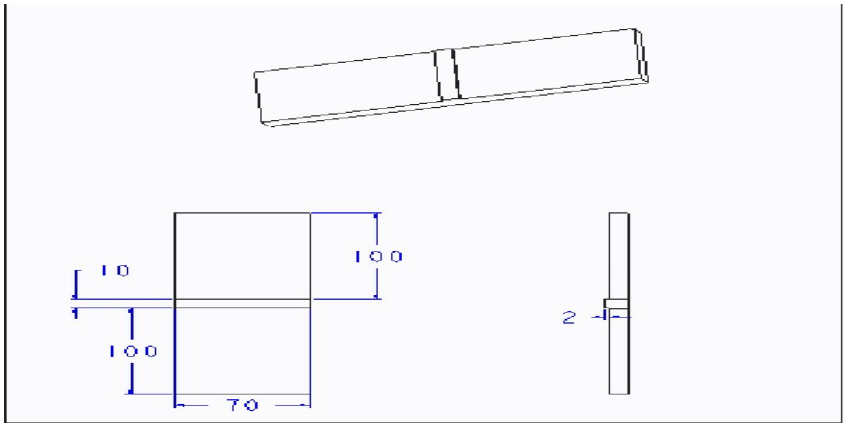

Fig.10: Schematic dimension of dies and work-piece

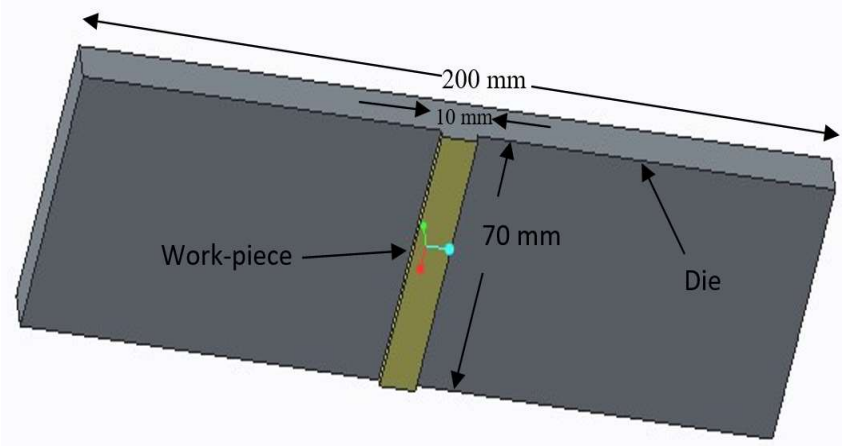

Fig. 11: The work-piece position and its die

The PBEMRF setup for finishing of EN-31 work-piece and various associated parts of the experimental setup is shown in Fig.12.

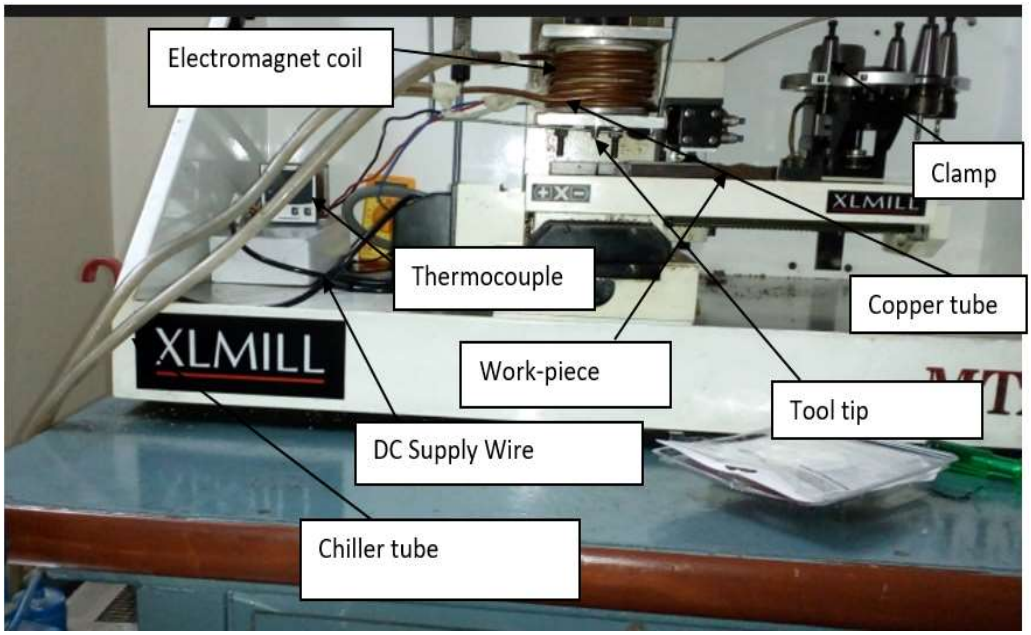

Fig.12: PBEMRF experimental setup

3.1.3 Chiller

A chiller is used to control the temperature of electromagnetic coil during finishing as shown in Fig.13. The water is used as a coolant medium in chiller tubes. This chiller tube is wrapped over the coil to overcome the overheating problem of the electromagnetic coil. The temperature of electromagnetic coil rises due to supply of current due to which coil may burn so that coolant is necessary for effectiveness of finishing process.

Fig.13: Chiller for cooling the electromagnetic coil

3.1.4 Thermocouple

PT100 thermocouple is inserted inside the coil to gives the reading of temperature during finishing of work-piece. The thermocouple is connected to a display which shows the reading of temperature. Thermocouple is used in the electromagnetic coil for safety of finishing tool as shown in Fig.14.

Fig.14: Thermocouple connected to display temperature reading

3.1.5 Pulse DC power supply

Pulse DC power supply is given to electromagnetic coil to energies it and a separate unit (HMI) is used to control the pulse on time, pulse off time as shown in Fig.15.

Fig.15: (a) Pulse DC power supply (b) HMI unit for adjusting pulse ON/pulse OFF value

3.1.6 CNC part Programming

Ball end magnetorheological finishing tool rotates over the reciprocating work-piece surface for finishing. Therefore, a CNC part program has been developed for finishing the work-piece using 3-axis CNC machine. Fig.16 shows the position of finishing tool when all the axis XYZ is set at zero. Finishing tool moves over EN-31 work-piece surface in X axis for 32.50 mm after execution of CNC part program as shown in Fig.17 and it will further move over the work-piece surface upto 50 mm during finishing.

```
G21 G94
G91 G28 Z0
G28 X0 Y0
M03 S300
G90 G00 X10 Y0
Z5
G01 Z0.1 F50
X50
M05
G91 G28 Z0
G28 X0Y0
M30
```

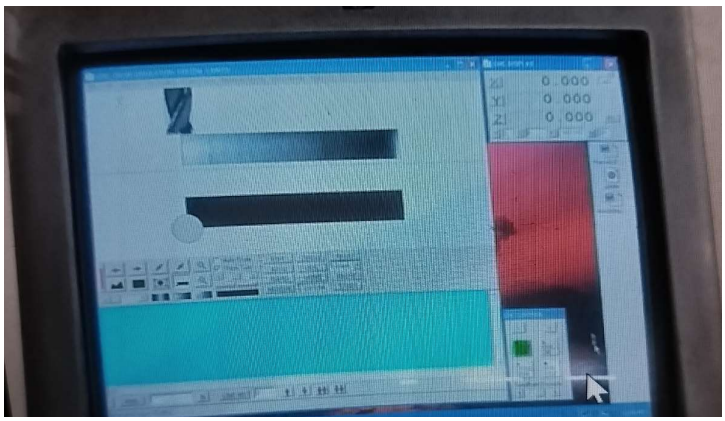

Fig.16: The position of tool before start the part program

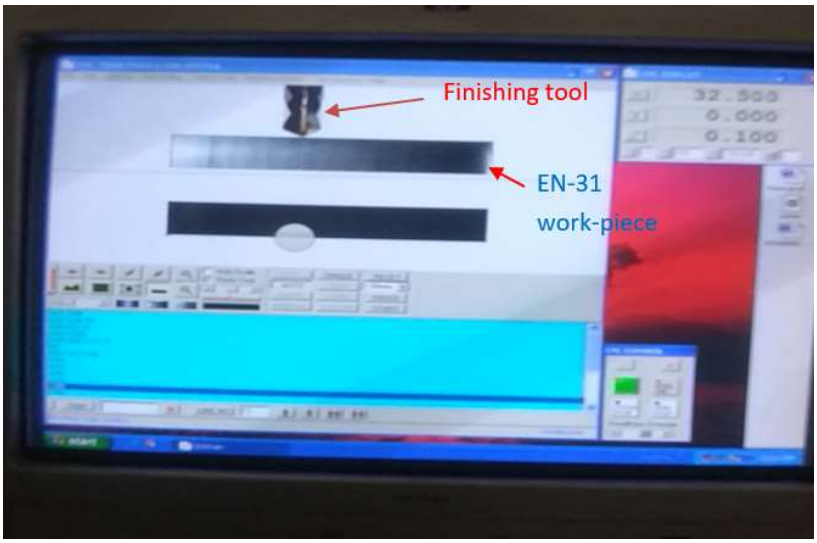

Fig.17: Finishing tool moves over EN-31 work-piece surface

3.1.7 Preparation of work-piece samples

EN-31 samples before grinding on surface grinder are shown in Fig.18. The chemical composition of EN-31 steel is measured and found as carbon (1.108%), manganese (0.462%), silicon (0.103%), sulphur (0.045%), chromium (1.153%), Phosphorus (0.037%) and remaining is iron. EN-31 steel has been highly used in automobile industry.

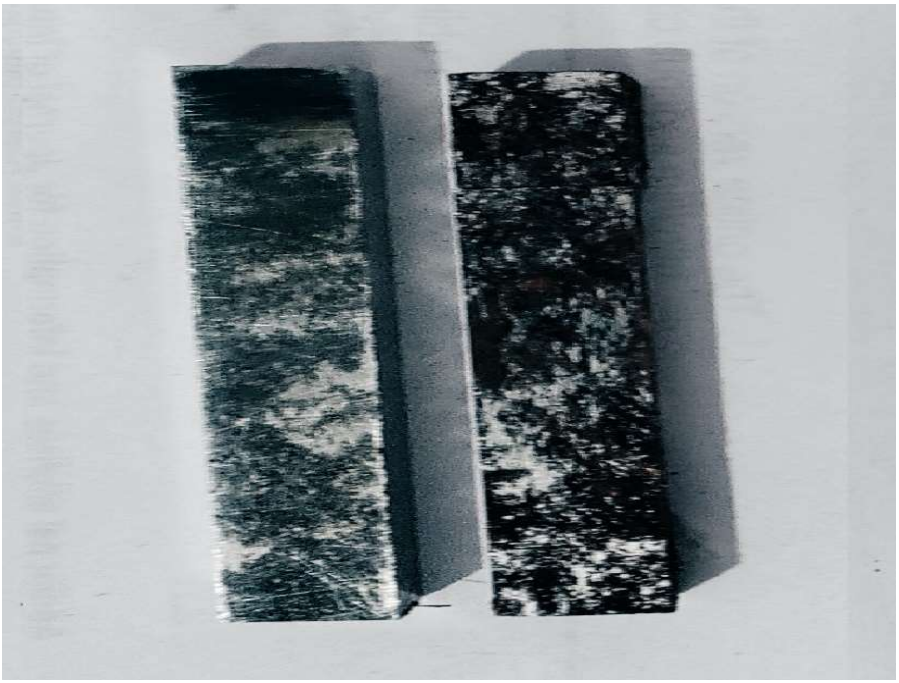

Fig.18: EN-31 samples before grinding

The mechanical properties of EN-31 steel are of young modulus elasticity (224 GPa), tensile strength (750 MPa) and yield stress (450MPa) and density of material (7800 Kg/m^3). EN-31 samples have been initially finished on surface grinder as shown in Fig.19. The specimens were fixed on the surface grinder machine using a magnetic bed.

Fig.19: EN-31 work-piece samples during finishing on Surface grinder

CHAPTER 4

COMPARATIVE STUDY WITH PULSE DC POWER SUPPLY AND WITHOUT PULSE DC POWER SUPPLY

In this chapter comparative study with pulse DC power supply and without pulse DC power supply has been carried out and the preliminary experiments were conducted on flat EN-31 steel work-piece surface with MR fluid on BEMRF process with and without pulse DC power supply.

4.1 Mechanism of material removal

In BEMRF process, the DC power supply is used to energize the electromagnetic coil due to which a semi solid hemisphere or ball shaped finishing spot of MR polishing fluid is established at the extremity end of the tool tip. The semi-solid finishing spot is generally used for finishing of surfaces such as flat, curved surface, 2D, 3D and stepped surfaces irrespective of movement of finishing tool. The semi-solid ball shaped finishing spot has more pliability to move over any kind of work-piece surface for finishing as shown in Fig.20.

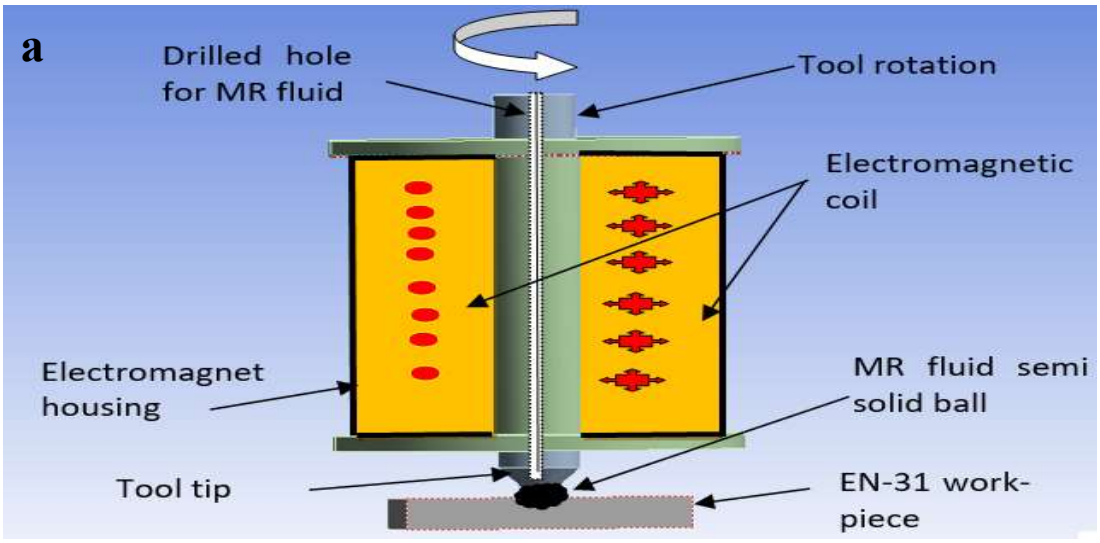

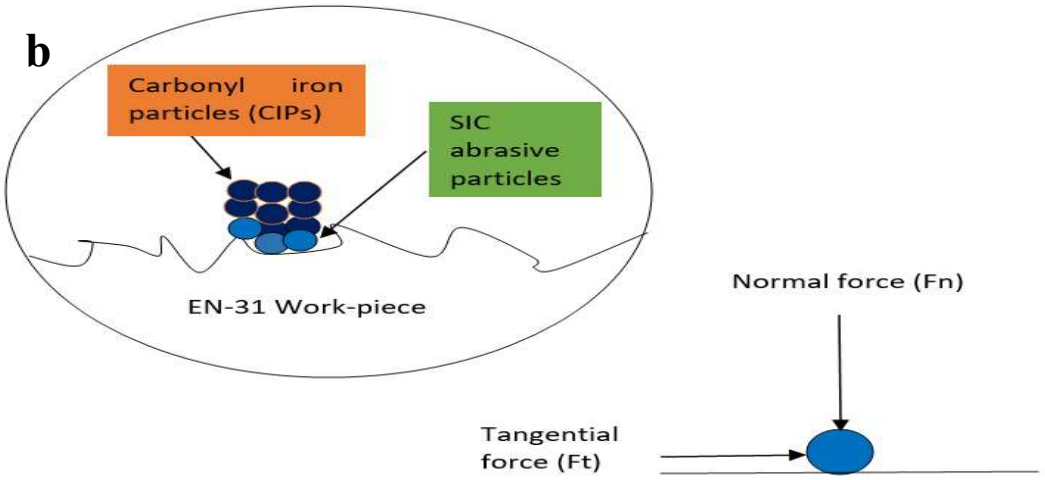

Fig. 20: (a) Semi solid ball is formed at finishing tool tip (b) Mechanism of material removal during finishing of EN-31 work-piece surface with force acting on single abrasive.

The semi solid ball moves over the work-piece surface and acts like as finishing tool to remove the peaks from the work-piece surface as shown in Fig.21.

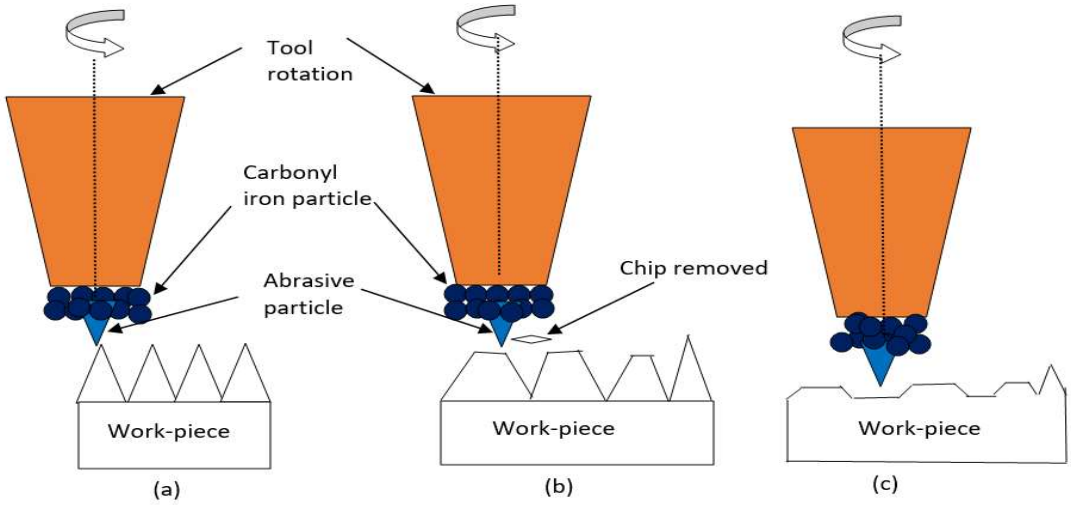

Fig.21: (a) Initial stage of EN-31 work-piece (b, c) Gradual removal of roughness peaks

In conventional MR finishing process, the abrasive particles in contact with the work-piece do not change their orientation in the entire finishing time due to fixed magnetic flux density. As a result, the cutting edges of the abrasive particles get dull resulting in poor surface finish. In order to further enhance the finishing efficiency, the fresh active abrasive particles are required again and again to finish the work-piece surface which is not possible with conventional MR finishing process. To overcome this limitation, an improvement has been done in the conventional MR finishing process by providing fluctuating DC power supply.

Pulse DC power supply is given to BEMRF finishing tool which produces fluctuating magnetic field on the tip of MR finishing tool. Therefore, fresh active abrasive grains may come outward or orientation of abrasive particles may get changed and finishing action of abrasive particles over the surface of work-piece in direct contact enhance the finishing efficiency of BEMRF process. During the process, the viscosity of MR polishing fluid reduces as soon as the DC power supply is get OFF for very short duration which results in changing semi-solid ball towards liquid state. As soon as the power supply is ON, the orientation of the abrasive particles gets changed due to fluctuating magnetic field or some new active abrasive grains may come outward. As soon as the power supply is again OFF and ON, the orientation of the abrasive particles gets changed due to fluctuating magnetic field. The frequent ON and OFF of DC power supply results in orientation change of abrasive particles hence fresh abrasive particles come in contact with work-piece surface during finishing.

On the use of pulse DC power supply in BEMRF process, higher reduction in surface roughness has been obtained as compared to reduction in surface roughness obtained with the use of continuous/conventional DC power supply without pulse. The Semi solid ball behavior at the tip of finishing tool with pulse ON conditions and with pulse OFF condition process is shown in Fig.22a and Fig.22b respectively. The schematic diagram of semi solid ball wear behavior at pulse ON, pulse OFF condition is shown in Fig.23.

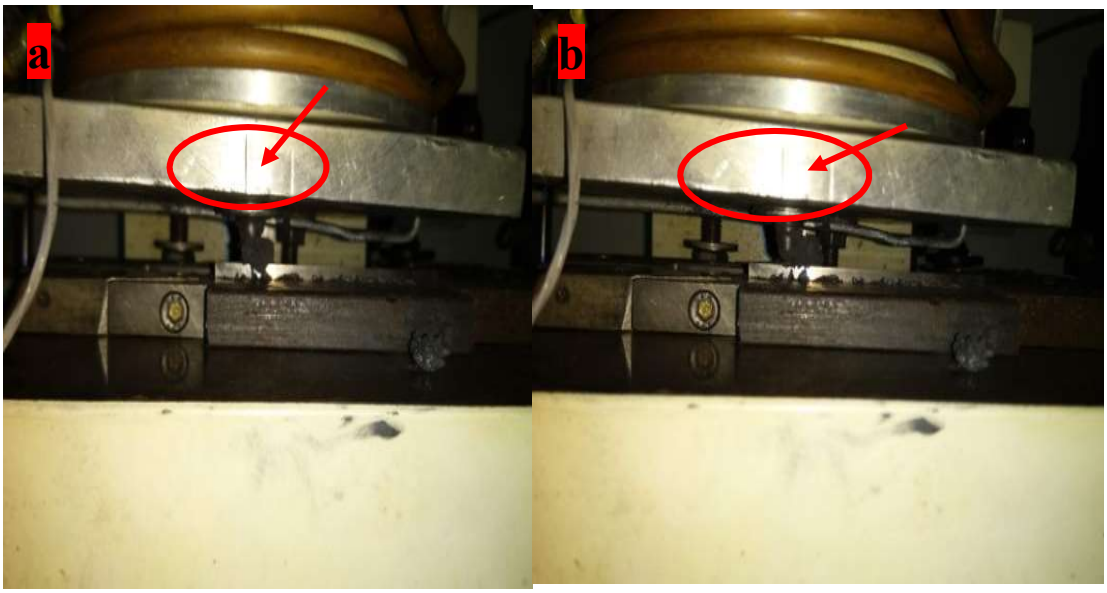

Fig.22: (a) Formation of semi solid ball at pulse ON condition(b) Destruction of semi solid ball at pulse OFF condition

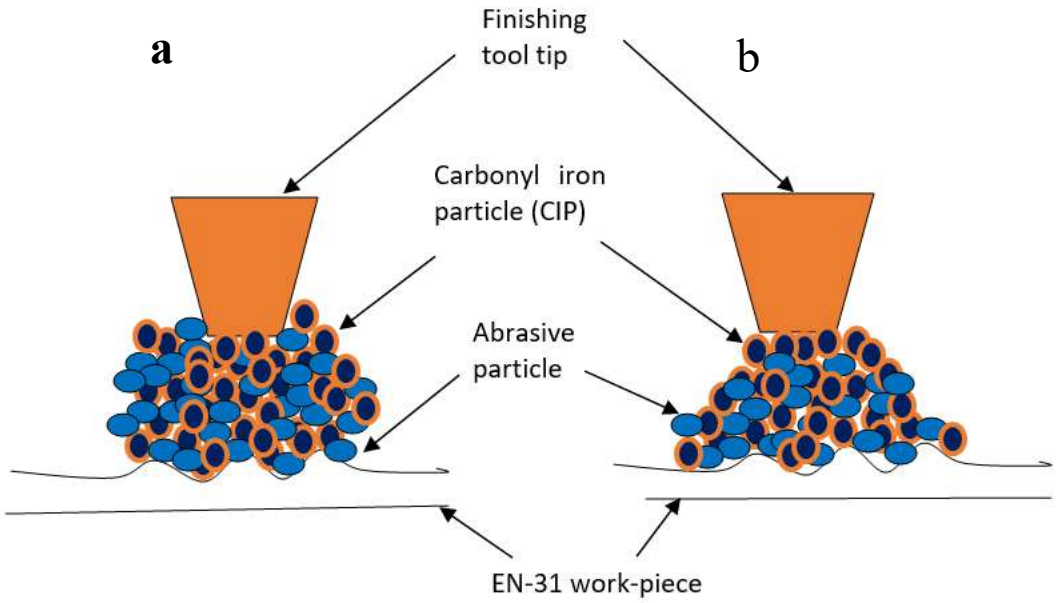

Fig.23: Schematic diagram (a) Formation of semi solid ball at pulse ON condition(b) Destruction of semi solid ball at pulse OFF condition

4.2 Preliminary Experimentations

The preliminary experiments were conducted on flat EN-31 steel work-piece surface with MR polishing fluid on BEMRF process using DC power supply with and without pulse. The MR polishing fluid consist of CI particles and SiC particles along with base fluids. These CIP and SiC particles are mixed with paraffin oil and grease which is used as slurry/finishing medium. This slurry/finishing medium forms a semi solid ball at the tip of finishing tool in presence of magnetic field which is responsible for finishing the work-piece surface. The experiments were conducted at magnetizing current 2.5A, tool rotational speed 500 rpm, working gap 1.5 mm, feed rate 50 mm/min and finishing time 30 min. The selection of parameters and their ranges has been taken on the basis of literature review.

The preparatory experiments were conducted to attain the intended purpose of getting finish on work-piece surface and to develop the ranges of the duty cycle parameters.

Equation 1 represents the Duty cycle *r*.

$$r = T_{ON}/(T_{ON} + T_{OFF}) \quad (1)$$

Here T_{ON} and T_{OFF} denotes ON time &OFF time of pulse DC power supply respectively. The approximate values for parameters are selected on the basis of the literature review. These parameters were employed with DC power supply at different duty cycles with and without pulses. The percent reduction in surface roughness ($\%\Delta Ra$) was calculated for preliminary experiments at various duty cycles and given in Table 2. A total of eighteen experiments were performed with three repletion for each sample (total number of samples = 6). The finished EN-31 work-piece with pulse DC power supply in BEMRF process as shown in Fig.24 and finishing of work-piece using DC power supply without pulse is shown in Fig.25 at same process parameters.

Fig.24: Finished EN-31 work-piece using pulse DC power supply at 2.5A, 50 mm/min, 1.5 mm and 500 rpm

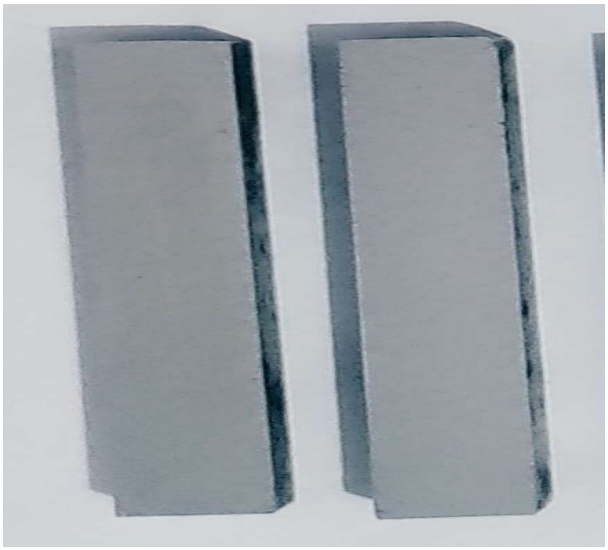

Fig.25: Finished EN-31 work-piece using DC power supply without pulse at 2.5A, 50 mm/min, 1.5 mm and 500 rpm

Table 1. Preliminary experimentation with pulse DC power supply

Exp. no.	**Duty cycle**	**ON-time [ms]**	**OFF-time [ms]**	**Pulse time**	**Initial *Ra* [µm]**	**Final *Ra* [µm]**	**%Δ*Ra***
1	**0.16**	**4**	**21**	**25**	**0.186**	**0.127**	**31.72**
2	0.27	4	11	15	0.197	0.149	24.36
3	0.36	4	7	11	0.194	0.161	17.01
4	0.45	4	5	9	0.197	0.172	12.69
5	0.61	4	3	7	0.197	0.185	6.09
6	0.67	4	2	6	0.185	0.176	4.86

Table 2. Preliminary experimentation using DC power supply without pulse

Experiment number	MC [A]	F [mm/ min]	WG [mm]	RST [rpm]	Time [min]	Initia l Ra [µm]	Final Ra [µm]	%ΔR a
1	2.5	50	1.5	500	30	0.187	0.161	13.44
2	2.5	50	1.5	500	30	0.191	0.165	13.10

From table.1, it is observed that as duty cycle increases, the %ΔRa decreases and vice versa. As the pulse OFF time starts then current in electromagnetic coil falls and before reaches the zero value again pulse ON time starts. The reshuffling of fresh grains is occurred in semi solid ball of MRP fluid due to inductance and energy stored in electromagnetic coil during pulse OFF time. The normal magnetic force is high during pulse ON time hence, depth of indentation is also high. In case of pulse OFF conditions Normal magnetic force and indentation depth are both low due to which semi solid ball becomes weak. In this instance, abrasive particles cannot endure the resistance provided by the work-piece. In this condition jumbling of CIP and SiC particle takes place in semi solid ball. The higher %ΔRa is achieved at low duty cycle and can be attributed to force ratio that depends upon the current ratio. The current ratio is given as maximum current in pulse to the minimum current in pulse. Maximum to minimum force ratio is greater at 0.16 duty. The better mixing of CIP and SiC particle is occurred

at higher current ratio. That's why higher %ΔRa is achieved with lowest duty cycle. However, for the constant duty cycle and low ON-time and high OFF time the value of pulse frequency is high.

It is observed from Fig.26 that the highest %Δ*Ra* is found to be 31.72 % at 0.16 duty cycle and is lowest at 0.67 duty cycle. The %Δ*Ra* is found to be 13.44 % on conducting the experiments with DC power supply without pulse. It has been observed from experimental study that the best %Δ*Ra* was found at 0.16 duty cycle.

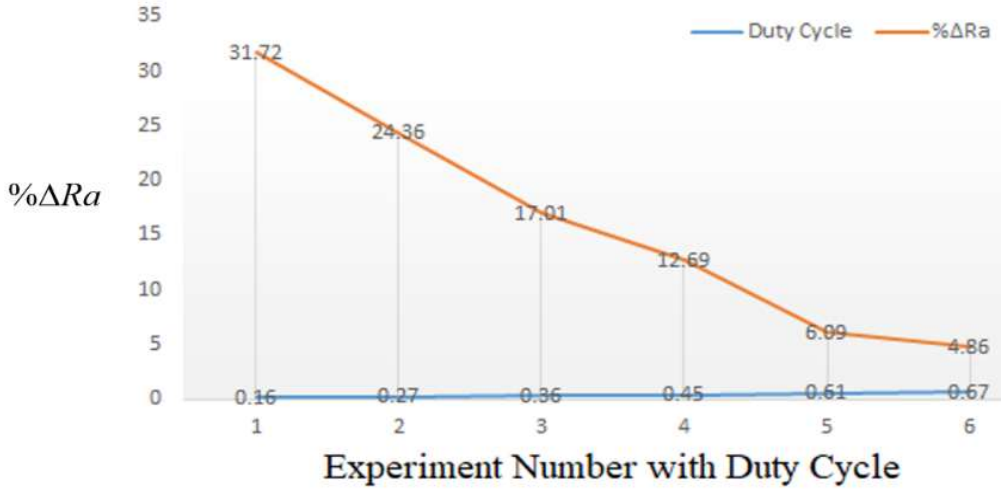

Fig.26: Graph between percent reductions in surface roughness with duty cycle

The response parameter percentage reduction in surface roughness (%Δ*Ra*) was calculated using;

$$\%\Delta R_a = \frac{\text{initial roughness - final roughness}}{\text{initial roughness}} \text{x} 100\% \qquad (2)$$

Taylor Hobson surface analyzer was used with cut-off length 0.8 mm and data length of 4 mm to measure surface roughness as shown in Fig.27. The roughness profile of EN-31 work-piece surface before finishing and after finishing at 2.5A current, 50 mm/min feed rate, 1.5 mm working gap and 500 rpm tool rotational speed with DC

power supply without pulse is shown in Fig.28 (a) and Fig.28 (b) respectively. The percent reduction in surface roughness (%Δ*Ra*) was calculated and given in Table 2.

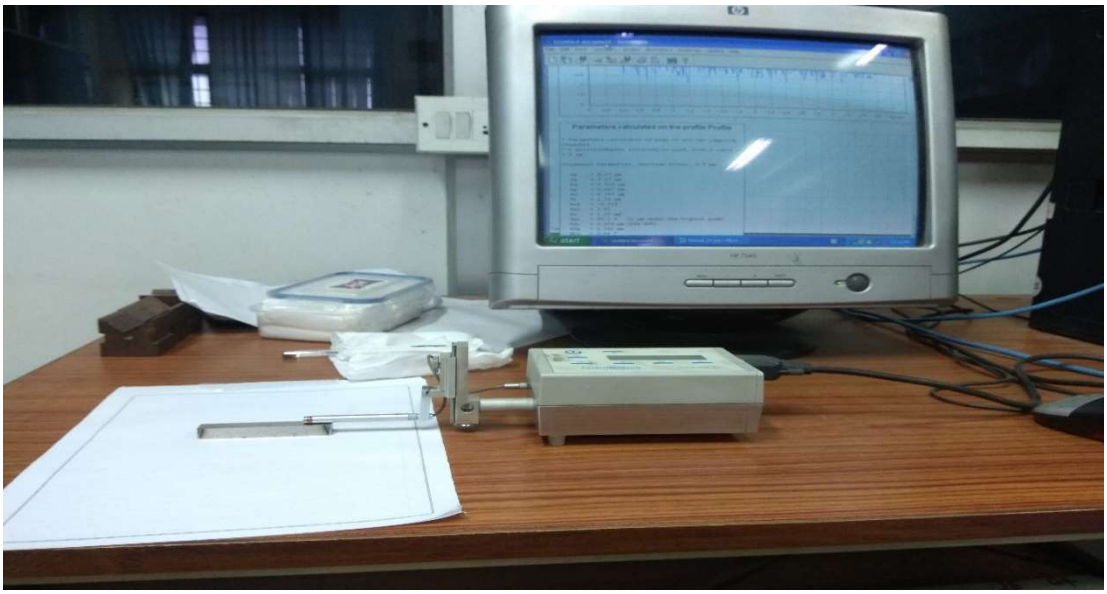

Fig.27: Taylor Hobson instrument during measurement of surface roughness

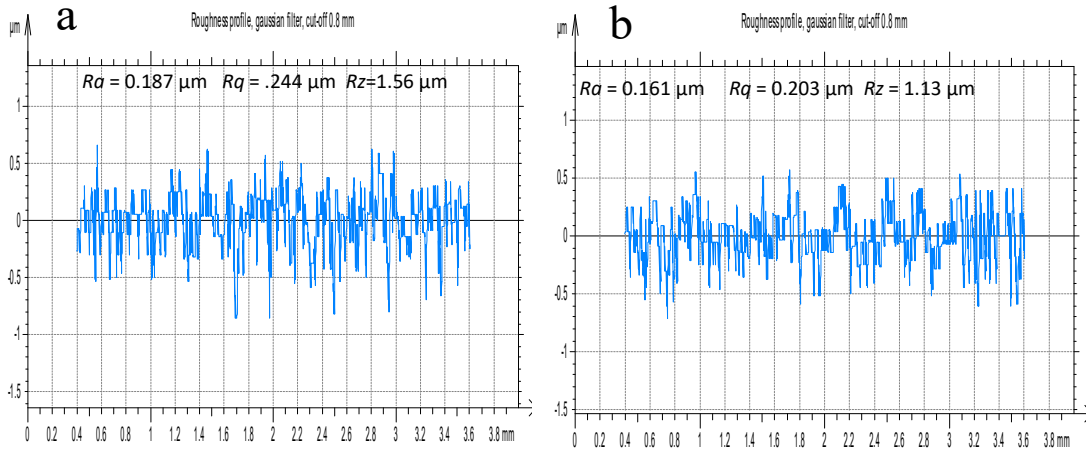

Fig.28: Surface roughness profile of EN-31 (a) Before finish (b) After finish using DC power supply without pulse

The roughness profile of finished EN-31 work-piece surface after conducting experiments at 2.5A current, 50 mm/min feed rate, 1.5 mm working gap and 500 rpm tool rotational speed with pulse DC power supply at 0.16 duty cycle as shown in Fig.29b. It is observed that the %Δ*Ra* has been found better by conducting the experiments with pulse DC power supply at 0.16 duty cycle as compared to %Δ*Ra* obtained by DC power supply without pulse.

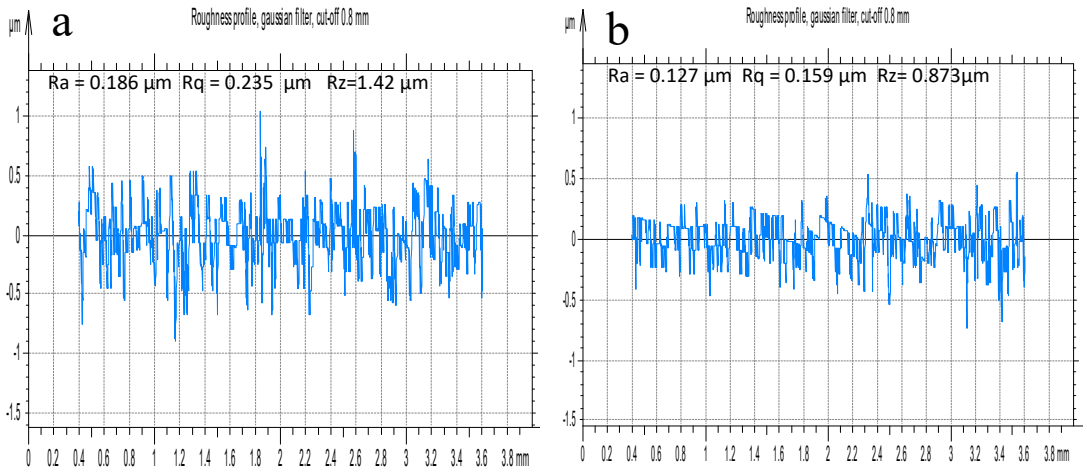

Fig.29: Surface roughness profile of EN-31(a) Before finish b) After finish with pulse DC power supply at 0.16 duty cycle

The surface roughness profile of finished EN-31 work-piece surface has been drawn after conducting experiments at 2.5A current, 50 mm/min feed rate, 1.5 mm working gap and 500 rpm tool rotational speed with pulse DC power supply at 0.27 duty cycle and is shown in Fig.30b.

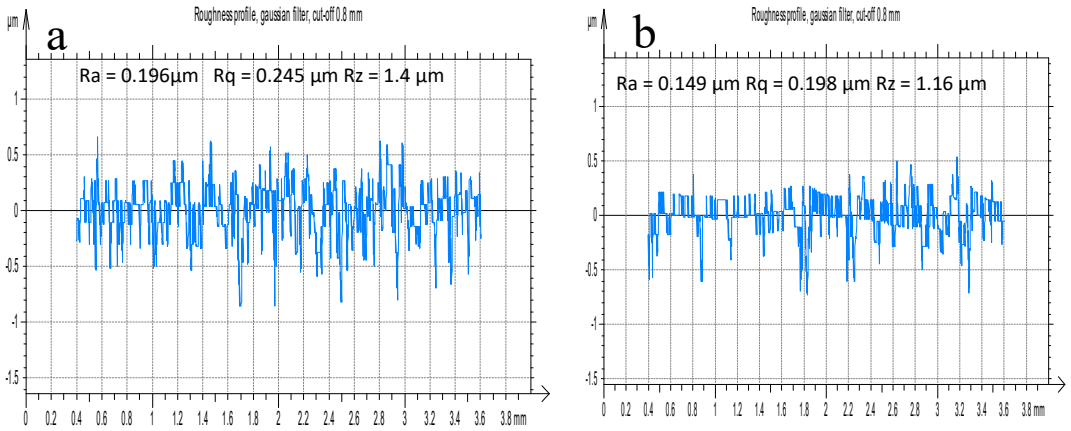

Fig.30: Surface roughness profile of EN-31(a) Before finish (b) After finish with pulse DC power supply at 0.27 duty cycle

The optical microscopic images are taken from the zeta instrument as shown in Fig.31. The optical microscopic images are taken at the scale of 9 µm. There is microscope field of view (FOV) 116µm×87µm with z-axis at 16 µm and L-axis at 109 µm. The optical microscopic views of finished EN-31 work-piece surface with and without pulse DC power supply are shown in Fig.32. The best texture of finished surface using pulse DC power supply was found at duty cycle 0.16 at 2.5A current, 50 mm/min feed rate, 1.5 mm working gap and 500 rpm tool rotational speed as shown in Fig. 32c as compare to finished surface with DC power supply without pulse at same process parameters as shown in Fig.32a. From optical microscopic views of finished surface, it was found that the surface texture is observed improved as the duty cycle decrease from 0.27 to 0.16.

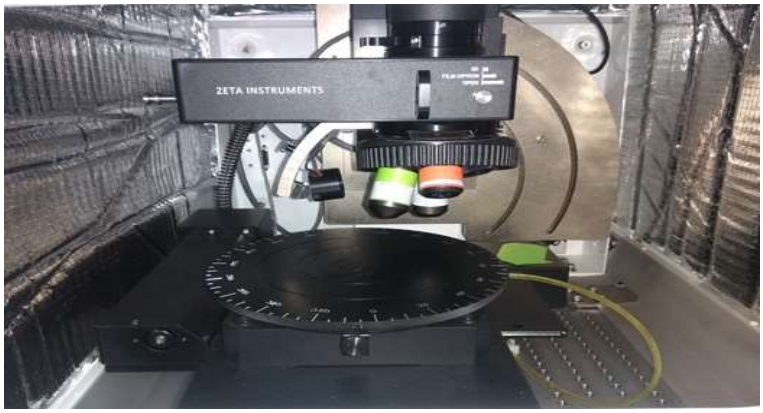

Fig.31: Zeta instrument for measurement of optical microscopic view

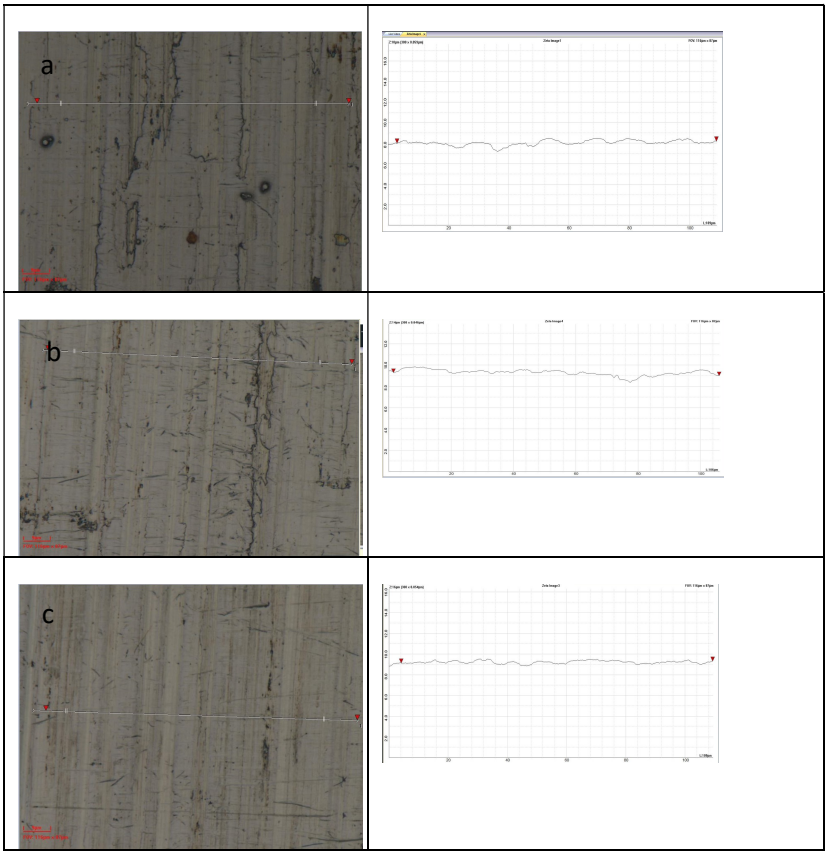

Fig.32: Optical microscopic views of finished surface (a) With DC power supply without pulse (b) With pulse DC power supply at 0.27 duty cycle (c) With pulse DC power supply at 0.16 duty cycle

Scanning electron micrograph of EN-31 samples have been taken at cross section of (10×10) mm as shown in Fig.33. Scanning electron micrograph (SEM) of EN-31 work-piece surface is shown at 100 µm resolution and 600× magnification as outlined in Fig.34. The lays are clearly visible in initial grinded surface as shown in Fig.34a. It is observed from the Fig.34c that more uniform finished surface is obtained with pulse DC power supply at 0.16 duty cycle at 2.5A current, 50 mm/min feed rate, 1.5 mm working gap and 500 rpm tool rotational speed as compared to the finished surface obtained with DC power supply without pulse at same process parameters as shown in Fig.34d from the Fig.34b and 34c is shown that as the duty cycle decreases from 0.27 to 0.16, better surface texture is achieved at 0.16 duty cycle.

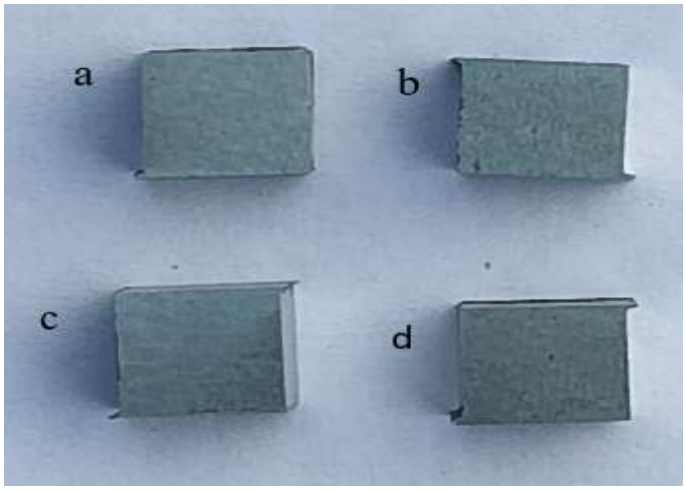

Fig.33: Images of work-piece surface (a) Before finish, (b) After finish at 0.27 duty cycle, (c) After finish at 0.16 duty cycle, (d) After finish with DC power supply without pulse

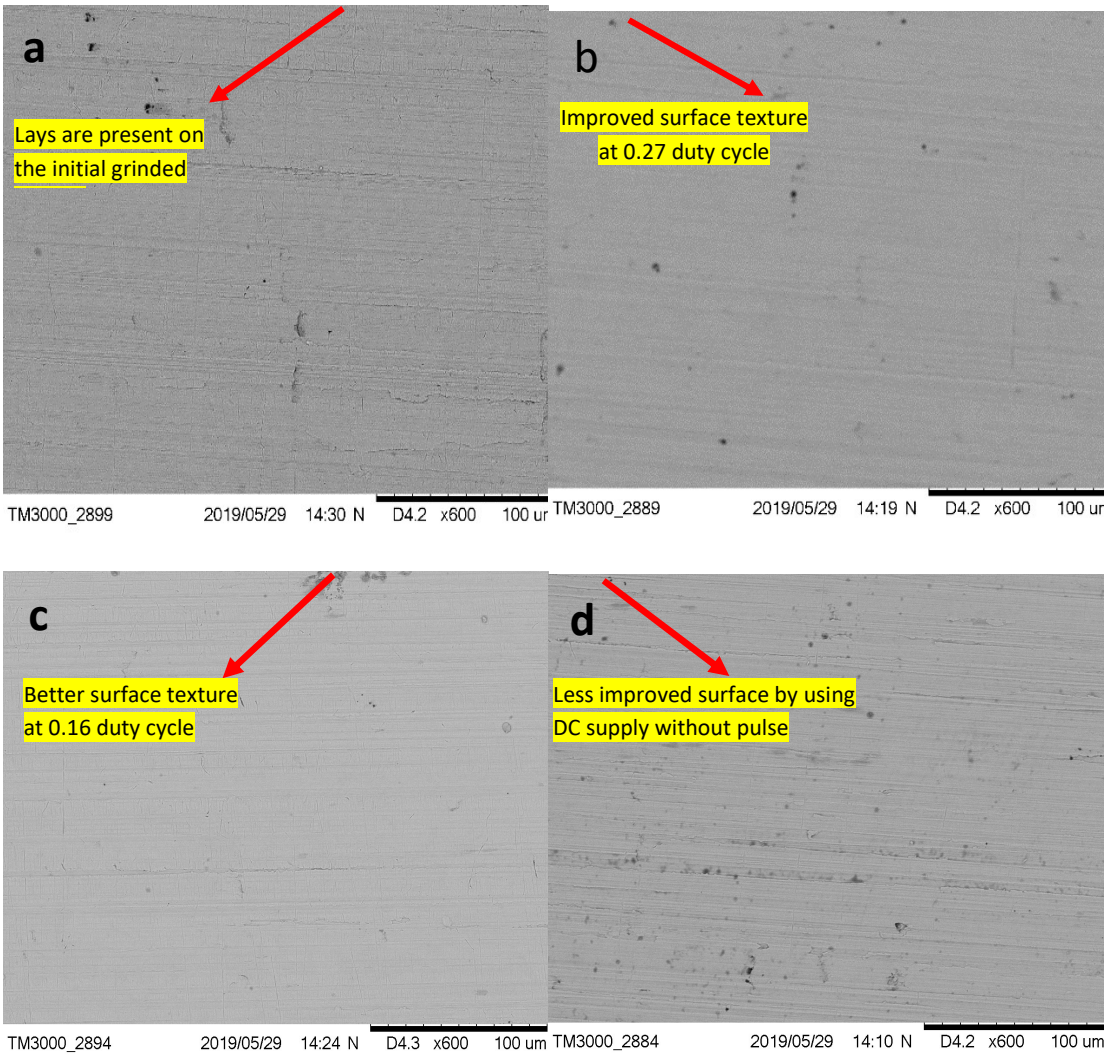

Fig.34: SEM images of work-piece surface at 600X magnification) (a) Before finish, (b) After finish at 0.27 duty cycle, (c) After finish at 0.16 duty cycle, (d) After finish with DC power supply without pulse

CHAPTER 5

DESIGN OF EXPERIMENT FOR PROCESS PARAMETERS

The Design of experiment is introduced in this chapter to help with proper experiment planning. To get the optimum response in the developed method, the Response Surface Methodology was further explored. This section also goes into detail about the importance and application of analysis of variance.

For clear and accurate conclusions from the preliminary experimental observations, a well-planned experimentation is crucial. The design of experiment is regarded as a particularly effective method for completing these tasks. In general, it defines the procedures for inferring conclusions from observations that are not precise but are variable. Second, it outlines the proper procedures for gathering the experimental data. Additionally, methods for accurate findings and interpretations are developed. The best response of the created procedure was used for the current experiment using the Response Surface Methodology. The following are some benefits of organizing the trials in accordance with the experimental design:

(a)Identification of crucial decision factors influencing and enhancing the effectiveness of the product or process

b) Significantly fewer trials (c) Finding the parameters ideal configuration

d) Determining the experimental error

e) It is possible to draw conclusions about how parameters affect the process' features.

5.1 Response Surface Methodology (RSM)

RSM is a group of mathematical and statistical methods that can be used to analyze issues when various independent factors have an impact on a dependent variable or response. The response will be optimized as a result. The independent variables, which

are continuous and subject to negligible error control by the experimenter, are considered to be x 1, x 2, x 3,.., x k. It is assumed that the response "y" is a random variable. This method explains how a specific response is impacted by a particular set of input factors and what level the input variables should be regulated to give the product the intended specifications. The following diagram illustrates the relationship between the dependent and independent variables:

$$y=f(x_1,x_2,x_3,\ldots\ldots\ldots..,x_k)+\varepsilon \quad (3)$$

Where ε displays the noise or error that was seen in the response "y."

If the anticipated response is indicated by:

$$E(y)=f(x_1,x_2,x_3,\ldots\ldots\ldots..,x_k)=\eta \quad (4)$$

Thereafter, the surface symbolized by:

$$\eta=f(x_1,x_2,x_3,\ldots\ldots\ldots..,x_k) \quad (5)$$

This surface is created between a variety of factors and some responses with levels "m", whose levels are indicated by, x_1, x_2, x_3,……., x_k.The values of variables are frequently the surface characteristic that interests the most arex_1, x_2, x_3,……., x_k,where m is either maximum or minimum.

Finding a good approximation for the real functional connection between y and a set of independent variables is the first stage in the response surface methodology. It is typical to utilize a low order polynomial in a portion of the independent variable. The first order model serves as the approximation function if the answer can be accurately predicted by

$$y=\beta_0x_0+\beta_1x_1+\beta_2x_2+\ldots\ldots\ldots\ldots\ldots+\beta_kx_k+\varepsilon \quad (6)$$

A higher degree polynomial, such as a second order model, must be utilized if the system is curved.

$$y=\beta_0 x_0 + \sum_{i=1}^{k} \beta_i x_i + \sum_{i=1}^{k} \beta_i x_i^2 + \sum_{i<j} \beta_{ij} x_i x_j + \varepsilon \quad (7)$$

The majority of issues are there with the response surface methodology relate to one of these models. Response surface design refers to designs for fitted response surfaces.

5.2 First order design

First-degree polynomials are used in this instance to fit the response surface.

$$\eta=\beta_0 x_0+\beta_1 x_1+\beta_2 x_2+\ldots\ldots\ldots\ldots+\beta_k x_k \quad (8)$$

Fitting a polynomial as a special instance of several linear regressions. For fitting a linear relationship between the response and variables in exploratory work, the 2k factorial design in single or fractional replication is useful. The experimental error variance is not estimated by the fractional designs. This can be obtained:

a) By carrying out the entire experiment again.

b) By using a prior experiment's estimate if there is strong evidence that error variance stays constant over time;

c) By adding a number of tests to the 2k factorial at the point where all 'x' have the value '0' on the coded scale.

5.3 Second order design

Second degree polynomials typically take the following form:

$$y = (b_0 x_0 + b_1 x_1 + b_2 x_2 + \ldots\ldots + b_k x_k) + (b_{12} x_1 x_2 + b_{13} x_1 x_3 + \ldots\ldots\ldots + b_{K-1} x_{K-1} x_k) + (b_{11} x_1^2 + b_{22} x_2^2 + \ldots\ldots + b_{kk} x_k^2) \quad (9)$$

The equation shows the linear terms, squared terms, and cross product terms. Each variable should have three levels in this model in order to estimate the regression coefficients. In this instance, a 3k factorial design is necessary. The 3k factorial design's drawback is that it requires extensive testing when employing more than three variables.

5.4 Non Central composite design

There are k extra points in this style of design, one for each element. When 2k factorial trials indicate that as opposed to the Center, the point of highest reaction is near one of the factor combinations, this form of design can be utilized.

5.5 Rotatable Second order design

In this design, the standard error is the same for all locations that are spaced the same distance apart from the region's Centre. If the region Centre for which the Y and X relation was being studied is point (0, 0,..., 0), then. Any point on the fitted surface can specify the standard errors of Y from any experimental result. For all places that are k distances apart from the region's center, the value of error will be the same due to the rotatability requirement. The equation below is valid under certain circumstances.

$x_1^2 + x_2^2 + x_3^2 + \ldots + x_k^2 = k^2 = \text{constant}$ (10)

5.6 Analysis of Variance

Analysis of variance (ANOVA) is a valuable technique for study in many disciplines and industry. When there are several sample cases, this method is employed. To ascertain the importance of the variance between the means of two samples, one can use either the z-test or the t-test. The problem occurs when more than two sample means need to be examined simultaneously. This simultaneous test can be carried out using the ANOVA technique, which makes it a valuable analytical tool in a researcher's arsenal.

By using this method, one may determine whether the samples came from populations with the same mean. The term "Variance" was first used by Professor R.A. Fisher, who also created a fairly complex theory on the ANOVA that explains its practical application. Later, Professor Snedecor and numerous other individuals helped to develop this method. ANOVA is primarily a method for evaluating the homogeneity of differences between various sets of data. The fundamental idea behind an ANOVA is to separate the entire variation.

Both variations within and between samples are possible. ANOVA involves dividing the variance into subsets for analytical reasons. It is therefore a technique for breaking down the various components of the variance that a response is exposed to into its distinct components, each of which corresponds to a different cause of variation. ANOVA) is also used to determine which cutting input factors have the greatest influence on the quality of the machined surface (surface roughness), as well as tool wear [135]. Different techniques such as Taguchi, grey relation analysis (GRA), factorial design, response surface methodology (RSM) etc are generally used. Response surface methodology (RSM) is selected for design of experiment in this study because it gives better reproducibility and requires minimum number of experimentation to understand the effect of all factor and also give the graphical representation. It also gives optimum combinations of all input parameters. Present work utilizes central composite design (CCD) under response surface methodology to design the experiments based on the preliminary study. In this regression analysis the significance of process parameters such as magnetizing current (*MC*), working gap (*WG*), feed rate (F) and rotational speed of tool (*RST*) on output response i.e. Percentage reduction in surface roughness (%ΔRa) is investigated. The level and ranges of the selected process parameters are given in table 3. In this work, 0.16 duty cycle was taken for 30sets of experimentation. Run order and results of output responses for finishing of EN-31work-piece surface through PBEMRF process are given table 4.

Table 3. Level and ranges of process parameters

S. No	**Process parameters**	**Units**	**Levels**				
			-2	**-1**	**0**	**1**	**2**
1	Magnetizing Current	A	1.5	2	2.5	3	3.5
2	Feed rate	mm/min	30	40	50	60	70
3	Working gap	mm	0.5	1	1.5	2	2.5
4	Rotational speed of tool	rpm	300	400	500	600	700

Table 4. Plan of experiments and output response in surface roughness (%Δ*Ra*)

Std	Run order	MC	F	WG	RST	%ΔRa
17	1	2	60	1	400	20.8
4	2	2.5	50	1.5	500	29.54
15	3	3	60	2	400	32.42
2	4	3	60	1	600	37.8
30	5	2.5	50	1.5	500	29.2
27	6	2.5	30	1.5	500	32.5
13	7	2	60	1	600	25.65
21	8	2	60	2	600	22.53
18	9	2	60	2	400	20.12
14	10	2	40	2	600	22.4
6	11	3	40	1	400	42.32
1	12	2	40	2	400	21.8
7	13	2.5	50	1.5	500	30.21
9	14	2	40	1	600	25.65
8	15	3	40	2	600	35.98
16	16	2.5	70	1.5	500	25.97
22	17	3	40	2	400	36.65
19	18	3	40	1	600	43.32
29	19	2.5	50	0.5	500	33.24
20	20	2.5	50	1.5	500	27.89
26	21	3	60	2	600	33.76
3	22	3.5	50	1.5	500	48.5
28	23	2.5	50	2.5	500	24.2
24	24	2.5	50	1.5	500	29.8
10	25	2.5	50	1.5	500	29.21

25	26	3	60	1	400	33.25
5	27	1.5	50	1.5	500	23.48
11	28	2.5	50	1.5	700	30.65
23	29	2.5	50	1.5	300	25.34
12	30	2	40	1	400	23.5

In the analysis, Design-Expert software version 13.0 has been used in which the quadratic model is selected on the basis of the lack of fit tests, since the cubic model is aliased. Table 5 shows the significant terms after analysis of variance (ANOVA). The *p*-value less than 0.05 shows that the model is found significant. In this model of ANOVA, following terms A, B, C, D, AB, AC, BC, CD, BD, A^2, D^2 are found to be significant as shown in table 5.

Table 5. ANOVA for Quadratic model

Source	**Sum of Squares**	**DF**	**Mean Square**	**F-value**	**p-value**
Model	1408.45	14	100.60	103.02	< 0.0001 significant
A-MC	1108.26	1	1108.26	1134.90	< 0.0001
B-F	61.28	1	61.28	62.75	< 0.0001
C-WG	83.29	1	83.29	85.29	< 0.0001
D-RST	30.04	1	30.04	30.76	< 0.0001
AB	17.62	1	17.62	18.04	0.0007
AC	5.21	1	5.21	5.33	0.0355
AD	0.8978	1	0.8978	0.9193	0.3529
BC	5.39	1	5.39	5.52	0.0329
BD	6.34	1	6.34	6.49	0.0223
CD	4.92	1	4.92	5.04	0.0404
A^2	67.46	1	67.46	69.08	< 0.0001
B^2	0.3984	1	0.3984	0.4080	0.5326
C^2	1.70	1	1.70	1.75	0.2063

D^2	5.08	1	5.08	5.21	0.0375
Residual	14.65	15	0.9765		
Lack of Fit	11.51	10	1.15	1.83	0.2616 **Not significant**
Pure Error	3.14	5	0.6283		
Cor Total	1423.09	29			

After dropping the insignificant terms AD, B^2 and C^2 in table 5 by backward elimination method, the F-value is found improved as 131.8 with p value as less than 0.0001as shown in table 6, which indicates that the model is found significant. There is only 0.01% possibility of this to occur due to noise. The contributions of each process parameters has been found from the table 6. From the table 6 it is observed that highest contributing parameter is magnetizing current followed by working gap, feed rate and tool rotational speed.

Table 6. ANOVA for Reduced Quadratic model

Source	**Sum of Squares**	**DF**	**Mean Square**	**F-value**	**p-value**	**Percentage contribution**
Model	1405.64	11	127.79	131.80	< 0.0001significant	
A-MC	1108.26	1	1108.26	1143.07	< 0.0001	77.88%
B-F	61.28	1	61.28	63.20	< 0.0001	4.30%
C-WG	83.29	1	83.29	85.91	< 0.0001	5.85%
D-RST	30.04	1	30.04	30.98	< 0.0001	2.11%
AB	17.62	1	17.62	18.17	0.0005	
AC	5.21	1	5.21	5.37	0.0324	
BC	5.39	1	5.39	5.56	0.0298	
BD	6.34	1	6.34	6.54	0.0198	
CD	4.92	1	4.92	5.07	0.0370	
A^2	74.14	1	74.14	76.47	< 0.0001	
D^2	4.20	1	4.20	4.33	0.0519	
Residual	17.45	18	0.9696			

Lack of Fit	14.31	13	1.10	1.75	0.2786	**Not significant**	
Pure Error	3.14	5	0.6283				
Cor Total	1423.09	29					
Std. Dev.			0.9847	**R²**			0.9877
Mean			29.92	**Adjusted R²**			0.9802
C.V. %			3.29	**Predicted R²**			0.9562
Adeq Precision	45.0706						

When the difference between the measured and estimated output values is less than 0.2, the adjusted R^2 for regression models is 0.9802, indicating a strong connection between the two. The signal to noise ratio is measured by Adeq Precision. The corrected and anticipated R^2 values are respectively 0.98 and 0.95, and the difference between them is 0.03, which is within the allowable range. The ideal ratio is greater than 4. A sufficient signal is shown by the value of 45.071. The following is the equation for %ΔRa in terms of the actual factor:

$$\%\Delta Ra = +15.034 - 4.780\times MC - 0.123\times F + 1.71\times WG + 0.0347\times RST - 0.2098\times MC\times F - 2.28^{*} MC^{*}WG + 0.116^{*}F^{*}WG + 0.000629^{*}WG^{*}RST - 0.019\times WG\times RST + 6.45\times MC^{2} - 0.000050^{*}RST^{2}$$

CHAPTER 6

RESULTS AND DISCUSSION

This chapter includes results and discussion part of the investigations performed in this thesis. In this regression analysis the significance of process parameters such as magnetizing current (MC), working gap (WG), feed rate (F) and rotational speed of tool (RST) on output response i.e. percentage reduction in surface roughness (%ΔRa) is investigated.

The results obtained after finishing of EN-31 using PBEMRF process and effect of process parameters on %Δ*Ra* are discussed in this section.

6.1 Effect of Magnetizing Current (MC) on %ΔRa

Magnetizing current is found as the highest contributing process parameter having value of 77.88 % (from model analysis) for percentage reduction in surface roughness (%Δ*Ra*). As the magnetizing current is increased the %Δ*Ra* also increases due to the increase in magnetic flux density at tip of the finishing tool [89]. The stiffness of semi sold MRPF ball is increased with increasing the magnetizing current and results in higher percentage reduction in surface roughness (%Δ*Ra*). Surrounding CIPs particles along with abrasives aggregates into chain like columnar structure and form strong chain structure at high magnetic field. The CIPs particles move towards the tool tip and pushes the abrasive particle into work-piece surface due to magnetic field gradient present in the working gap. The normal magnetic force (F_n) acting on the abrasives is increased with increase of magnetizing current due to which higher reduction in surface roughness is observed. The normal magnetic force (F_n) acting on the abrasives is responsible to penetrate the abrasives on to the work-piece surface. This trend can be observed in Fig.35.1 representing the effect of magnetizing current on %Δ*Ra.*

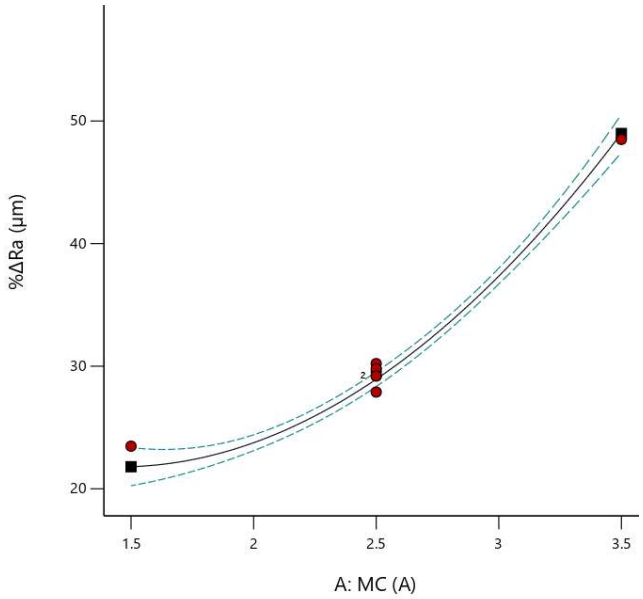

Fig. 35.1: Effect of magnetizing current (MC) on %ΔRa

6.2 Effect of Feed rate on %ΔRa

Thepercentage reduction in surface roughness (%Δ*Ra*) decreases with the increase in feed rate (F) as shown in Fig.35.2. This is due to the reason that the CIP chains remain intact at low feed rate and get separated when feed rate further increases resulting in getting partly out of contact from the work-piece [89]. During finishing the two forces on the abrasive particle are involved, normal force (F_n) due to magnetic field and tangential force (F_t) due to tool rotation. The normal magnetic forces are responsible for packing of CIPs particle in the working gap due to which micro indentation occurs into the work-piece surface. The tangential force (F_t) is responsible for removing the microchips from the work-piece surface. These two forces are decreased as feed rate are increased due to which less %Δ*Ra* is observed. The percentage contribution of feed rate on %Δ*Ra* is found as 4.30 % as depicted from model analysis.

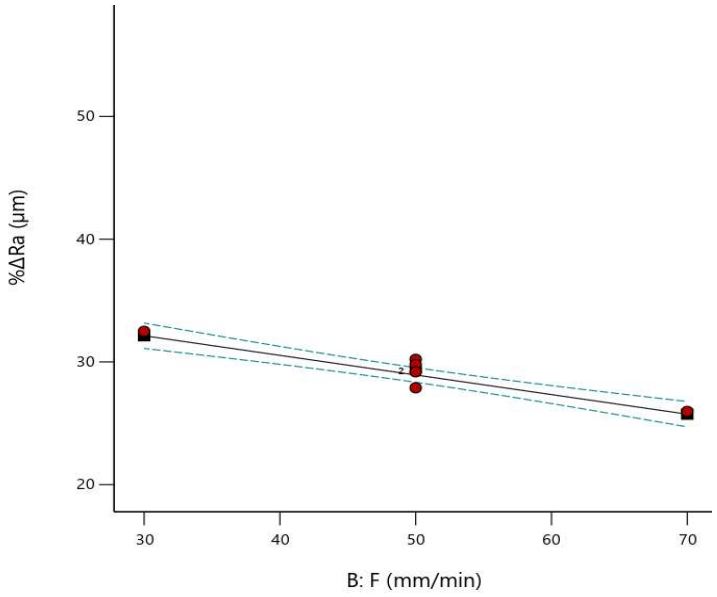

Fig. 35.2: Effect of feed rate (F) on %ΔRa

6.3 Effect of Working Gap (WG) on %ΔRa

Thepercentage reduction in surface roughness (%Δ*Ra*) has been found increased with decreasing the working gap as shown inFig.35.3. It is due to the reason that the magnetic flux density on work-piece surface is increased with the reduction in working gap. The magnetic flux density is inversely proportional to the working gap [81]. The normal magnetic force due to magnetic field is increased as the working gap decreased and hence, strength of CIP chain structure in MRPF increased. In this situation, stiffness of MRPF ball is increased which interact directly with the work-piece surface during finishing action and is responsible for increased material removal rate as well as increased percentage reduction in surface roughness(%Δ*Ra*). It is also seen from the perturbation or 3D surface diagram as shown in Fig.35.5 (a) and (c). The % contribution of feed rate is found as 5.85 % from model analysis.

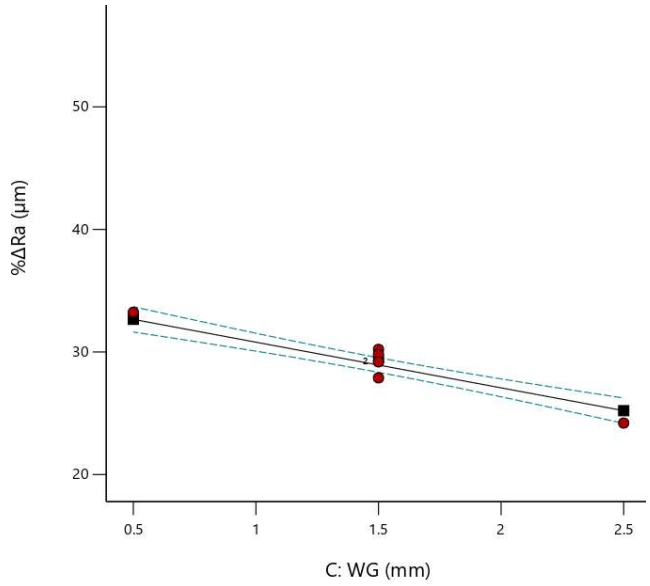

Figure.35.3: Effect of working gap (WG) on %ΔRa

6.4 Effect of Rotational Speed of Tool (RST) on %ΔRa

Thepercentage reduction in surface roughness (%Δ*Ra*) slightly increases with the increase in rotational speed of tool (RST) as shown in Fig.35.4. The asperities on the work-piece surface are the cause of this because the abrasive particles caught in the CIP chains move more quickly against them and remove the peak more quickly. As the rotational speed of tool is increased, tangential force (Ft) acts on abrasive particle increases which is responsible for material removal rate. Therefore %ΔRa is increased with increase of rotational speed of tool. Furthermore, if RST increases beyond 700 rpm, %ΔRa may slightly decrease. It is due to the reason that the centrifugal force acting on the abrasive particle increases. The active abrasive particles thrown away from the working area due to this high centrifugal force and hence reduces %ΔRa [137]. The effect of RST from model analysis reveals that it is the least contributing parameter on %ΔRa. The percentage contribution of rotational speed of tool is found as 2.11% on %ΔRa from model analysis.

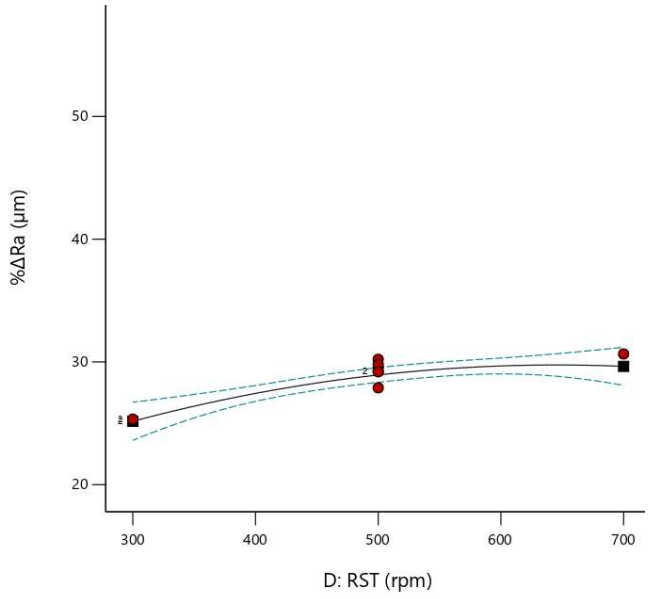

Fig.35.4: Effect of rotational speed of tool (RST) on %ΔRa

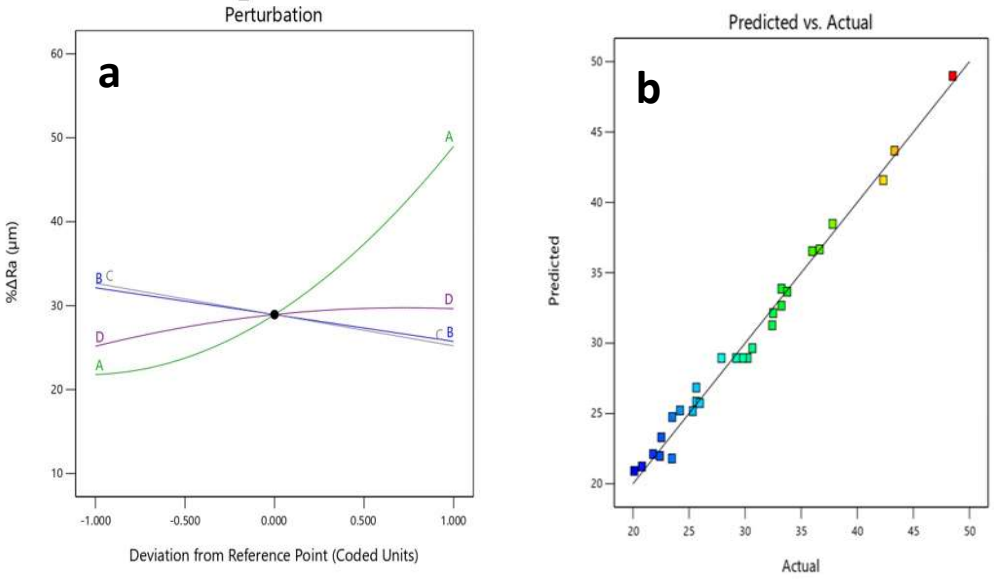

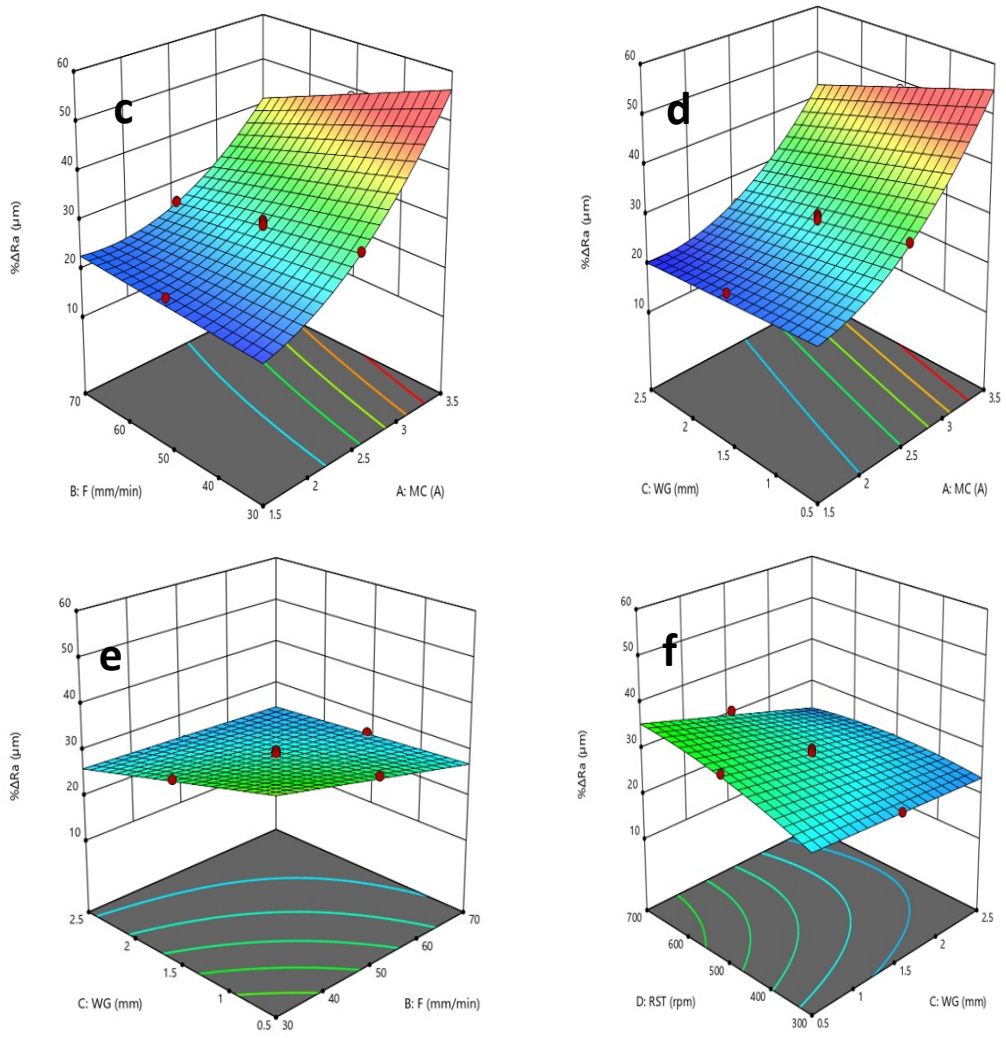

Fig. 35.5: a) Perturbation diagram for %Δ*Ra* with (A – Magnetization current, B – Feed rate, C- working gap, D – Rotational speed of tool) b) Actual vs. Predicted graph c) 3-D surface graph between feed rate and MC on %ΔRa d) 3-D surface graph between WG and MC on %ΔRa e) 3-D surface graph between WG and F for %ΔRa f) 3-D surface graph between RST and WG on %ΔRa

The perturbation diagram as in Fig.35.5 (a) shows the individual effect of process parameters on *%Δ Ra*. Fig.35.5 (b) shows that the predicted value of %ΔRa which is close to the actual value obtained after experimentation. The regression model's incredible acceptability is displayed in Fig. 35.5b. Every value shown was in line with

the model's projected value, as shown in Fig. 35.5b. The projected line is rather consistent with the actual values, as seen in Fig. 35.5b. The experimental values are satisfying the projected results since the actual value points were closer to the predicted line. The 3-D surface diagram for interaction of process parameters are shown in Fig.35.5(c,d,e,f).The interaction of process parameters on %ΔRa can also be observed through contour surface graphs shown in Fig.35.6 (a, b, c, d).

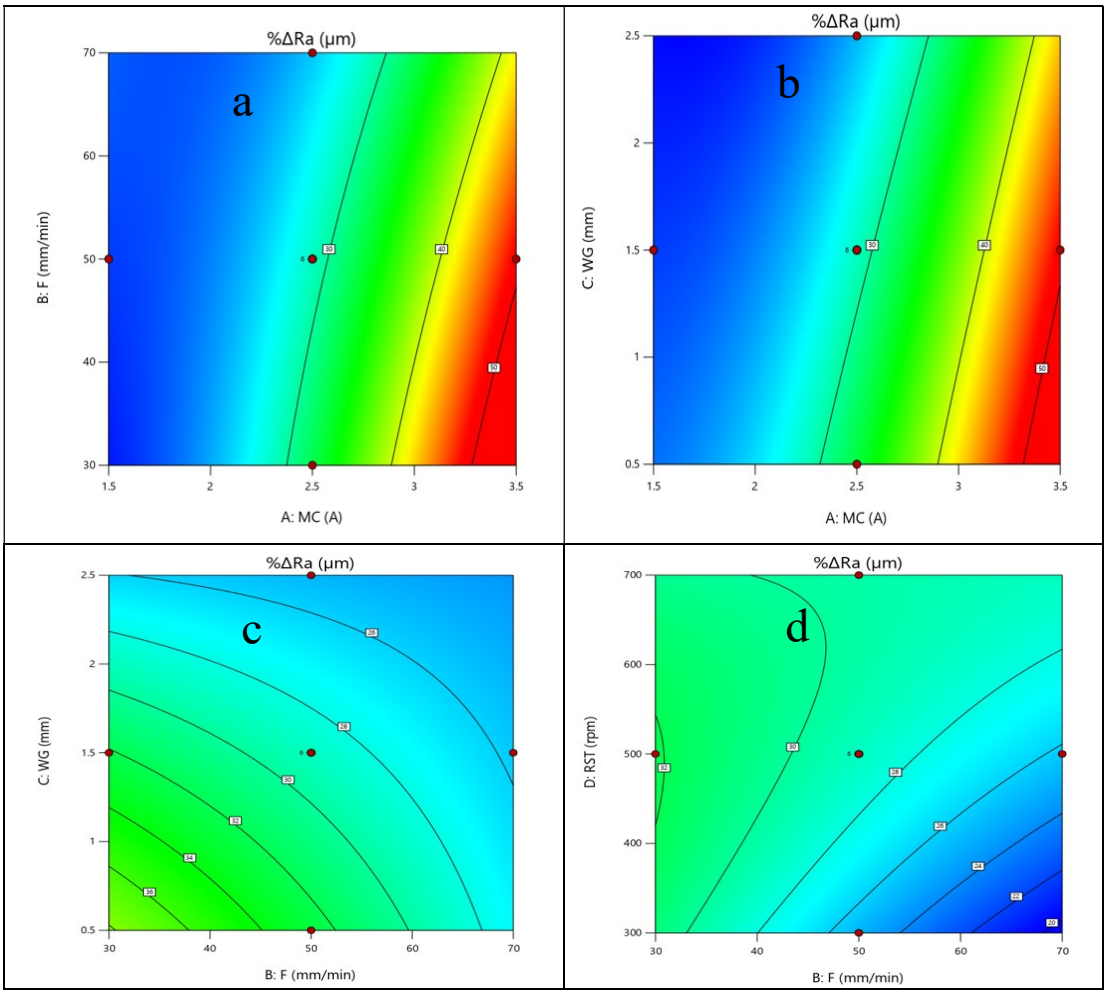

Fig.35.6: Contour surface graph between (a) Feed rate and Magnetizing Current (b) Working Gap and Magnetizing Current (c) Working Gap and Feed rate (d) Rotational Speed of Tool and Working Gap on %ΔRa

The effect of process parameters has also been studied through interaction graph. The %ΔRa found increased with increasing the magnetizing current and %ΔRa found reduced with increasing of feed rate as shown in Fig.35.7. The %ΔRa increases with increasing the magnetizing current and %ΔRa reduces with increasing of working gap as shown in Fig.35.8. The %ΔRa reduces with increasing the feed rate and %ΔRa increasing with reducing the working gap as shown in Fig.35.9. The %ΔRa increases with increasing the rotational speed of tool and %ΔRa reduces with increasing of feed rate as shown in Fig.35.10.

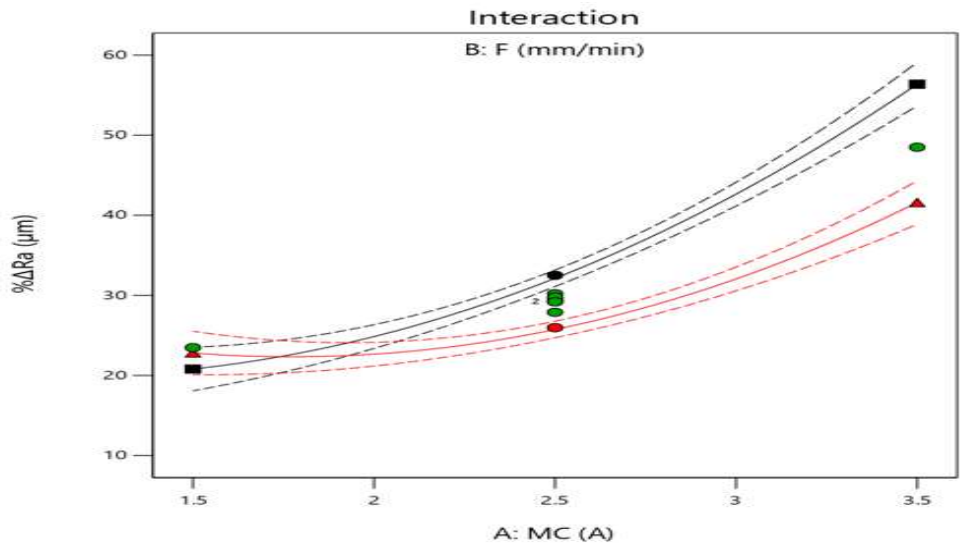

Fig. 35.7: Interaction graph between Magnetizing Current and Feed rate on %ΔRa

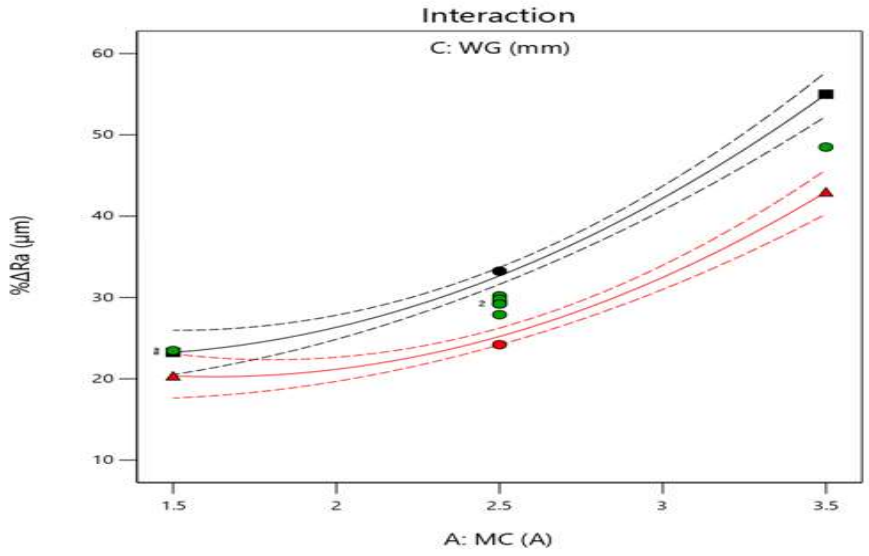

Fig. 35.8: Interaction graph between Magnetizing Current and Working Gap on %ΔRa

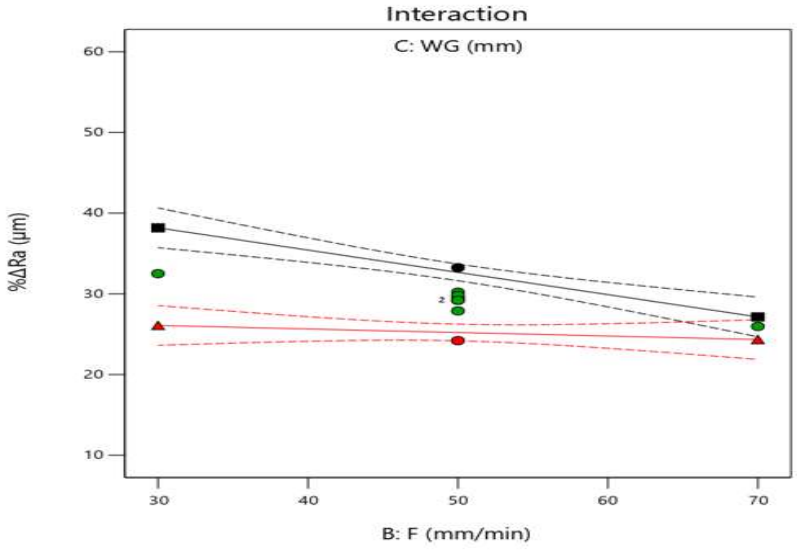

Fig.35.9: Interaction graph between Feed rate and Working Gap on %ΔRa

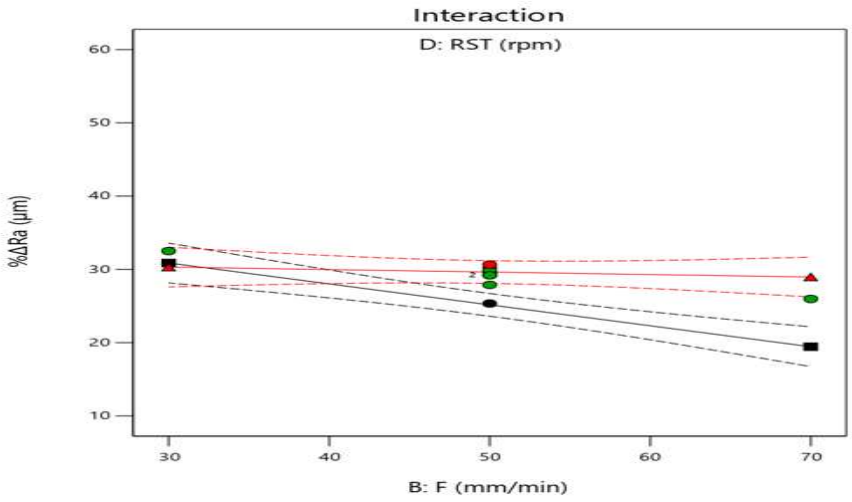

Fig.35.10: Interaction graph between Feed rate and Rotation Speed of Tool on %ΔRa

6.5 Validation of results through confirmatory experiment

Statistical analysis revealed that the predicted *%ΔRa* has been found to be maximum as 55.52% through actual regression equation at 3.5A magnetizing current, 30 mm/min feed rate, 0.5mm working gap, 700 rpm rotational speed of tool. The experiment has been conducted on work-piece surface with PBEMRF process at 0.16 duty cycle and at selected optimum process parameters 3.5A magnetizing current, 30 mm/min feed rate, 700 rpm rotational speed of tool and 0.5 mm working gap. The %ΔRa obtained through experimentation was found to be 51.23% and is shown in table 7. The results obtained after experimentation are found close to the predicted value of%ΔRa and a 4.29% error is obtained as shown in table 7. The surface roughness profile of EN-31 work-piece before and after finishing though PBEMRF process is shown in Fig.36.

Table 7. Confirmatory experiment after finishing of work-piece using PBEMRF

S. No	MC (A)	F(mm/min)	RST (rpm)	WG(mm)	Predicted %ΔRa	Actual %ΔRa	% Error
1.	3.5	30	700	0.5	55.52%	51.23%.	4.29

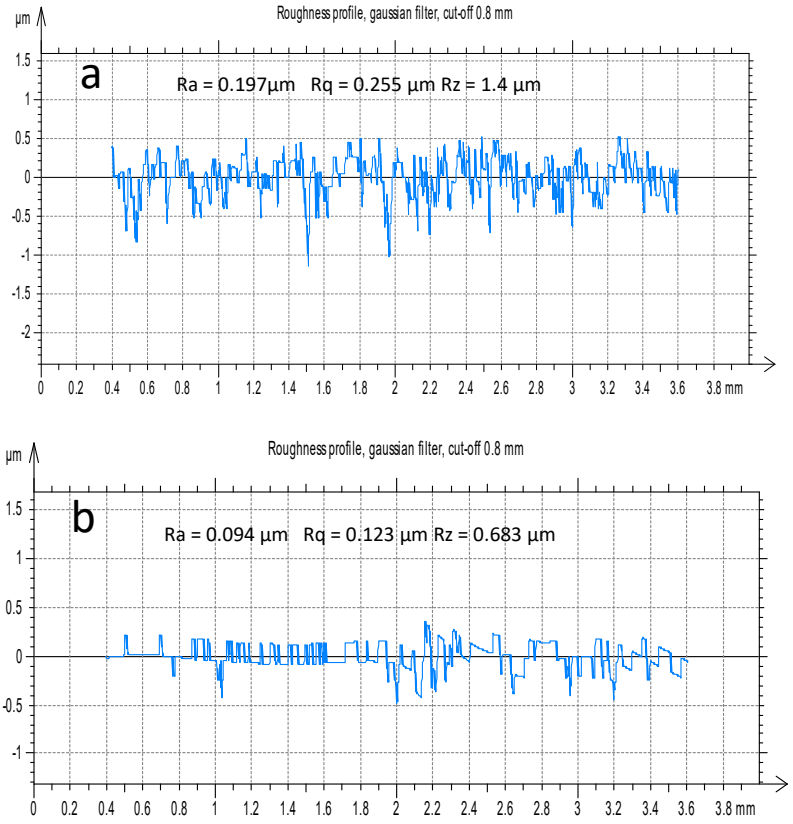

Fig.36: Surface roughness profile (a) Before finishing (b) After finishing with PBEMRF process at optimum process parameters (3.5A, 30 mm/min, 0.5 mm and 700 rpm.

6.6 Numerical optimization

Design Expert software has been used to perform response optimization. Table 8 shows the 10 best solutions obtained using the desirability method. The highest desirability value obtained is 1, which means that when finishing EN-31 work-piece, the maximum percentage surface roughness reduction can be obtained as 52.856% at 3.237 A magnetizing current, 33.03 mm/min feed rate, 0.832 mm working gap and 688.675 rpm rotational speed of tool.

Table 8. Best solutions through numerical optimization

Number	MC	F	WG	RST	%ΔRa	Desirability	
1	**3.237**	**33.03**	**0.832**	**688.675**	**52.856**	**1**	**Selected**
2	3.229	35.23	0.774	588.673	52.643	**1**	
3	3.466	44.778	1.239	582.766	52.335	**1**	
4	3.441	38.491	1.404	640.952	52.19	**1**	
5	3.479	56.117	0.861	651.34	52.017	**1**	
6	3.448	50.535	0.664	482.868	51.941	**1**	
7	3.325	49.674	0.658	686.429	51.866	**1**	
8	3.479	33.794	1.699	640.497	51.862	**1**	
9	3.467	41.523	1.005	340.562	51.818	**1**	
10	3.417	41.115	1.217	474.117	51.654	**1**	

CHAPTER 7

SURFACE TEXTURE ANALYSIS THROUGH SCANNING ELECTRON MICROGRAPH AND ATOMIC FORCE MICROSCOPY

In this chapter scanning electron micrograph (SEM) and atomic force microscopy (AFM) has been studied after finishing the work-piece surface using PBEMRF process at optimum process parameters

7.1 SEM ANALYSIS

Scanning electron micrograph (SEM) of EN-31 work-piece surface before and after finishing with PBEMRF process at optimum process parameter as 3.5A magnetizing current, 30 mm/min feed rate, 700 rpm rotational speed of tool and 0.5 mm working gap is obtained at different magnification and resolution as outlined in Fig.37. As observed from Fig. 37(a), the lays are clearly visible at 300X magnification on initial grinded work-piece surface. The SEM image of work-piece surface as in Fig. 37(b) after finishing with PBEMRF process at optimum parameters has very fine lays at 300X magnification as compared to initial grinded work-piece surface at the same magnification and resolution. The SEM images of finished work-piece surface through PBEMRF process at optimum parameters at 600X and 1200X magnifications are shown in Fig.37 (c) & (d).

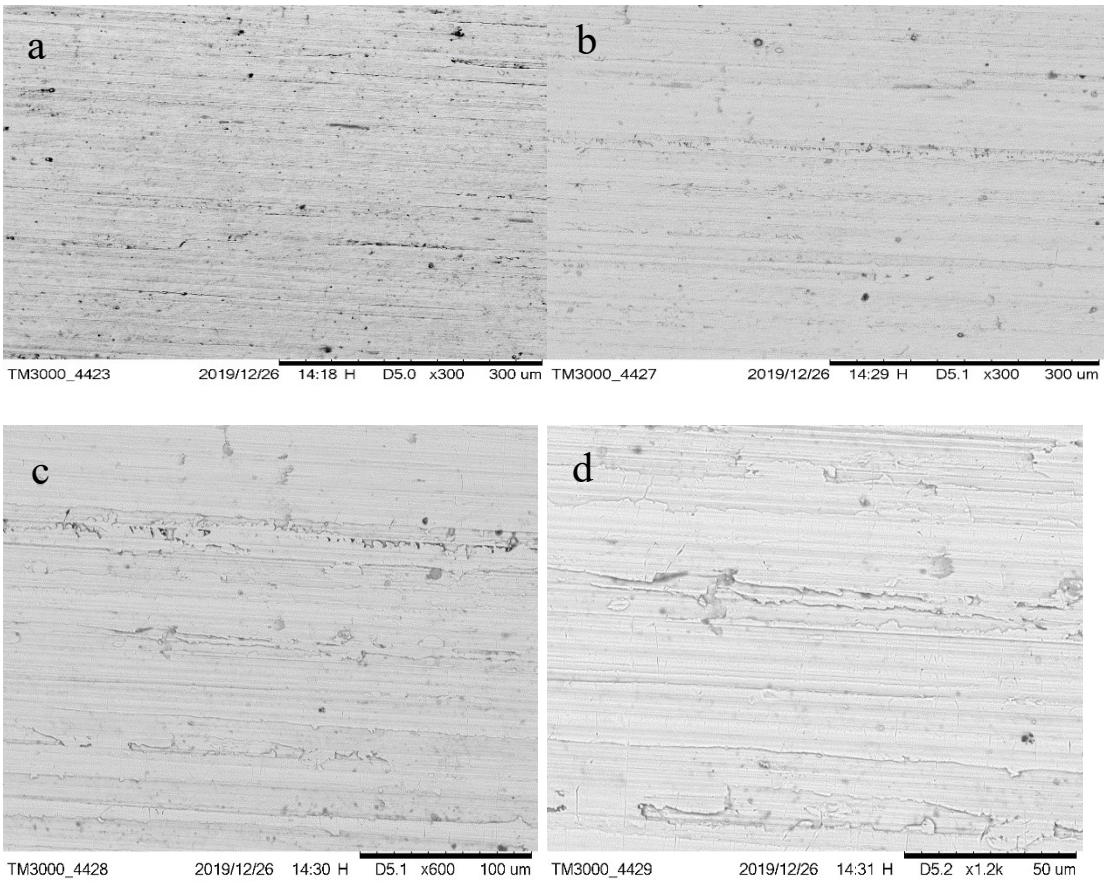

Fig.37: Scanning electron micrograph a) Before finish at 300X b) After finish at 300X c) After finish at 600X d) After finish at 1200X

7.2 AFM ANALYSIS

Atomic force microscopy (AFM) images of work-piece surface taken at the scale of 10 μm are shown in Fig.38. More number of lays are seen on grinded work-piece surface after process on surface grinder as shown in Fig.38 (a). The density of lays on work-piece surface is 0.301 (/μm²) and mean height of peak is 5.4541 (º). The surface texture produced using BEMRF process with pulse DC power supply at optimum parameters (3.5A, 30 mm/min, 700 rpm, and 0.5 mm and 0.16 duty cycle) has very fine lays as compared to the surface texture obtained after grinded work-piece surface as shown in Fig.38 (b).

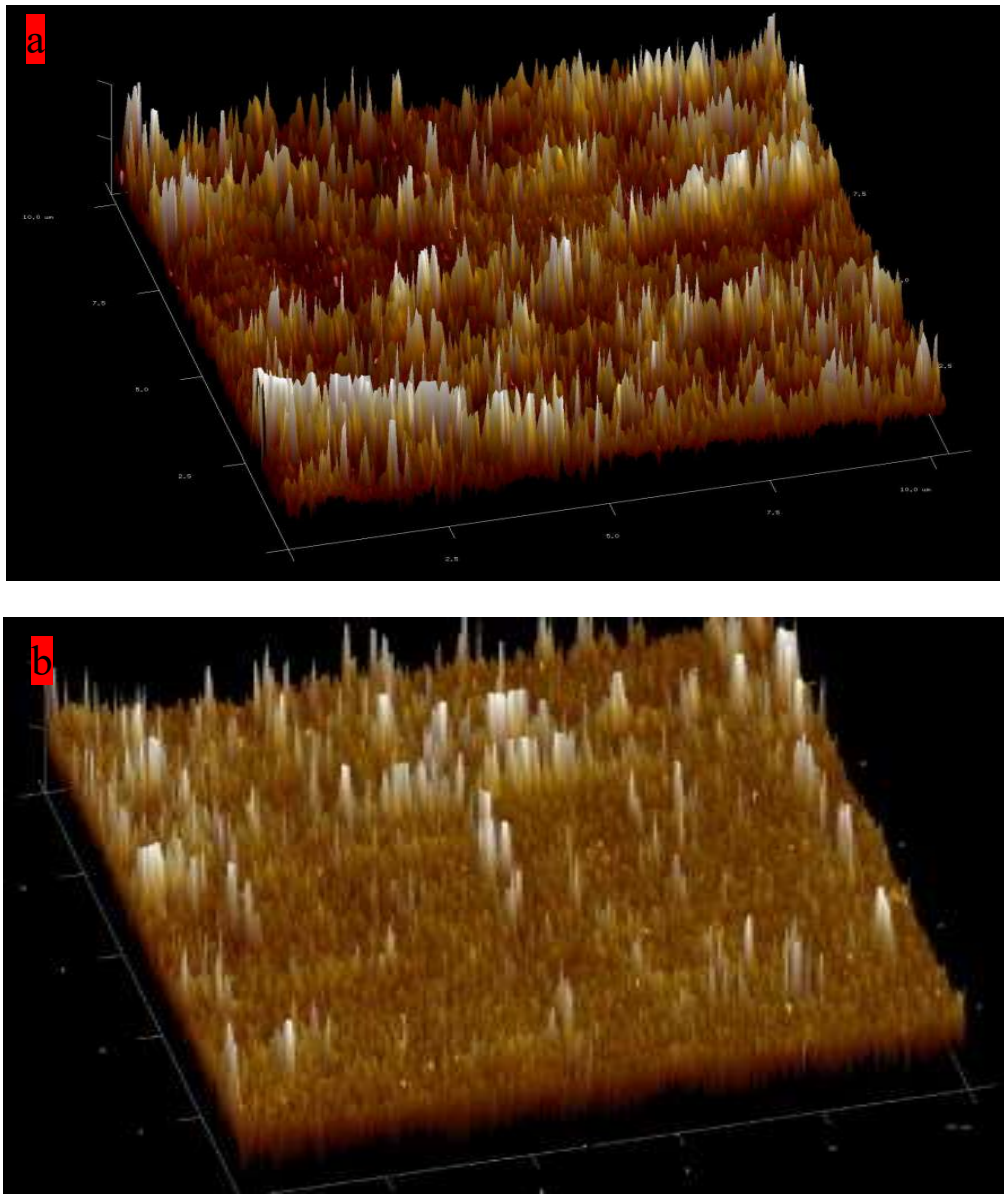

Fig.38: Atomic force micrograph of (a) Grinded work-piece surface (b) Finished work-piece surface with PBEMRF process at optimum process parameters

CHAPTER 8

STUDY OF RESIDUAL STRESS

In this chapter study of the residual stress of grinded work-piece surface before BEMRF process and after conducting experiments on BEMRF process with pulse DC power supply or without pulse DC power supply were measured using x- ray residual stress analyzer. The percentage of residual stress that had been reduced (%RS) was then determined. This chapter also includes optimization using Response surface methodology along with Analysis of variance (ANOVA). Optimization was performed for response parameters percentage reduction in residual stress. In this regression analysis the significance of process parameters such as magnetizing current (MC), working gap (WG), feed rate (F) and rotational speed of tool (RST) on output response i.e. percentage reduction in residual stress (%ΔRS) is investigated.

8.1 Study of Residual stress

The residual stress developed on the work surface is one of many unfavorable impacts on components of manufactured items caused by various machining techniques. The residual stress is caused by variety of reasons, including temperature changes, volume changes in phases, resolidification, melting, and phase transformations. The product's reliability is reduced as a result of this residual stress, which also increases the likelihood that manufactured goods will fail. Therefore, it was essential to research on residual stress in order to reduce these stresses and improve product reliability. Different categories, including destructive testing, semi-destructive testing, and non-destructive testing, has been used to categories residual stress measurement methodologies (NDT).

8.2 Destructive and nondestructive technique

Compared to destructive and semi-destructive testing, non-destructive testing has a number of benefits. A large range of materials can be tested non-destructively, and

measurement precision is quite good. There are several NDT techniques for assessing residual stress, Berkhausen noise, neutron diffraction method, and ultrasonic diffraction including X-ray diffraction. Because X-ray diffraction approach may be used for measurements of residual stress over a large range of materials, it offers various advantages over other methods. Additionally, the handheld nature of the X-ray diffraction technique allows for readings to be taken in any angle while simultaneously allowing for the analysis of both micro and macro residual stress.

8.3 Residual stress analyzer

The residual stress measurements were taken by μX-360 pulstec machine (Japanese built) as shown in Fig.39.

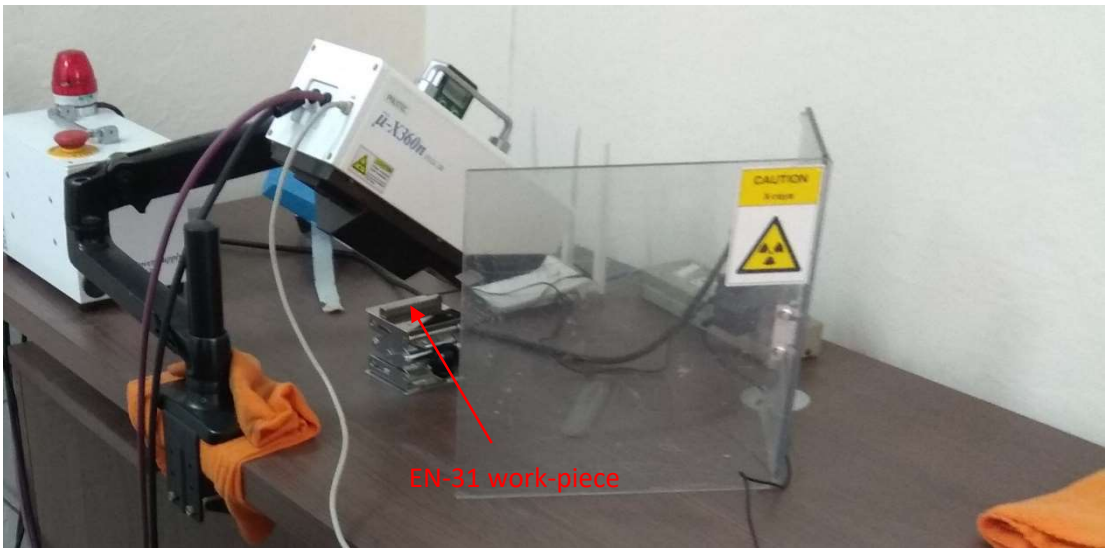

Fig.39: Residual stress analyzer with position of EN-31 work-piece

The computer, sensor unit, and power unit are the major three components of the machine. The system comprises of a 30-KV X-ray tube, a 2-D X-ray sensor, and a power supply unit to generate X-rays. One reading of residual stress is taken by an X-ray in 90 seconds. The machine features an air conditioning element that makes it very effective. The sample was 38mm away from the X-ray focusing lens and the X-

ray tube current was 1mA. The specimen to be studied was given information on its lattice constant, inter-planar spacing, and diffraction planes (h, k, and l), as well as its crystal structure, poison's ratio, and Young's modulus. The incidence angle for X-rays was fixed at 35 degrees. The X-ray machine required an AC supply with the specifications of 240V and 50/60Hz to function, although it could alternatively be powered by a battery-powered 24 V source. A unique air cooling element that was included with the machine ensured its efficient operation. Between the sample and the machine's focusing lens, the incidence angle for X-rays striking the sample surface was adjusted at 35º. Lattice constant 2.86A; inter planar distance 1.17 m; diffraction plane 2, 1, 1; diffraction angle156.390; crystal structure BCC; poison's ratio 0.28; and young's modulus 224 GPa were the values for residual stress measurement. Full width at half maximum (FWHM), an expression of a function's range, is the product of the highest and minimum values of peak diffraction, indicated as -max and -min, respectively (profile peak diffraction). There are four stages to the residual stress measurement process. The sample location and sample picture capturing are included in the first stage. The incidence of X-rays and their detection by a 2-D sensor are included in the second stage. The third stage comprises residual stress computation, and the fourth stage includes residual stress output data results and value of full width half maximum (FWHM). In order to ensure the repeatability of the reading, the output reading additionally computes the standard deviation in the reading that was acquired.

8.4 X-ray Diffraction

The working principle of residual stress is based on X-ray diffraction scattering as per Bragg's law given by Eq.

$$n\lambda=2d\sin\theta \tag{11}$$

In this equation, the order of reflection is denoted by the integer "n," the incoming X-wavelength ray's is denoted by " λ " the crystal's inter-planar spacing is denoted by "d," and the angle of incidence is denoted by θ as shown in Fig.40.The difference in

the crystal's orientation causes the diffracted X-ray to form a cone around the incident X-ray axis, which also causes the production of a ring of residual stress known as the Debye-Scherrer ring as illustrated in Fig.41. This Debye ring is the result of a single, brief X-ray irradiation. By precisely measuring the location of the Debye-Scherrer rings, it is possible to calculate the residual stress, and these positions are a direct indicator of strain.

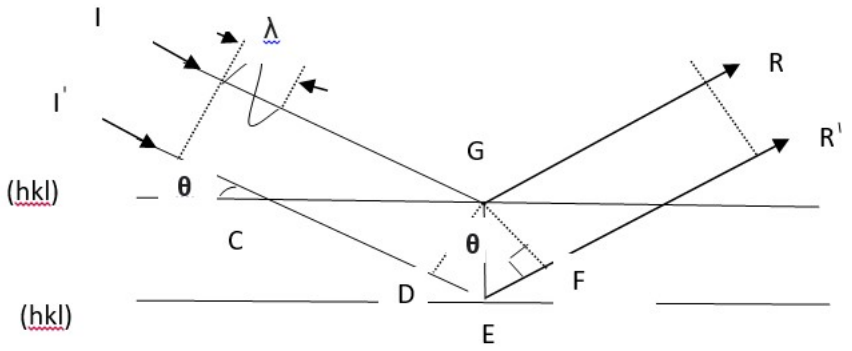

Fig.40: Diffraction of X-ray from work-piece surface

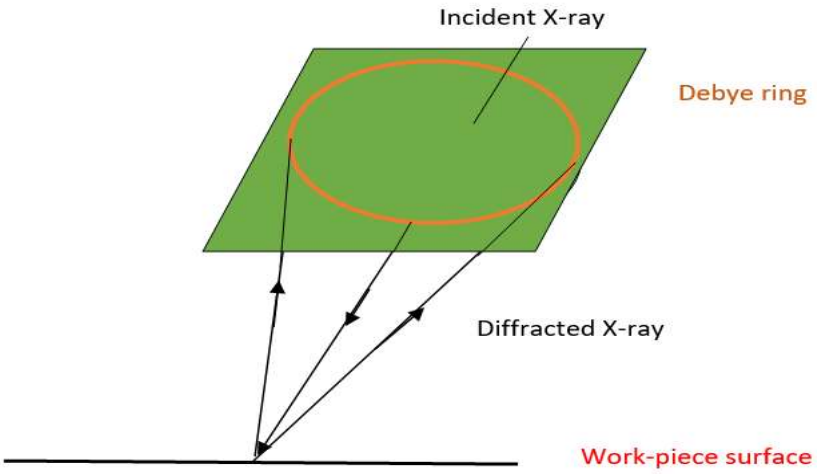

Fig.41: Formation of Debye-Scheerer ring

8.5 Preliminary experimentation for residual Stress

The residual stress of grinded surface before BEMRF process and after conducting experiments with BEMRF process were measured using X- ray residual stress analyzer. Thereafter percent reduction in residual stress (%ΔRS) was calculated. In the present work, Cosα method has been applied to measure the residual stress of EN-31 finished surface by PBEMRF and BEMRF process. The comparative results of residual stress after conducting experiments with BEMRF process with and without pulse are shown in table 9& 10 respectively. The %ΔRS is calculated as:

$$\%\Delta RS = \frac{(Initial\ residual\ stress - Final\ residual\ stress)}{Initial\ residual\ stress} \times 100 \qquad (12)$$

The residual stress has been measured efficiently by detecting the full Debye ring data from a single incident X-ray angle. The material under study was α Fe (211) having lattice constant (a) 2.8664 A.

The residual stress of initial grinded work-piece surface was measured efficiently by detecting the full Debye ring data from a single incident X-ray angle (35^{o}) and diffraction angle (2Θ) is 156.39^{o}. Fig. 25 shows the Debye ring 3(D) and Distortion ring taken under normal incidence.

Table 9. Experimental results for residual stress by DC power supply without pulse

S.No	MC (A)	F (mm/min)	WG (mm)	RST (rpm)	Initial Residual Stress (MPa)	Final Residual Stress (MPa)	%ΔRS
1.	2.5	50	1.5	500	130	90	30.76
2.	**2.5**	**50**	**1.5**	**500**	**122**	**78**	**36.06**
3.	2.5	50	1.5	500	125	84	32.8

Table 10: Experimental results for residual stresses with pulse DC power supply

S.N	Duty cycle	MC (A)	F (mm/min)	WG (mm)	RST (rpm)	Initial Residual Stress	Final Residual Stress	%ΔRS
1.	0.16	2.5	50	1.5	500	124	70	**43.54**
2.	0.16	2.5	50	1.5	500	129	69	**45.51**
3.	**0.16**	**2.5**	**50**	**1.5**	**500**	**102**	**55**	**46.07**

8.5.1 Residual stress analysis of finished surface with BEMRF process using DC power supply without pulse

The Debye ring and distortion ring of grinded work-piece surface has higher irregularity in intensity which represent texture of surface is shown in Fig.42a.The Debye ring and Distortion ring of finished surface using BEMRF process without pulse DC power supply which has less irregularity. The irregularity of intensity distribution is reduced in Debye-Scherrer ring with finished surface as shown in Fig.42b. The Debye ring and distortion ring represents the texture of surface. The FWHM is minimum for the grinding work-piece surface and FWHM of finished surface is increased using BEMRF process without pulse DC power supply.

Peak diffraction values were reported as having maximum and minimum values of -max and -min, respectively, although the full width at half maximum (FWHM) is a measure of the size of a function. The FWHM graph of initial grinded work-piece surface with peak strength are given in Fig.43. The value of FWHM 3.35lies between (3.23-3.47) and α_{max} 341.28 and α_{min} 234 with peak strength (Ave) 165k. After finishing with BEMRF process without pulse DC power supply the value of FWHM 3.52 lies between (3.39-3.64) and α_{max} 31.68 and α_{min} 317.52with peak strength 138k as shown in Fig.44. The peak strength is maximum of initial grinded work-piece surface and minimum for finished surface which indicate the intensity of residual stress.

In fig.45, the x-axis Cosα represents cos of azimuth angle of Debye sheerer ring and y-axis represents strain (εα1). The inclination angle of bend was measured as the residual stress. The measured value of residual stresses after grinded surfaces of EN-31 are observed as 122 MPa as shown in Fig.45 (a). The Residual stress was reduced to 78 MPa using BEMRF process without DC power supply as given in Fig.45 (b). The percentage reduction in residual stress (%ΔRS) is calculated from equation 12 and it was found to be 36.06% as shown in table 9.

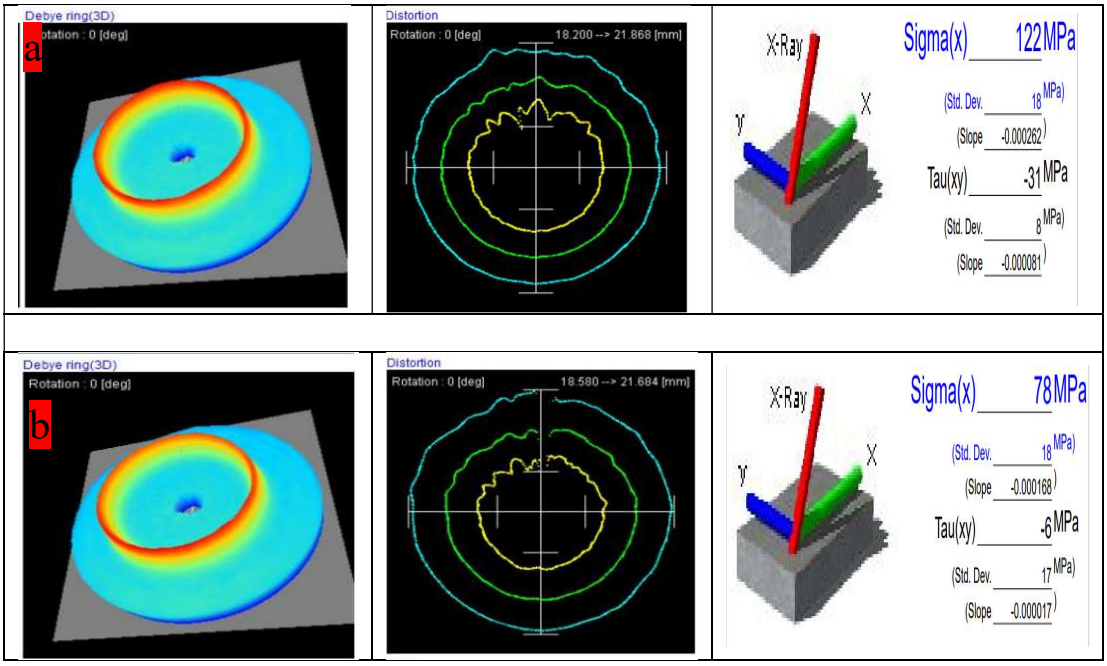

Fig.42: Debye ring (3D) and Distortion ring of (a) Initial grinded work-piece at 122 MPa, FWHM= 3.35 (b) Finished work-piece surface at 78MPa, FWHM= 3.52 without pulse DC power supply in BEMRF process.

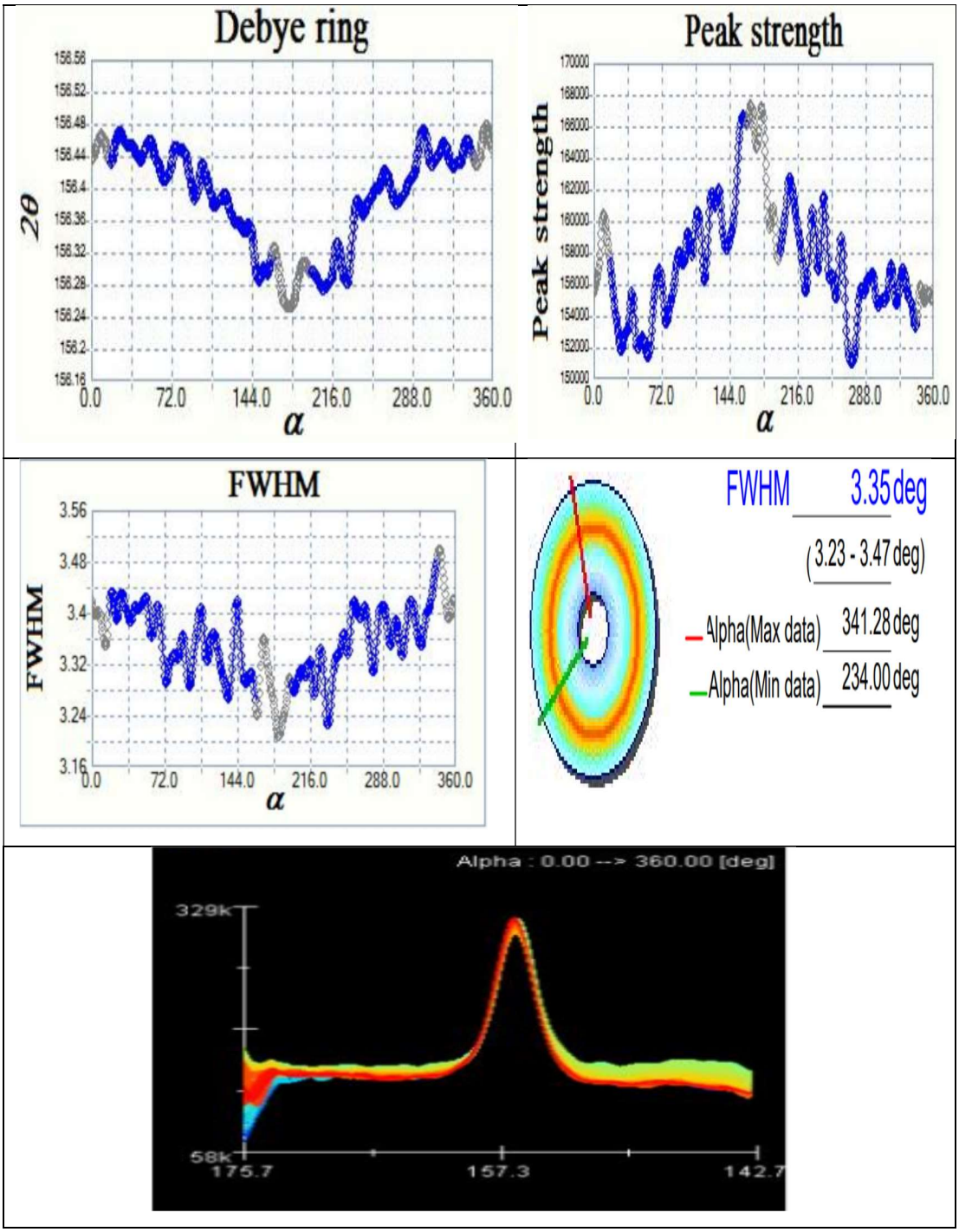

Fig.43: FWHM graph with peak strength of initial grinded work-piece surface

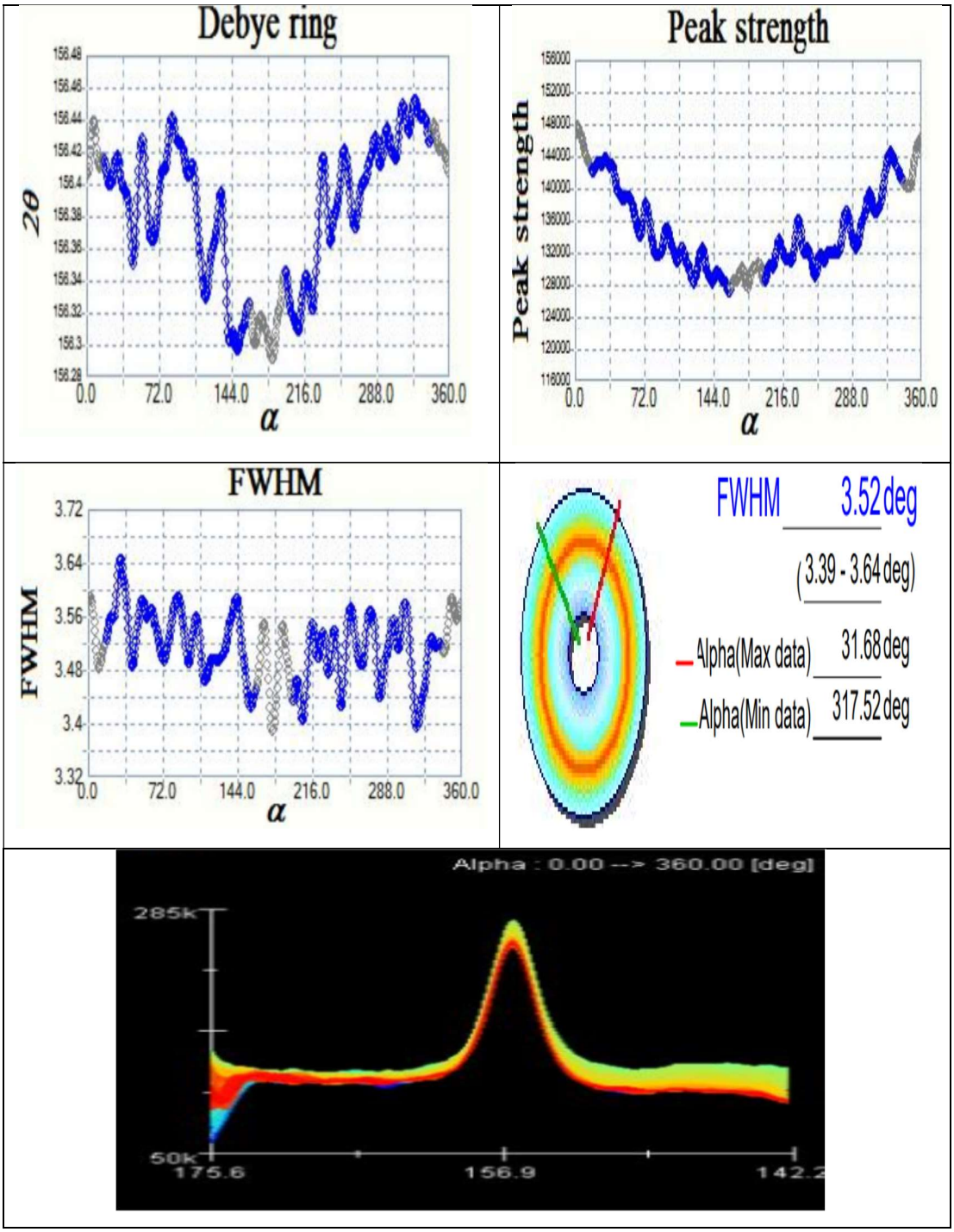

Fig.44: FWHM graph with peak strength of finished work-piece surface using DC power supply without pulse

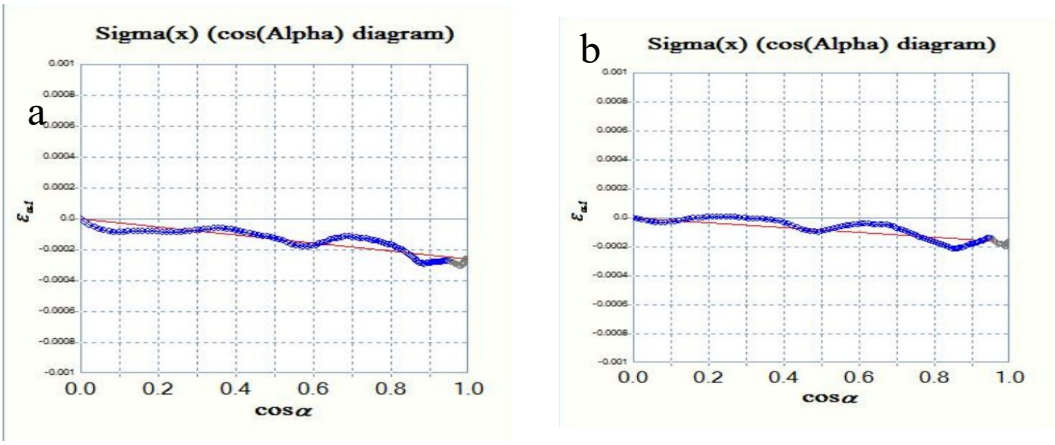

Fig.45: Residual stress graph of (a) Initial grinded surface at 122 MPa (b) Finished surface by BEMRF without pulse at 78 MPa.

8.5.2 Residual stress analysis of finished surface with PBEMRF process with pulse DC power supply

The Debye ring and distortion ring of grinded work-piece as shown in Fig.47a. The Debye ring and Distortion ring of finished surface using BEMRF process with pulse DC power supply which has less irregularity shown in Fig.46b. In fig. 49 a &b, x-axis Cosα represents cos of azimuth angle of Debye sheerer ring and y-axis represents strain (εα1).

The Debye ring and distortion ring represents the texture of work-piece surface. The FWHM is minimum for the grinding surface of work-piece and FWHM is increased with pulse DC power supply in BEMRF process. The FWHM graph of initial grinded work-piece surface with peak strength are given in Fig.47. The value of FWHM 3.32ºlies between (3.20º-3.45º) and α_{max}341.28º and α_{min} 218.16º with peak strength (Ave) 154k. After finishing with BEMRF process using DC power supply without pulse, the value of FWHM 3.43º lies between (3.24º-3.53º) and α_{max}58.32º and α_{min} 198º with peak strength 135k as shown in Fig.48. The peak strength is maximum of

initial grinded work-piece surface and it reduced for finished surface which indicate the intensity of residual stresses.

The inclination angle of bend was measured as the residual stress. The measured value of residual stresses after grinded surfaces of EN-31 are observed as 102 MPa as shown in Fig.49 (a). The residual stress of finished surface was reduced to 55 MPa with pulse DC power supply on BEMRF process at 2.5 A, 0.5 mm, 500 rpm, 50 mm/min and 0.16 duty cycle as shown in Fig.49b. The percentage reduction in residual stress (%ΔRS) is calculated from equation 12 and it was found to be 46.07% as shown in table10.

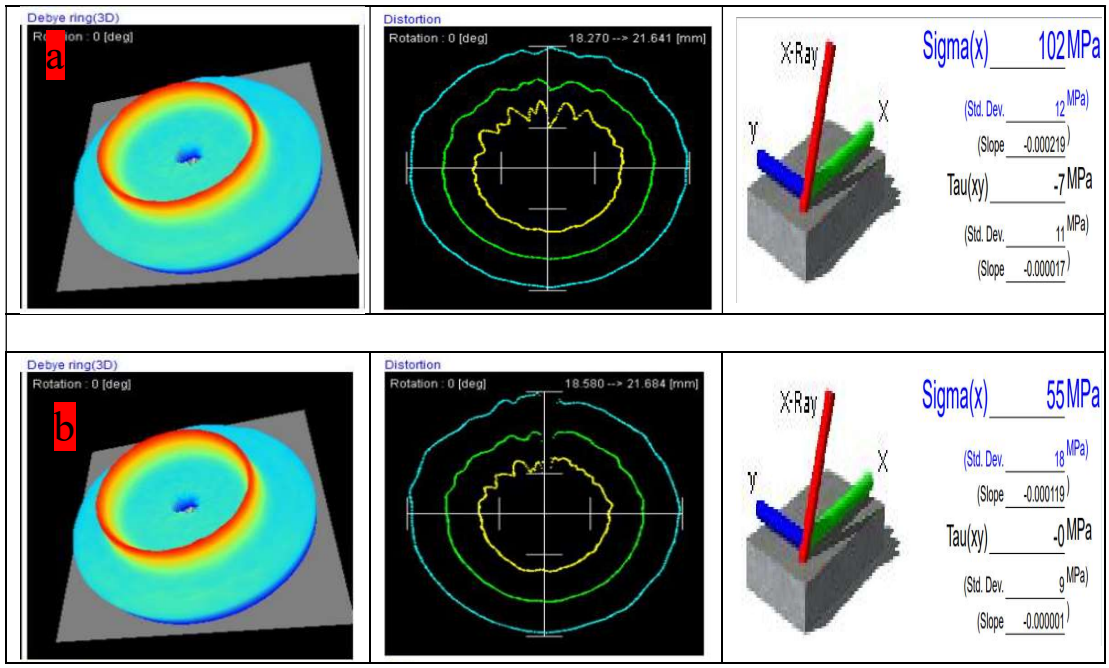

Fig.46: Debye ring (3D) and Distortion ring of (a) Initial grinded surface at 102 MPa, FWHM= 3.32º(b) Finished surface at 55 MPa, FWHM=3.43º with PBEMRF.

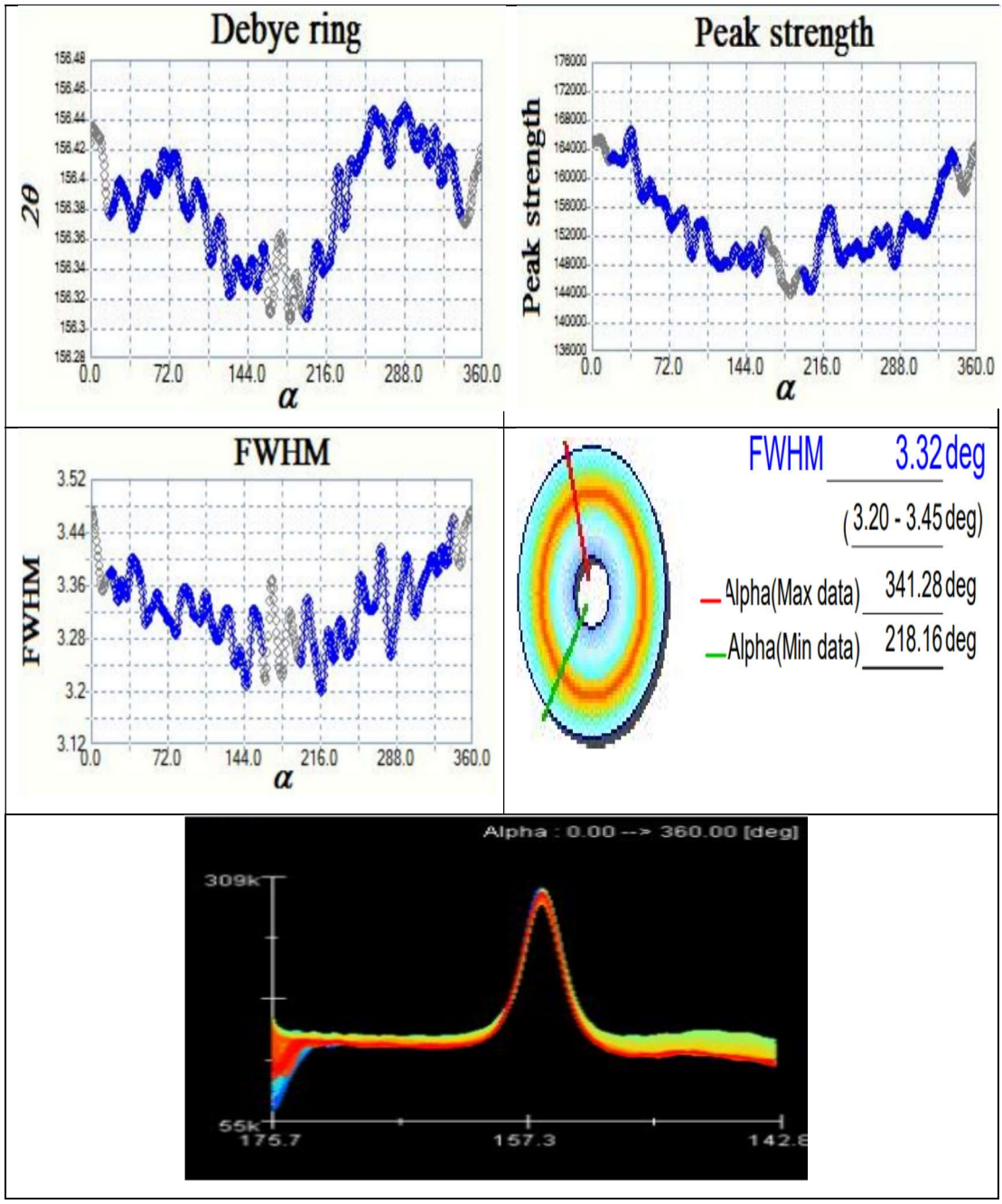

Fig.47: FWHM graph with peak strength of initial grinded work-piece surface

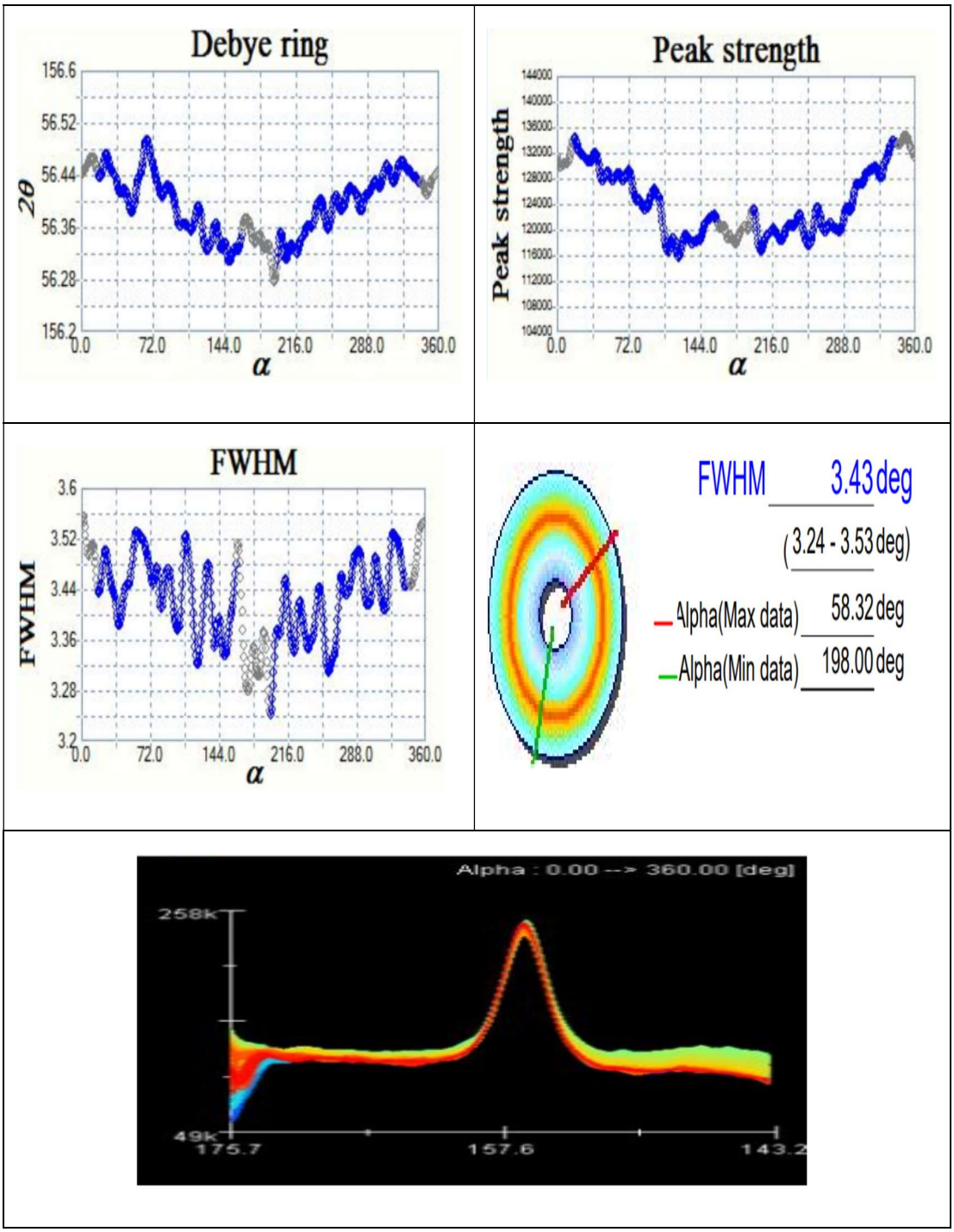

Fig.48: FWHM graph with peak strength of finished surface with PBEMRF Process

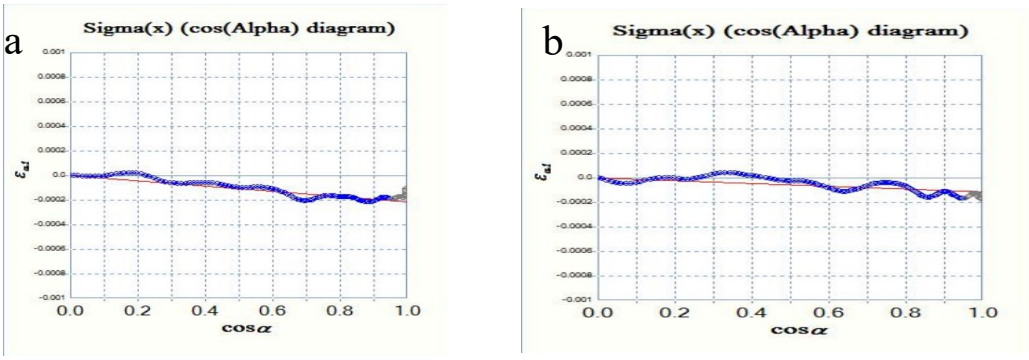

Fig.49: Residual stress graph of (a) Initial grinded surface at 102 MPa (b) Finished surface by PBEMRF at 55 MPa

A drastic reduction in residual stresses was observed after conducting the preliminary experimental study on EN-31 steel surface using BEMRF process DC power supply with and without pulse.

Debye ring and Distortion ring of finished surface using BEMRF process without pulse DC power supply which has less uniform ring and then finished surface using BEMRF process with pulse DC power supply. The Residual stress graph also represents that higher reduction in residual stress was achieved using DC power supply with pulse at same process parameters (2.5 A magnetizing current, 50 mm/min Feed rate, 0.5 mm working gap, 500 rpm rotational speed of tool). Further these process parameters are to be optimize through design of experiment.

8.6 Residual stress analysis through Design of experiment for process parameters

Central composite design (CCD) under response surface methodology was used to design the experiments based on the preliminary study. In this regression analysis the significance of process parameters such as magnetizing current (*MC*), working gap (*WG*), feed rate (F) and rotational speed of tool (*RST*) on output response i.e. percentage reduction in residual stress (%ΔRS) is investigated. The level and ranges

of the selected process parameters are given in table 11. In this work, 0.16 duty cycle was taken for all experimentation. Run order and results of output responses for finishing of EN-31 through PBEMRF process are given table no.12.

Table 11. Level and ranges of process parameters

S. No	Process parameters	Units	Levels				
			-2	-1	0	1	2
1	Magnetizing Current	A	1.5	2	2.5	3	3.5
2	Feed rate	mm/min	30	40	50	60	70
3	Working gap	mm	0.5	1	1.5	2	2.5
4	Rotational speed of tool	rpm	300	400	500	600	700

Table 12. Design and result of output response in surface roughness (%Δ*RS*)

Std	Run order	MC	F	WG	RST	%ΔRS
13	1	3	60	1	600	46.47
14	2	2.5	50	1.5	500	38.9
6	3	2.5	30	1.5	500	41.34
15	4	2	60	1	400	28.7
17	5	2.5	50	1.5	500	37.1
30	6	3	60	2	400	42.4
1	7	2	60	1	600	39.44
21	8	2	60	2	600	32.34
4	9	2	60	2	400	30.54
2	10	2	40	2	600	33.8
27	11	3	40	1	400	51.55
18	12	2	40	2	400	31.97
7	13	2.5	50	1.5	500	39.85

9	14	2	40	1	600	37.89
8	15	3	40	2	600	45.49
16	16	2.5	70	1.5	500	36.8
22	17	3	40	2	400	46.8
19	18	3	40	1	600	52.84
29	19	2.5	50	0.5	500	44.26
20	20	2.5	50	1.5	500	36.59
25	21	3	60	1	400	45.64
5	22	1.5	50	1.5	500	34.42
11	23	2.5	50	1.5	700	39.54
23	24	2.5	50	1.5	300	34.9
12	25	2	40	1	400	33.9
26	26	3	60	2	600	42.72
3	27	3.5	50	1.5	500	58.32
28	28	2.5	50	2.5	500	35.46
24	29	2.5	50	1.5	500	38.9
10	30	2.5	50	1.5	500	40.3

The statistical analysis has been done with Design-Expert software using response surface methodology. The quadratic model is selected on the basis of the lack of fit tests, since the cubic model is aliased. Table 13 shows the significant terms after analysis of variance (ANOVA). The *p*-value less than 0.05 shows that the model parameters are significant. In the model of ANOVA following terms A, B, C,D, AB,AC,BC,CD,BD, A^2, D^2 are found to be significant as shown in table 13.

Table 13. ANOVA for Quadratic model

Source	Sum of Squares	DF	Mean Square	F-value	p-value
Model	1319.29	14	94.23	48.30	< 0.0001
A-MC	977.03	1	977.03	500.77	< 0.0001
B-F	51.25	1	51.25	26.27	0.0001
C-WG	95.88	1	95.88	49.14	< 0.0001
D-RST	34.49	1	34.49	17.68	0.0008
AB	10.42	1	10.42	5.34	0.0355
AC	3.81	1	3.81	1.95	0.1825
AD	18.55	1	18.55	9.51	0.0076
BC	2.15	1	2.15	1.10	0.3101
BD	3.89	1	3.89	1.99	0.1783
CD	12.62	1	12.62	6.47	0.0225
A^2	95.07	1	95.07	48.73	< 0.0001
B^2	0.0371	1	0.0371	0.0190	0.8922
C^2	1.51	1	1.51	0.7716	0.3936
D^2	4.97	1	4.97	2.55	0.1313
Residual	29.27	15	1.95		
Lack of Fit	18.34	10	1.83	0.8397	0.6207
Pure Error	10.92	5	2.18		
Cor Total	1348.55	29			

After dropping the insignificant terms in above table 13 by backward elimination method, the model F value has been found improved as 73.28 with p value less than 0.0001 which indicates that the model is significant as shown in table 14. There is only 0.01% possibility of this to occur due to noise**.** P-values less than 0.0500 indicates that the model terms are significant. In this case A, B, C, D, AB,

AD, CD, A^2 are significant model terms. Values greater than 0.1000 indicate the model terms are not significant.

Table 14. ANOVA for Reduced Quadratic model

Source	Sum of Squares	DF	Mean Square	F-value	p-value		Percentage contribution
Model	1301.92	8	162.74	73.28	< 0.0001	significant	
A-MC	977.03	1	977.03	439.95	< 0.0001		72.47 %
B-F	51.25	1	51.25	23.08	< 0.0001		3.80 %
C-WG	95.88	1	95.88	43.17	< 0.0001		7.11 %
D-RST	34.49	1	34.49	15.53	0.0007		2.56 %
AB	10.42	1	10.42	4.69	0.0420		
AD	18.55	1	18.55	8.35	0.0088		
CD	12.62	1	12.62	5.68	0.0266		
A^2	101.68	1	101.68	45.78	< 0.0001		
Residual	46.64	21	2.22				
Lack of Fit	35.71	16	2.23	1.02	0.5396	Not significant	
Pure Error	10.92	5	2.18				
Cor Total	1348.55	29					

Table 15. Fit statics of reduced quadratic model

Std. Dev.	1.49	**R^2**	0.9654
Mean	39.97	**Adjusted R^2**	0.9522
C.V. %	3.73	**Predicted R^2**	0.9240
Adequate precision	35.30		

The coefficient of correlation, R^2as 0.9654, demonstrates that the measured and computed values of the output have a satisfactory relationship. Adequate Precision measures the signal to noise ratio. The corrected and anticipated R^2 values are respectively 0.95 and 0.92, and the difference between them is 0.03, which is within the allowable range. A ratio greater than 4 is desirable. The value of 35.30 indicates an adequate signal. Final equation in terms of actual factor are given below:

$$\%\Delta RS = 0.4341 - 5.9808MC + 0.257312\ F + 4.88375\ WG + 0.092475\ RST - 0.161375\ MC * F - 0.021537\ MC * RST - 0.017763\ WG * RST + 7.51583\ MC^2 \quad \ldots\ldots\ldots\ldots (13)$$

The effect of different process parameters has been studied from analysis of variance on percentage reduction in residual stress (%ΔRS).

8.6.1 Effect of Magnetizing Current (MC) on %ΔRS

Magnetizing current is the highest contributing parameter for %Δ*RS* having value of 72.47% (from model analysis). As the magnetizing current is increased the %Δ*RS* also increases due to the increase of magnetic flux density on high magnetizing current at finishing tool. This trend can be observed from Fig.50.1 representing the effect of magnetizing current on %Δ*RS.*

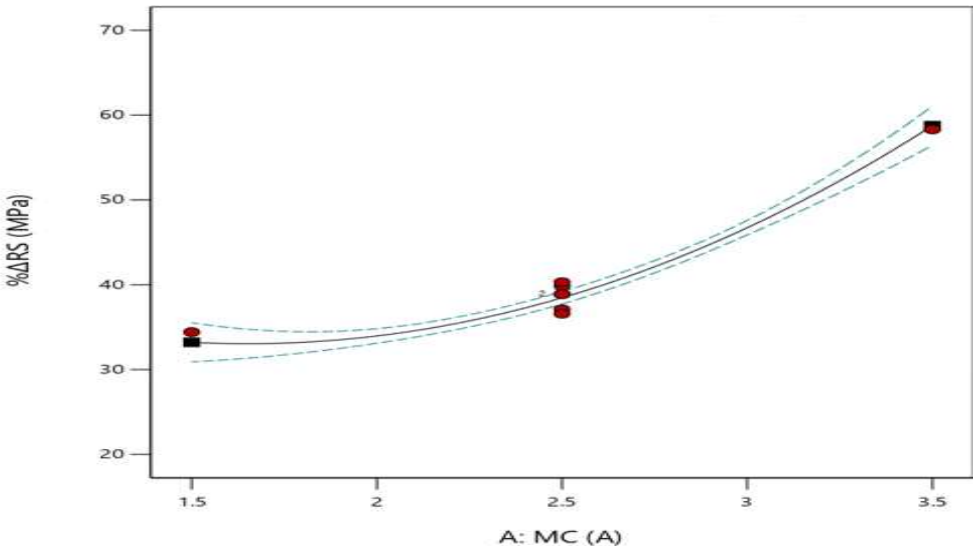

Fig. 50.1: Effect of Magnetizing Current on %ΔRS

8.6.2 Effect of Feed rate on %ΔRS

The %Δ*RS* slightly decreases with the increase in feed rate (F) as shown in Fig.50.2. This is due to the reason that the CIP chains remain intact at low feed rate and get separated when feed rate further increases resulting in getting partly out of contact from the work-piece. The percentage contribution of feed rate parameter on %Δ*RS* is 3.80 % as depicted from model analysis.

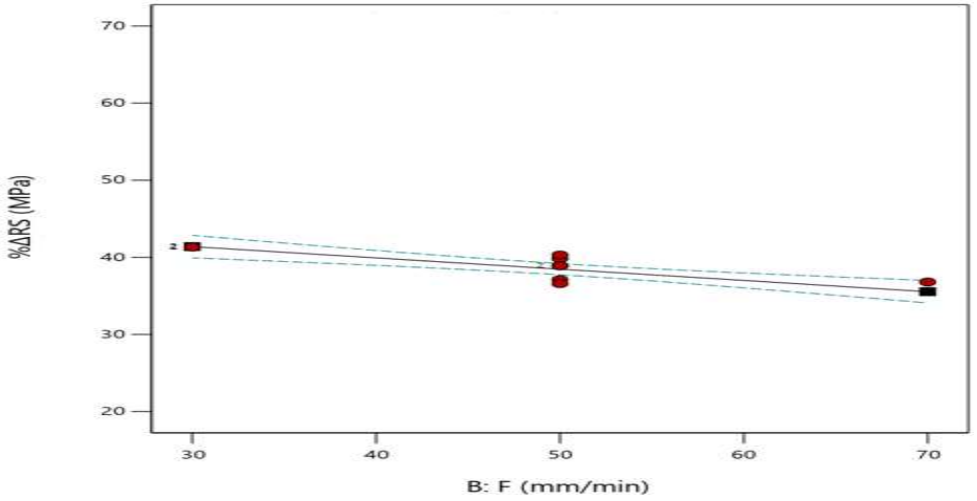

Fig. 50.2: Effect of Feed rate on %ΔRS

8.6.3 Effect of Working Gap (WG) on %ΔRS

The %ΔRS has been found decreased with increasing the working gap as shown in Fig 50.3. It is also seen from the perturbation or 3D surface diagram as shown in Fig.50.5 (a) and (c). The % contribution of feed rate is 7.11% from model analysis.

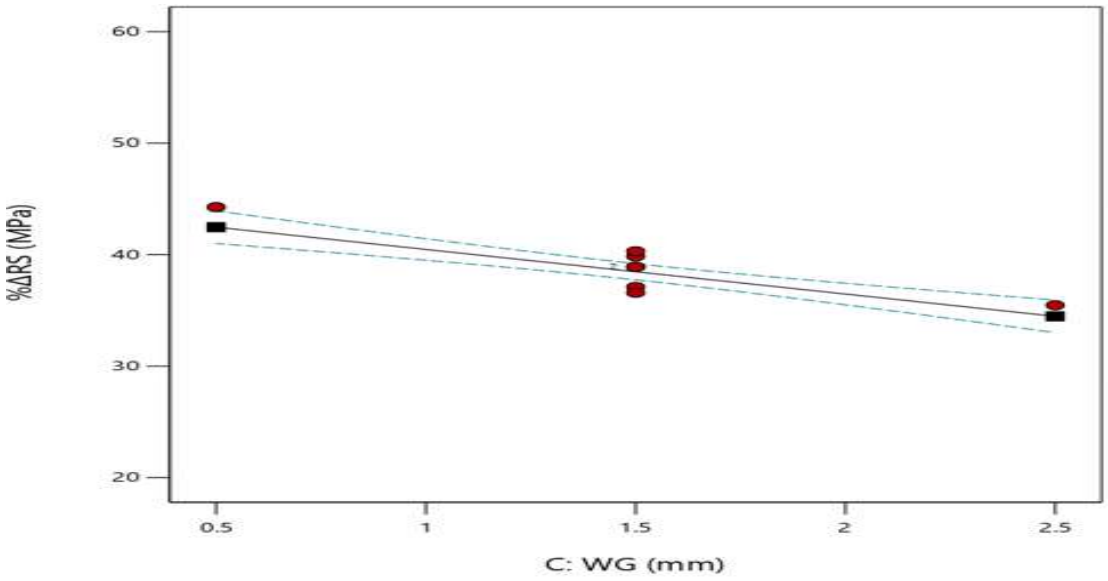

Fig.50.3: Effect of Working Gap on %ΔRS

8.6.4 Effect of Rotational Speed of Tool (RST) on %ΔRS

Fig.50.4 shows that the %Δ*RS* slightly increases with the increase in *RST*. The percentage contribution of rotational speed of tool is 2.56% on %Δ*RS* from model analysis.

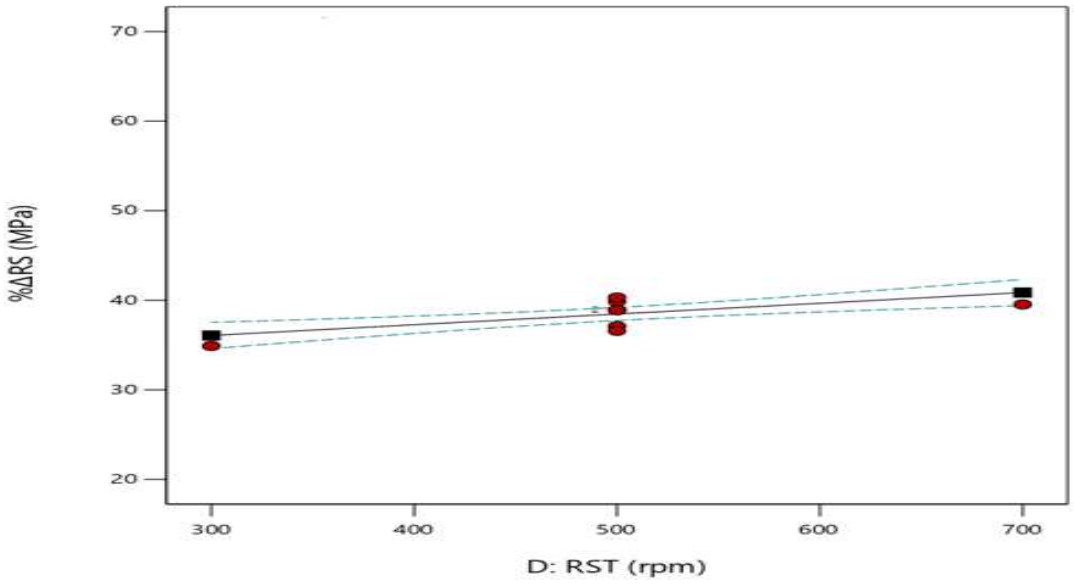

Fig.50.4: Effect of Rotational Speed of Tool on %ΔRS

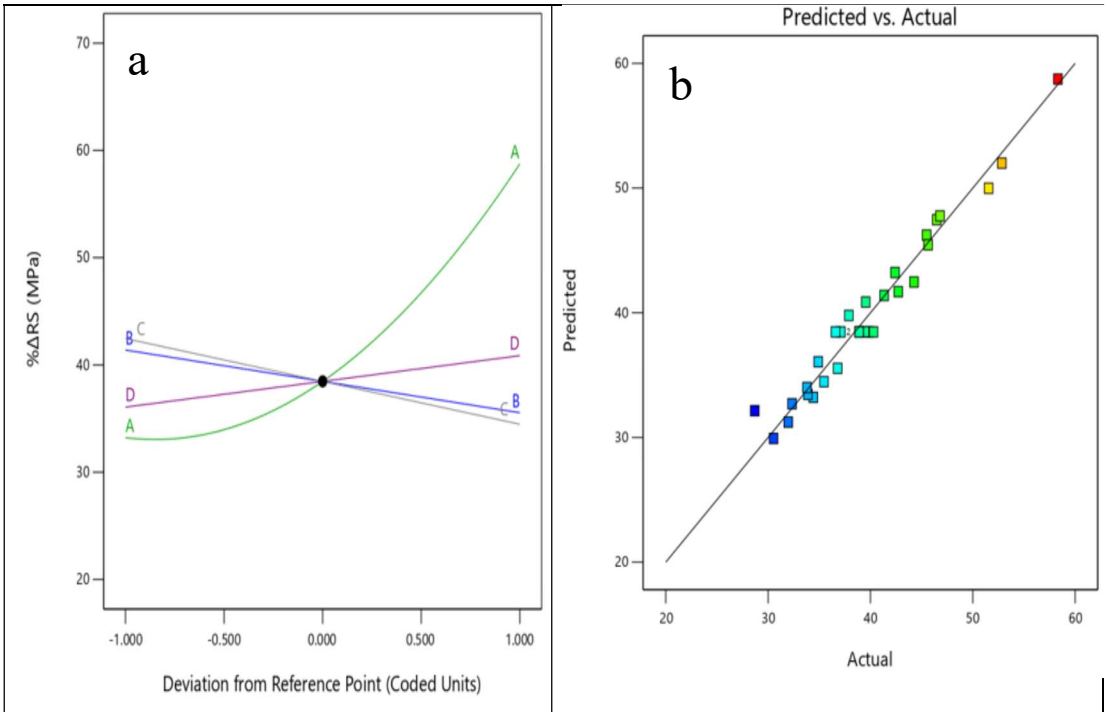

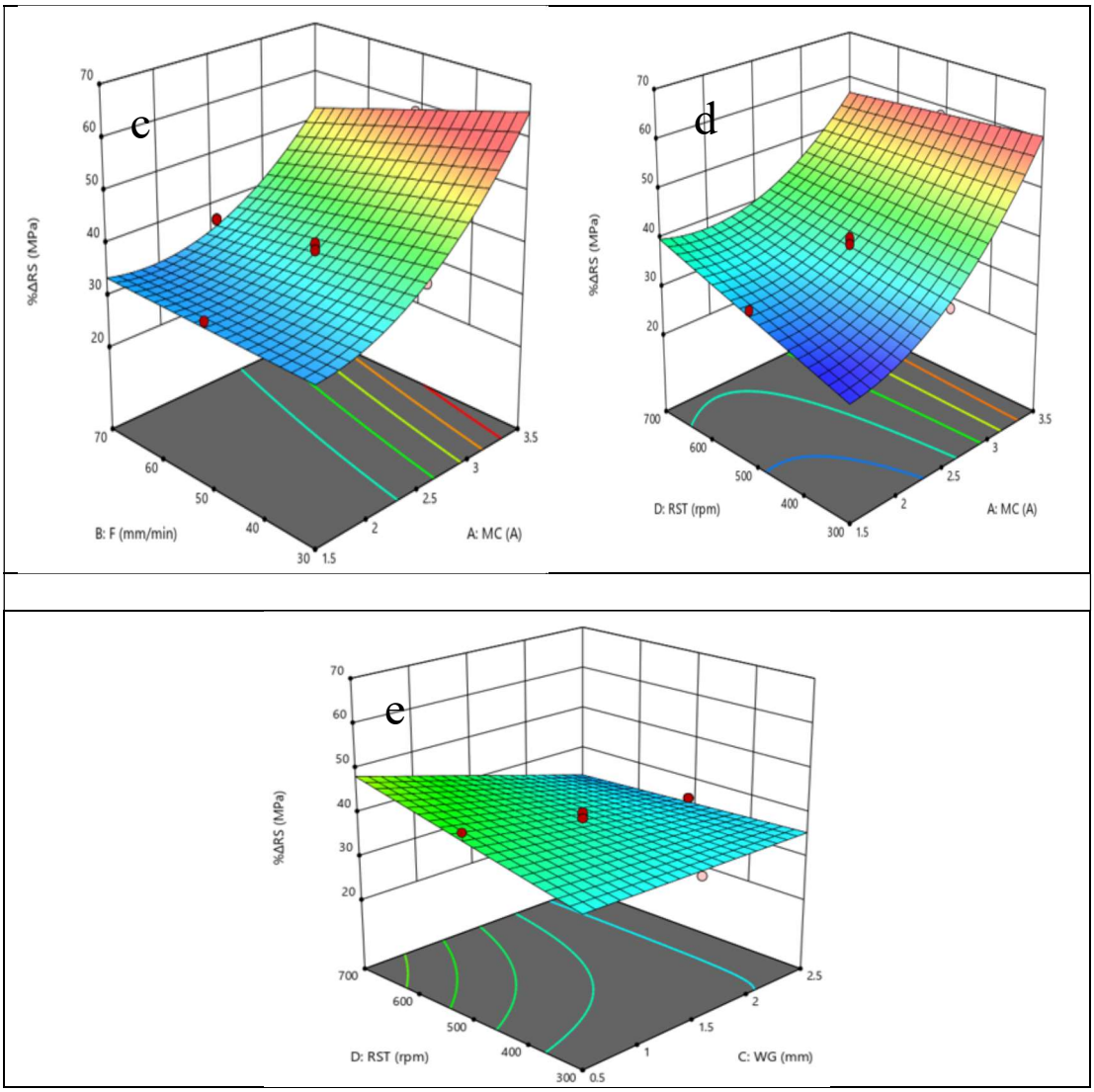

Fig.50.5:(a) Perturbation diagram for %Δ*RS* with (A –Magnetization current, B – Feed rate, C- working gap, D – Rotational speed of tool) (b) Actual vs. Predicted graph (c) 3-D surface graph between feed rate and MC on %ΔRS (d) 3-D surface graph between RST and MC on %ΔRS (e) 3-D surface graph between WG and F for %ΔRS

The perturbation diagram shows the individual effect of process parameters on *%ΔRS* in Fig.50.5 (a). Fig.50.5 (b) shows that the predicted value of *%ΔRS* is close to the

actual value obtained after experimentation. Fig.50.5b shows a magnificent acceptability of the regression model. Every observed value was comparable to the predicted value which can be taken from the model as shown in Fig.50.5b and shows a fair consistency of the predicted value with the actual values. The actual value points were nearer to the predicted line which means that the experimental values are satisfying the predicted results.3-D surface diagram for interaction of process parameters are shown in Fig.50.5(c, d, e). The interaction of process parameters on %ΔRS can also be observed through contour surface graphs shown in Fig.50.6.

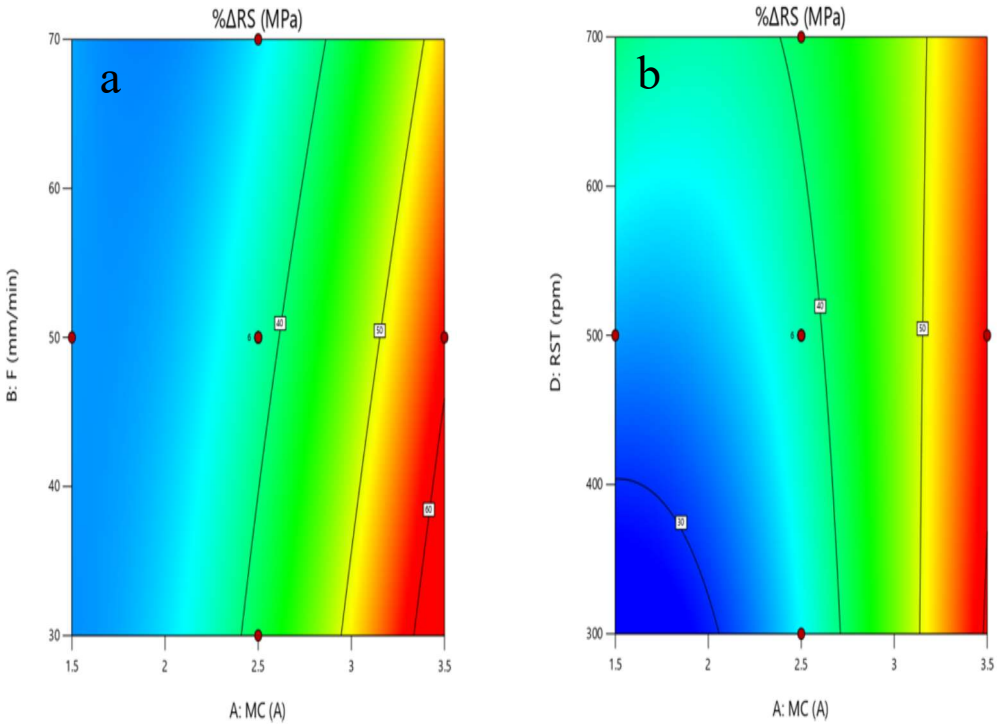

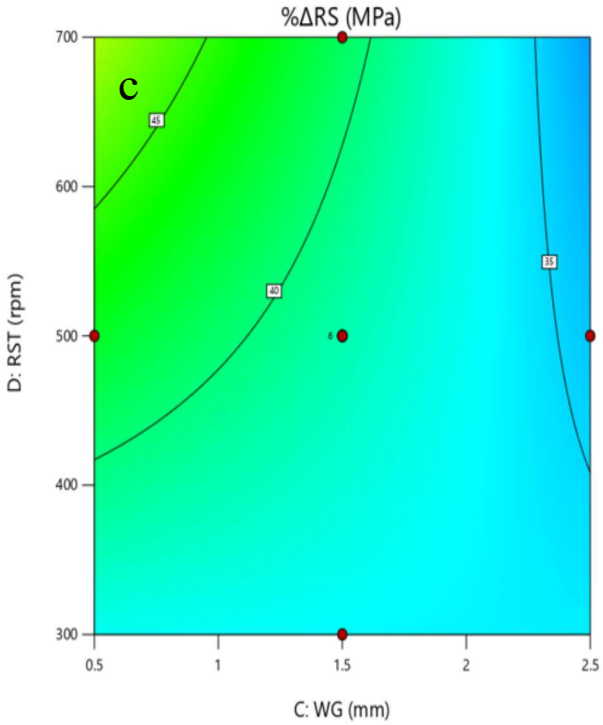

Fig.50.6: Contour surface graph between (a) Feed rate and Magnetizing Current (b) Rotation Speed of Tool and Magnetizing Current (c) Rotation Speed of Tool and Working Gap for %ΔRS

The effect of process parameters has also been studied through interaction graph. The %ΔRS increases with increasing the magnetizing current and reduces with increasing of feed rate as shown in Fig.50.7. The %ΔRS increases with increasing the magnetizing current and rotational speed of tool as shown in Fig.50.8. The %ΔRS reduces with increasing the working gap and %ΔRS increasing with RST as shown in Fig.50.9.

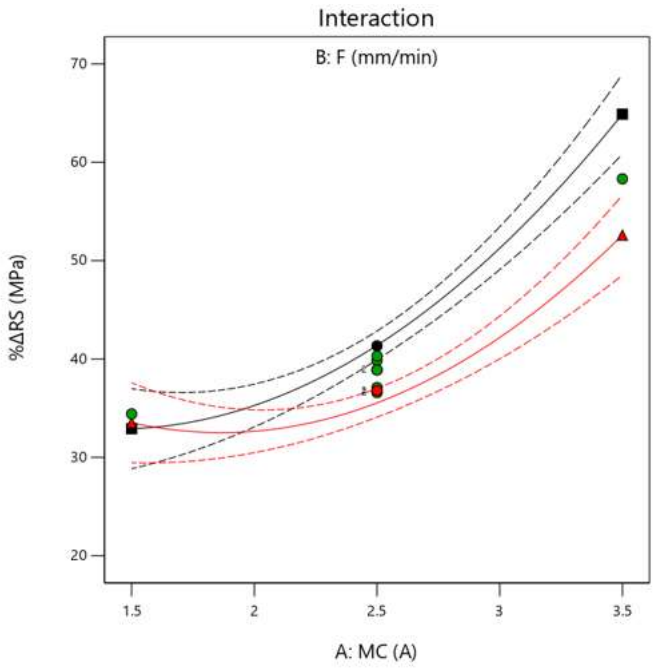

Fig. 50.7: Interaction graph between Magnetizing Current and Feed rate on %ΔRS

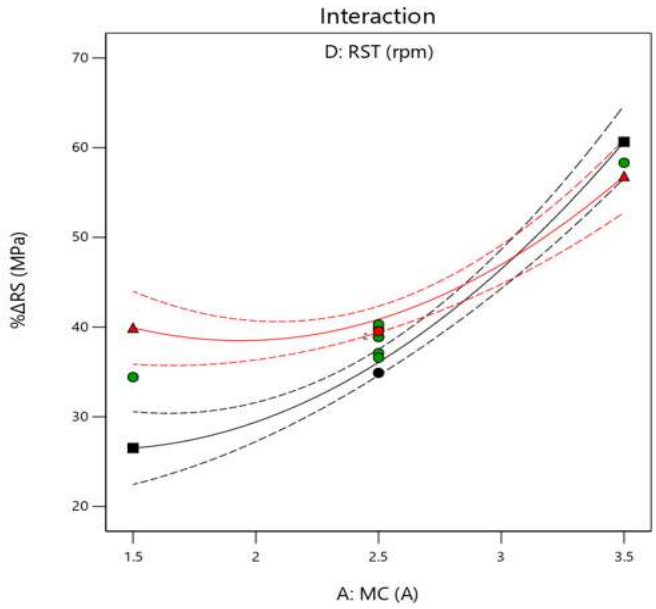

Fig. 50.8: Interaction graph between Magnetizing Current and Rotation Speed of Tool on %ΔRS

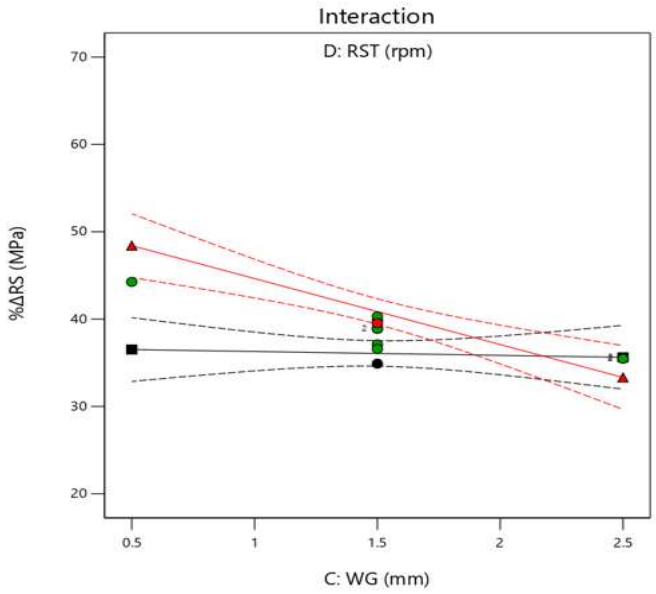

Fig. 50.9: Interaction graph between Working Gap and Rotation Speed of Tool on %ΔRS

8.6.5 Residual stress at optimum process parameters

The experiments have been conducted on work-piece surface with pulse BEMRF process at optimum process parameters obtained by statistical analysis as 3.5A current, 30 mm/min feed rate, 0.5 mm working gap, and 700 rpm rotational speed of tool. Thereafter residual stress has been measured. The residual stress has been measured efficiently by detecting the full Debye ring data from a single incident X-ray angle. The Debye ring and distortion ring of initial grinded work-piece has higher irregularity as shown in Fig.51a. The Debye ring and Distortion ring of finished surface using PBEMRF process has very less irregularity as shown in Fig.51b.The FWHM graph of initial grinded work-piece surface with peak strength are given in Fig.52. The value of FWHM 3.31ºlies between (3.18º-3.41º) and α_{max}39.60º and α_{min} 214.56º with peak strength (Ave) 157k.After finishing the work-piece surface with PBEMRF process, the value of FWHM 3.50º lies between (3.32º-3.64º) and α_{max}66.24º and α_{min} 216º with peak strength 134k as shown in Fig.53. The peak

strength is maximum of initial grinded work-piece surface and it reduced for finished surface which indicated the intensity of residual stresses.

X-axis Cosα represents cos of azimuth angle of Debye sheerer ring and y-axis represents strain (εα1). The inclination angle of bend was measured after grinded surfaces of EN-31 are observed as 119 MPa and after finishing the work-piece surface with PBEMRF process, the residual stress was observed 42 MPa. Residual stress was relieved from the work-piece surface from 119 MPa to 42 MPa after finishing with PBEMRF process at optimum process parameters 3.5A current,30 mm/min feed rate, 0.5 mm working gap, 700 rpm rotational speed of tool as given in Fig.54(a-b). The maximum %ΔRS has been found as 64.70% at optimum process parameters.

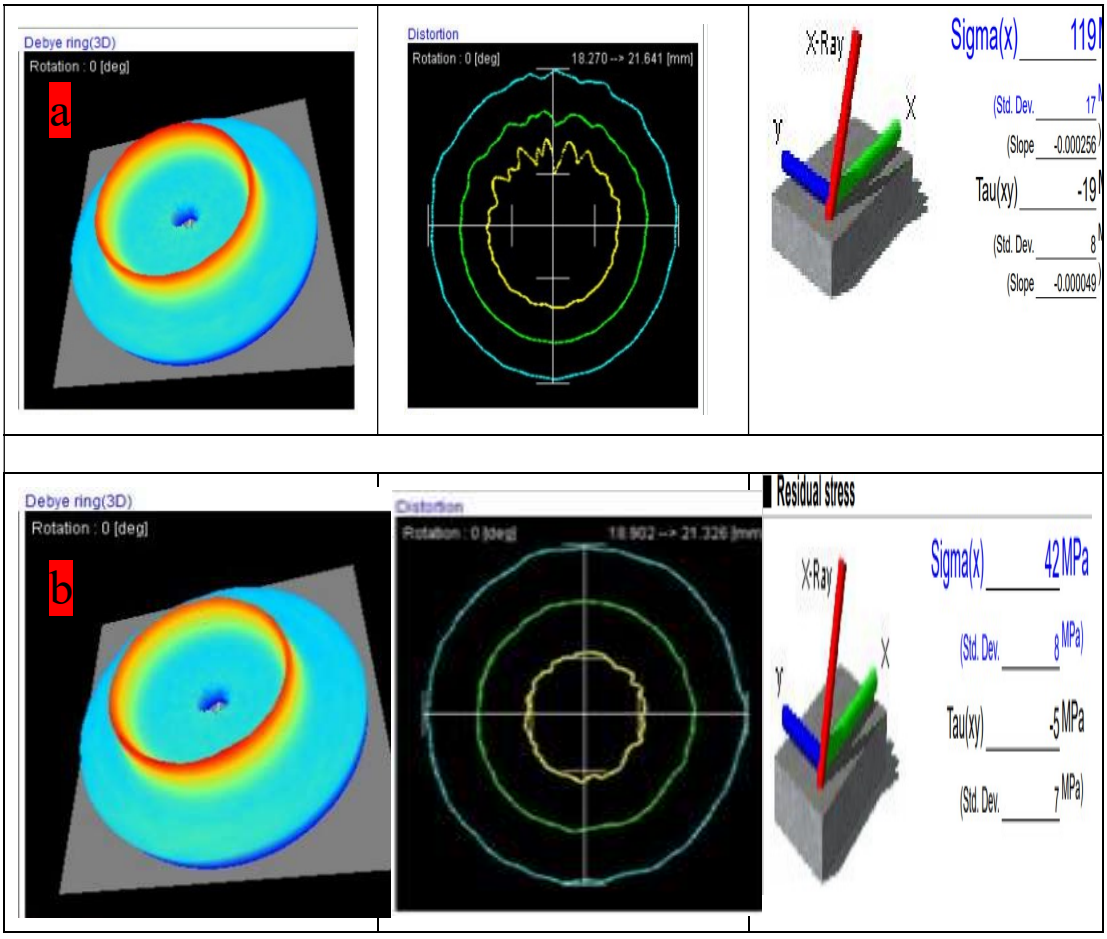

Fig. 51: Debye ring (3D) and Distortion ring of (a) Initial grinded work-piece

surface at 119MPa, FWHM= 3.31 (b) Finished surface at 42 MPa, FWHM= 3.50 by PBEMRF process

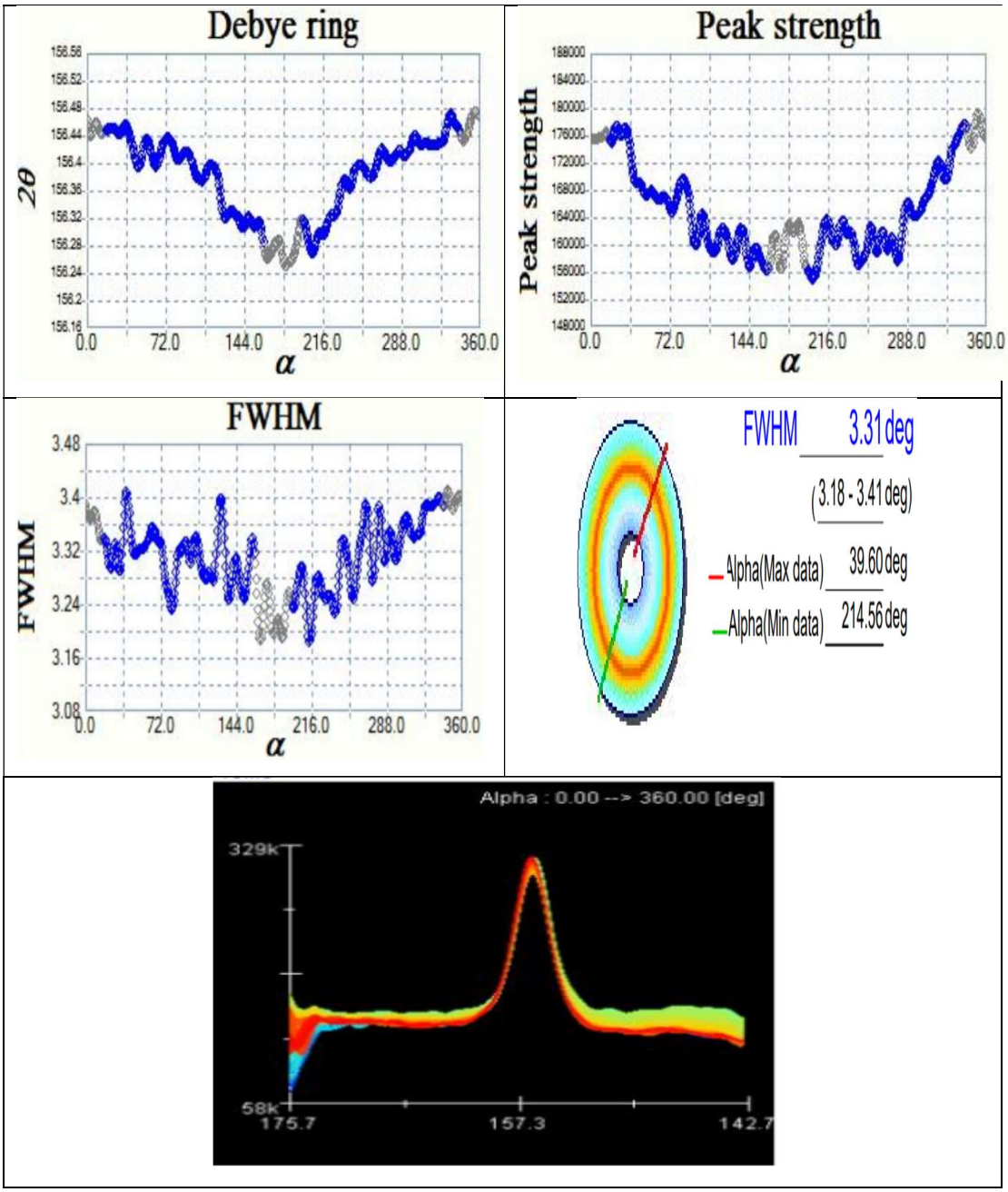

Fig.52: FWHM graph with peak strength of initial grinded work-piece surface

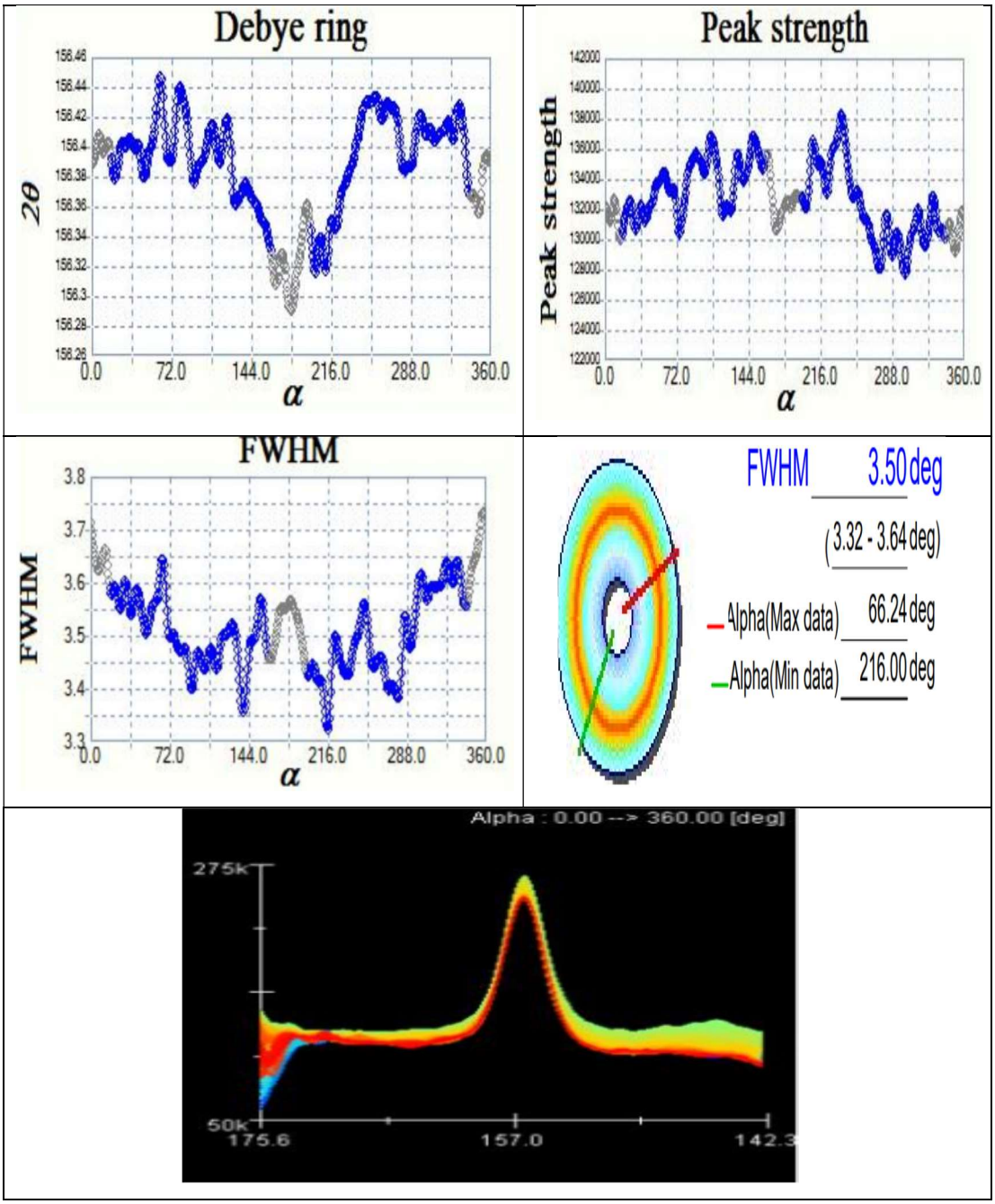

Fig.53: FWHM graph with peak strength of finished surface with PBEMRF process at optimum process parameters (3.5A, 30 mm/min, 0.5 mm, 700 rpm)

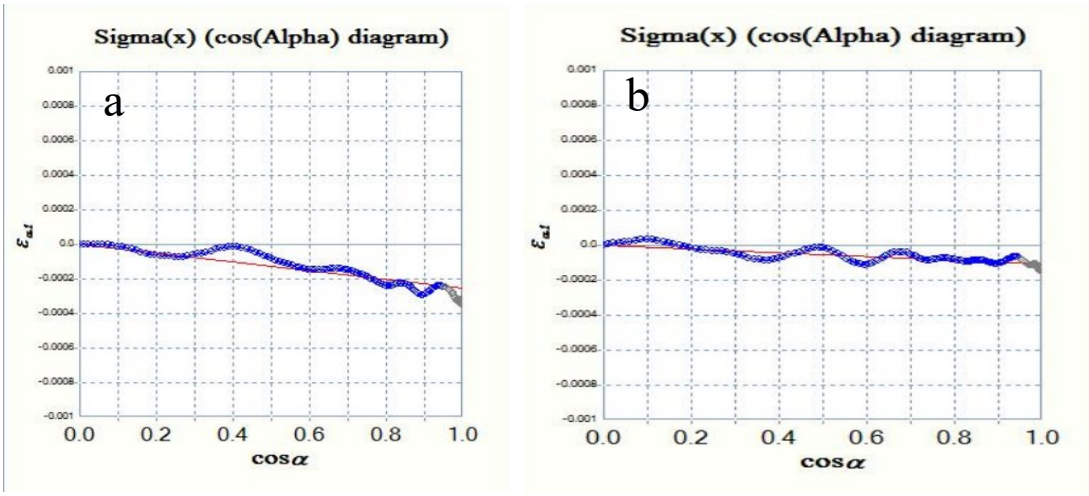

Fig.54: (a) Residual stress graph of initial Grinding surface is 119MPa (b) Residual graph of finished surface with PBEMRF process is 42 MPa at 3.5 A, 30 mm/min, 700 rpm, 0.5 mm

The value of %ΔRS obtained by statistical analysis was found to be 70.35% at optimum process parameters as 3.5A magnetizing current, 30 mm/min feed rate, 0.5mm working gap, 700 rpm rotational speed of tool. After conducting the experiment at optimum process parameters the actual%ΔRShas been found to be 64.70 % The results obtained after experimentation are close to the predicted value of %ΔRS and 5.65% error is calculated as shown in table 16.

Table 16. Confirmatory experiment after finishing work-piece using PBEMRF

S.No	MC (A)	F(mm/min)	RST (rpm)	WG(mm)	Predicted %ΔRS	Actual %ΔRS	% Error
1.	3.5	30	700	0.5	70.35%	64.70%.	5.65

CHAPTER 9

CONCLUSIONS AND SCOPE OF FUTURE WORK

This chapter describes the conclusions obtained from experimental investigations on EN-31 work-piece surface with ball end magnetorheological finishing process using DC power supply with and without pulse. The process is thoroughly analyzed for surface roughness and residual stress by statistical analysis using response surface methodology. The results have been explained in brief and scope of future work is discussed.

9.1 Conclusions

The following conclusions are drawn based on experimental investigations into pulsed ball end magnetorheological finishing of hard metal-

1. Experiments have been conducted on EN-31 work-piece surface using BEMRF process with the use of DC power supply with and without pulse at process parameters 2.5A current, 500 rpm tool rotational speed, 0.5 mm working gap and feed rate 50 mm/min. It was observed that the better percentage reduction in surface roughness (%Δ*Ra*) of 31.72 at 0.16 duty cycle was achieved with the use of pulse DC power supply than%Δ*Ra of 13.44* without pulse DC power supply at same process parameters.
2. The experiments have been conducted on EN-31 work-piece surface with pulse BEMRF process using design of experiment. The statistical analysis has been carried out to see the effect of various process parameters on percentage reduction in surface roughness (%Δ*Ra*). The maximum percentage contribution of 77.87 was found for magnetizing current followed by percentage contribution of 5.85 for working gap, 4.21% for feed rate and 2.21% for tool rotational speed.
3. It was observed that, the %Δ*Ra* increases with increase in the magnetizing

current in the given range and %ΔRa was observed to be maximum at 3.5A. While the %ΔRa is found decrease on increase the feed rate. It was also found that %ΔRa decreases with increase the working gap. The %ΔRa was found to be increase on increase of tool rotational speed in given range.

4. The maximum predicted %ΔRa of 55.52was found by statistical analysis at optimum process parameters 3.5A current,30 mm/min feed rate,700 rpm tool rotational speed and 0.5 mm working gap.
5. The experiment has been conducted at 3.5A current,30 mm/min feed rate,700 rpm tool rotational speed and 0.5 mm working gap and %ΔRa was found as 51.23% which is very close to predicted %ΔRa with error of 4.29%.
6. The surface texture of grinded EN-31 work-piece surface and after finishing with pulse BEMRF process at optimum process parameters has been studied by scanning electron microscope at 300X magnification. It was observed from scanning electron micrograph that scratch marks and lays were seen on the initial grinded work-piece surface while very fine lays on the work-piece surface has been observed after finishing with pulse BEMRF process. The abrasion marks were significantly removed on finished surface as compared to initial grinded work-piece surface.
7. The surface texture of grinded EN-31 work-piece surface and after finishing with PBEMRF process has been studied by atomic force microscope (AFM) at 10 μm resolution. It was observed that high density of lays was found on initial grinded work-piece surface and most of these lays are removed after finishing with pulse BEMRF process.
8. The residual stress of grinded work-piece surface and finished surface by pulse BEMRF process has been studied. It has been observed that the better percent reduction in residual stress was achieved with pulse BEMRF process as compared to BEMRF process without pulse DC power supply. The percent reduction in residual stress (%ΔRS) is found as 46.07% at 0.16 duty cycle with

pulse BEMRF process while %ΔRS 36.06 using DC power supply without pulse in BEMRF process at same process parameters. A drastic percentage reduction in residual stresses was observed after conducting the experimental study on EN-31 steel surface using pulse DC power supply and without pulse DC power supply in BEMRF process.

9. The statistical analysis has been carried out to see the effect of various process parameters on percentage reduction in residual stresses (%Δ*RS*). The maximum percentage contribution of 72.47 was found for magnetizing current followed by percentage contribution of 7.11 for working gap, 3.80 % for feed rate and 2.56 % for tool rotational speed. It was observed that, the %Δ*RS* increases with increase in the magnetizing current in the given range and %ΔRS was observed to be maximum at 3.5A. While the %ΔRS is found decrease on increase the feed rate. It was also found that %ΔRS decreases with increase the working gap. The %ΔRS was found to be increase on increase of tool rotational speed in given range.
10. The maximum predicted %ΔRS of 70.35% was found by statistical analysis at optimum process parameters 3.5A current, 30 mm/min feed rate, 700 rpm tool rotational speed and 0.5 mm working gap. The experiment has been conducted at 3.5A current, 30 mm/min feed rate,700 rpm tool rotational speed and 0.5 mm working gap and %ΔRS was found as 64.70% which is very close to predicted %ΔRa with error of 5.65%.

9.2 Scope of future work

(1) Bi-disperse MR polishing fluid can be used to improve finishing efficiency. Nano size magnetic powder such as cobalt, nickel and carbonyl iron can also be explored to further improve the process efficiency.

(2) Carbon Nano tubes filled with magnetic materials such as Fe, Co and Ni can also be explored in the process for betterment.

(3) Mathematical modeling and simulation can also be done.

(4) The results can be analyzed for different industrial materials.

(5) The process can be optimized for variety of MRP fluid composition, different shapes and types of work-piece materials.

REFRENCES

[1] Kordonski, W., and Golini D. (1998), Magnetorheological suspension-based high precision finishing technology (MRF), Journal of Intelligent Material Systems and Structures,9(8), 650- 654.

[2] Jha, S., jain, V.K., and Komanduri R. (2007), Effect of extrusion pressure and number of finishing cycles on surface roughness in magnetorheological abrasive flow finishing (MRAFF) process, International Journal of Advanced Manufacturing Technology,33(7-8), 725-729.

[3] Singh, A.K., Jha, S., and Pandey, P.M.(2011), Design and development of nanofinishing process for 3D surfaces using ball end MR finishing tool, International Journal of Machine Tools and Manufacture,51(2), 142-151.

[4] Simon,T.M., Reitch, F., Jolly, M.R., Ito, K., and Banks, H.T. (2001), The effective magnetic properties of magnetorheological fluids, International journal of mathematical & computing modelling, 33, 273-284.

[5] Sidpara, A., Das, M., and Jain, V.K. (2009), Rheological characterization of magnetorheological finishing fluid. *Materials and Manufacturing Processes*, *24*(12), 1467-1478.

[6] Kala, P., Sharma, V., and Pandey, P.M.(2017), Surface roughness modelling for Double Disk Magnetic Abrasive Finishing process, Journal of Manufacturing Processes 25, 37–48.

[7] Srinivasan G., Shanmugan and Palani (2016),Application of Magnetorheological Fluid in Machining Process, International journal control theory and applications, 9(9), 3705-3712.

[8] Singh, A.K., Jha, S., and Pandey, P.M. (2015), Performance analysis of ball end magnetorheological finishing process with MR polishing fluid, *Materials and Manufacturing Processes*, *30*(12), 1482-1489.

[9] Saraswathamma, K., Jha, S., and Rao, P. V. (2015), Experimental investigation into ball end magnetorheological finishing of silicon, *Precision Engineering*, *42*, 218-223.

[10] Das, M., Jain, V.K., and Ghosh dastidar, P.S. (2012), Nanofinishing of flat work-pieces using rotational–magnetorheological abrasive flow finishing (R-MRAFF) process, *International Journal of Advanced Manufacturing Technology*, *62*(1), 405-420.

[11] Singh, A.K., Jha, S., and Pandey, P.M. (2012), Magnetorheological ball end finishing process. *Materials and Manufacturing Processes*, *27*(4), 389-394.

[12] Kim, J. D., and Choi, M. S. (1997), Study on magnetic polishing of free-form surfaces, *International Journal of Machine Tools and Manufacture*, *37*(8), 1179-1187.

[13] Yan, B. H., Chang, G. W., Chang, J. H., and Hsu, R. T. (2004), Improving electrical discharge machined surfaces using magnetic abrasive finishing, *Machining science and technology*, *8*(1), 103-118.

[14] Yin, S., and Shinmura, T. (2004), Vertical vibration-assisted magnetic abrasive finishing and deburring for magnesium alloy, *International Journal of Machine Tools and Manufacture*, *44*(12-13), 1297-1303.

[15] Chang, G.W., Yan, B.H., and Hsu, R.T. (2002), Study on cylindrical magnetic abrasive finishing using unbonded magnetic abrasives, *International Journal of Machine Tools and Manufacture*, *42*(5), 575-583.

[16] Yan, B. H., Chang, G. W., Cheng, T. J., and Hsu, R. T. (2003), Electrolytic magnetic abrasive finishing, *International Journal of Machine Tools and Manufacture*, *43*(13), 1355-1366.

[17] Yamaguchi, H., Shinmura, T., and Sekine, M. (2005), Uniform internal finishing of SUS304 stainless steel bent tube using a magnetic abrasive finishing process, Journal of Manufacturing Science & Engineering, 127, 605-611.

[18] Shinmura, T., Takazawa, K., and Hatano, E. (1987), Study on magnetic abrasive finishing: effects of various types of magnetic abrasives on finishing characteristics, *Bulletin of the Japan Society of Precision Engineering*, *21*(2), 139-141.

[19] Shinmura, T., Takazawa, K., Hatano, E., Matsunaga, M., and Matsuo, T. (1990), Study on magnetic abrasive finishing. *CIRP annals*, *39*(1), 325-328.

[20] Shinmura, T., Takazawa, K., and Hatano, E. (1985), Study on Magnetic-Abrasive Process, Application to Edge Finishing, *Bull. Jpn. Soc. Precis. Eng.*, *19*(3), 218-220.

[21] Jain, V.K., Singh, D.K., and Raghuram, V. (2008), Analysis of performance of pulsating flexible magnetic abrasive brush (P-FMAB). *Machining science and technology*, *12*(1), 53-76.

[22] Paul, A., and Akash, P.S. (2015), Residual Stress Analysis of Mild Steel ASTM A36 in Milling & Drilling, *International Journal of Science and Research (IJSR)*, *78*(96), 1517-1521.

[23] Jang, D.Y., Watkins, T.R., Kozaczek, K.J., Hubbard, C.R., and Cavin, O.B. (1996), Surface residual stresses in machined austenitic stainless steel, *Wear*, *194*(1-2), 168-173.

[24] Henriksen, E.K. (1951), Residual stresses in machined surfaces. Transactions of the American Society of Mechanical Engineers, 73(1), 69-76.

[25] Mishra, A., and Prasad, T. (1985). Residual stresses due to a moving heat source. International Journal of Mechanical Sciences, 27(9), 571-581.

[26] Iqbal, F., and Jha, S. (2019), Experimental investigations into transient roughness reduction in ball-end magneto-rheological finishing process. Materials and Manufacturing Processes, 34(2), 224-231.

[27] Arrasmith, S.R., Jacobs, S.D., Lambropoulos, J.C., Maltsev, A., Golini, D., and Kordonski, W.I. (2001), Use of magnetorheological finishing (MRF) to relieve residual stress and subsurface damage on lapped semiconductor silicon wafers, Optical manufacturing and testing IV (4451), 286-294.

[28] Kordonski, W.I., and Jacobs, S.D. (1996), Magnetorheological finishing, *International Journal of modern physics B*, *10*(23-24), 2837-2848.

[29] Jacobs, S.D., and Arrasmith, S. (1999), Overview of magnetorheological finishing,for precision optics manufacturing, *Ceram*. Trans, 102, 185-199.

[30] Cheng, H.B., Feng, Y.P., Ren, L.Q., To, S., and Wang, Y.T. (2009), Material removal and micro-roughness in fluid-assisted smoothing of reaction-bonded silicon carbide surfaces, Journal of Materials Processing Technology, 209(9), 4563-4567.

[31] Cheng, H.B., Yam, Y., and Wang, Y.T. (2009), Experimentation on MR fluid using a 2-axis wheel tool, *Journal of Materials Processing Technology*, *209*(12-13), 5254-5261.

[32] Schinhaerl, M., Smith, G., Stamp, R., Rascher, R., Smith, L., Pitschke, E., and Geiss, A. (2008), Mathematical modelling of influence functions in computer-controlled polishing: Part II, Applied Mathematical Modelling, 32(12), 2907-2924.

[33] Jha, S., and Jain, V.K.(2004), Design and development of the magnetorheological abrasive flow finishing (MRAFF) process, International Journal of Machine Tools and Manufacture, 44(10), 1019-1029.

[34] Jha, S., and Jain, V.K. (2006), Nano-finishing of silicon nitride work-pieces using magnetorheological abrasive flow finishing. International Journal of Nano-manufacturing, 1(1), 17-25.

[35] Jha, S., and Jain, V.K. (2009), Rheological characterization of magnetorheological polishing fluid for MRAFF. International Journal of Advanced Manufacturing Technology, 42(7), 656-668.

[36] Jha, S., Jain, V.K., and Komanduri, R. (2007), Effect of extrusion pressure and number of finishing cycles on surface roughness in magnetorheological abrasive flow

finishing (MRAFF) process, International Journal of Advanced Manufacturing Technology, 33(7), 725-729.

[37] Sadiq, A., and Shunmugam, M. S. (2009), Investigation into magnetorheological abrasive honing (MRAH). International Journal of Machine Tools and Manufacture, 49(7-8), 554-560.

[38] Sadiq, A., and Shunmugam, M. S. (2009), Magnetic field analysis and roughness prediction in magnetorheological abrasive honing (MRAH), Machining science and technology, 13(2), 246-268.

[39] Das, M., Jain, V.K., and Ghoshdastidar, P.S. (2012), Nanofinishing of flat work-pieces using rotational–magnetorheological abrasive flow finishing (R-MRAFF) process, International Journal of Advanced Manufacturing Technology, 62(1), 405-420.

[40] Das, M., Jain, V.K., & Ghoshdastidar, P.S. (2010), Nanofinishing of stainless-steel tubes using rotational magnetorheological abrasive flow finishing process, Journal of Machining Science and Technology, 14(3), 365-389.

[41] Kordonski, W.I., Shorey, A.B., and Tricard, M. (2006), Magnetorheological jet (MR Jet TM) finishing technology, Journal of Fluids Engineering ,128(1), 20-26.

[42] Jain, V.K., Ranjan, P., Suri, V.K., and Komanduri, R. (2010), Chemo-mechanical magneto-rheological finishing (CMMRF) of silicon for microelectronics applications, CIRP annals, 59(1), 323-328.

[43] Rabinow, J. (1948). The magnetic fluid clutch, *Electrical Engineering*, *67*(12), 1167-1167.

[44] López-López, M.T., De Vicente, J., González-Caballero, F., and Durán, J.D.G. (2005), Stability of magnetizable colloidal suspensions by addition of oleic acid and

silica nanoparticles, Colloids and Surfaces A Physicochemical and Engineering Aspects, 264(1-3), 75-81.

[45] Phulé, P.P., and Ginder, J.M. (1999), Synthesis and properties of novel magnetorheological fluids having improved stability and redispersibility, International Journal of Modern Physics B, 13(14 and16), 2019-2027.

[46] Phule, P.P. (2001), Magnetorheological (MR) fluids: principles and applications. Smart Materials Bulletin, 2001(2), 7-10.

[47] Park, J. H., Chin, B. D., and Park, O. O. (2001), Rheological properties and stabilization of magnetorheological fluids in a water-in-oil emulsion, Journal of Colloid and Interface Science, 240(1), 349-354.

[48] Lee, S.N., Park, S.J., Lee, J.I., Yook, J.G., Kim, Y.J., and Lee, S.J. (2005), Application of MRF scheme for low-loss transmission lines on CMOS-grade silicon, In Proceedings Electronic Components and Technology(IEEE), 1514-1518.

[49] Rankin, P.J., Horvath, A.T., & Klingenberg, D.J. (1999), Magnetorheology in viscoplastic media, Rheologica Acta, 38(5), 471-477.

[50] Kordonski, W., & Golini, D. (1998), Magnetorheological suspension-based high precision finishing technology (MRF), Journal of intelligent material systems and structures, 9(8), 650-654.

[51] Ginder, J.M. (1998), Behavior of magnetorheological fluids, *Bulletin*, *23*(8), 26-29.

[52] Ginder, J.M., Davis, L.C., and Elie, L.D. (1996), Rheology of magnetorheological fluids: models and measurements, International journal of modern physics, 10(23-24), 3293-3303.

[53] Miao, C., Shafrir, S.N., Lambropoulos, J.C., Mici, J., and Jacobs, S.D. (2009), Shear stress in magnetorheological finishing for glasses, Applied optics, 48(13), 2585-2594.

[54] Jha, S., and Jain, V.K. (2009), Rheological characterization of magnetorheological polishing fluid for MRAFF, International Journal of Advanced Manufacturing Technology, 42(7), 656-668.

[55] Sidpara, A., Das, M., and Jain, V.K. (2009), Rheological characterization of magnetorheological finishing fluid, Materials and Manufacturing Processes, 24(12), 1467-1478.

[56] Golini, D., Dumas, P., Kordonski, W., Hogan, S., and Jacobs, S. (1997), Precision optics fabrication using magnetorheological finishing, Optical Fabrication and Testing (https://doi.org/10.1364/OFT.1998.OMD.1).

[57] Shorey, A.B. (2000), Mechanisms of material removal in magnetorheological finishing (MRF) of glass, University of Rochester.

[58] Shorey, A.B., Jacobs, S.D., Kordonski, W.I., and Gans, R.F. (2001), Experiments and observations regarding the mechanisms of glass removal in magnetorheological finishing, Applied Optics, 40(1), 20-33.

[59] Gorodkin, S., Zhuravski, N., and Kordonski, W. (2002), Surface shear stress enhancement under MR fluid deformation, Electrorheological Fluids and Magnetorheological Suspensions, 847-852.

[60] Bombard, A.J., Knobel, M., Alcantara, M.R., and Joekes, I. (2002), Evaluation of magnetorheological suspensions based on carbonyl iron powders, Journal of intelligent material systems and structures, 13(7-8), 471-478.

[61] Kordonski, W., and Golini, D. (2002), Multiple application of magnetorheological effect in high precision finishing, Journal of intelligent material systems and structures, 13(7-8), 401-404.

[62] See, H., and Tanner, R. (2003), Shear rate dependence of the normal force of a magnetorheological suspension, Rheologica acta, 42(1), 166-170.

[63] Kim, W.B., Lee, S.H., and Min, B.K. (2004), Surface finishing and evaluation of three-dimensional silicon microchannel using magnetorheological fluid, Journal of Manufacturing Science and Engineering, 126(4), 772-778.

[64] Tricard, M., Dumas, P.R., and Golini, D. (2004), New industrial applications of magnetorheological finishing (MRF), Optical fabrication and testing (https://doi.org/10.1364/OFT.2004.OMD1).

[65] Jayaswal, S.C., Jain, V.K., and Dixit, P. (2005), Modeling and simulation of magnetic abrasive finishing process, International Journal of Advanced Manufacturing Technology, 26(5), 477-490.

[66] Singh, D. K., Jain, V.K., and Raghuram, V. (2005), On the performance analysis of flexible magnetic abrasive brush, Journal of Machining science and technology, 9(4), 601-619.

[67] Singh, D.K., Jain, V.K., and Raghuram, V. (2006), Experimental investigations into forces acting during a magnetic abrasive finishing process, International Journal of Advanced Manufacturing Technology, 30, 652-662.

[68] Jha, S., and Jain, V.K. (2006), Modeling and simulation of surface roughness in magnetorheological abrasive flow finishing (MRAFF) process, Wear, 261(7-8), 856-866.

[69] Olabi, A. G., and Grunwald, A. (2007), Design and application of magneto-rheological fluid, Materials & design, 28(10), 2658-2664.

[70] De Groote, J.E., Marino, A.E., Wilson, J.P., Bishop, A.L., Lambropoulos, J.C., and Jacobs, S.D. (2007), Removal rate model for magnetorheological finishing of glass, Journal of Applied optics, 46(32), 7927-7941.

[71] Miao, C., Shafrir, S. N., Romanofsky, H., Mici, J., Lambropoulos, J. C., and Jacobs, S. D. (2008), Frictional investigation for magnetorheological finishing (MRF) of optical ceramics and hard metals, Optical Fabrication and Testing (https://doi.org/10.1364/OFT.2008.OThB4).

[72] Kim, D.W., Cho, M.W., Seo, T.I., and Shin, Y.J. (2008). Experimental study on the effects of alumina abrasive particle behavior in MR polishing for MEMS applications, Sensors, 8(1), 222-235.

[73] Seok, J., Lee, S.O., Jang, K.I., Min, B.K., and Lee, S.J. (2009), Tribological properties of a magnetorheological (MR) fluid in a finishing process, Tribology Transactions, 52(4), 460-469.

[74] Fang, F.F., Kim, J.H., and Choi, H.J. (2009), Synthesis of core–shell structured PS/Fe3O4 microbeads and their magnetorheology, Polymer, 50(10), 2290-2293.

[75] Sadiq, A., and Shunmugam, M.S. (2009), Magnetic field analysis and roughness prediction in magnetorheological abrasive honing (MRAH), Journal of Machining science and technology, 13(2), 246-268.

[76] Miao, C., Shafrir, S.N., Lambropoulos, J.C., Mici, J., and Jacobs, S.D. (2009), Shear stress in magnetorheological finishing for glasses, Applied optics, 48(13), 2585-2594.

[77] Sim, W.M., (2010), Challenges of residual stress and part distortion in the civil airframe industry, International Journal of Microstructure and Materials Properties, 5(4-5), 446-455.

[78] Miao, C., Lambropoulos, J.C., and Jacobs, S.D. (2010), Process parameter effects on material removal in magnetorheological finishing of borosilicate glass, Applied optics, 49(10), 1951-1963.

[79] Jang, K.I., Seok, J., Min, B.K., and Lee, S.J. (2010), An electrochemomechanical polishing process using magnetorheological fluid, International Journal of Machine Tools and Manufacture, 50(10), 869-881.

[80] Singh, A.K., Jha, S., and Pandey, P.M. (2012), Nanofinishing of a typical 3D ferromagnetic work-piece using ball end magnetorheological finishing process, International Journal of Machine Tools and Manufacture, 63, 21-31.

[81] Sidpara, A., and Jain, V.K. (2012), Theoretical analysis of forces in magnetorheological fluid based finishing process, International Journal of Mechanical Sciences, 56(1), 50-59.

[82] Katiyar, A., Singh, A.N., Shukla, P., and Nandi, T. (2012), Rheological behavior of magnetic nanofluids containing spherical nanoparticles of Fe–Ni, *Powder Technology*, *224*, 86-89.

[83] Yamaguchi, H., Srivastava, A.K., Tan, M.A., Riveros, R.E., and Hashimoto, F. (2012), Magnetic abrasive finishing of cutting tools for machining of titanium alloys, CIRP annals, 61(1), 311-314.

[84]Hezaveh, H., Fazlali, A., and Noshadi, I. (2012), Synthesis, rheological properties and magnetoviscos effect of Fe_2O_3/paraffin ferrofluids, Journal of the Taiwan Institute of Chemical Engineers, 43(1), 159-164.

[85] Khalaj Amineh, S., Fadaei Tehrani, A., and Mohammadi, A. (2013), Improving the surface quality in wire electrical discharge machined specimens by removing the recast layer using magnetic abrasive finishing method, International Journal of Advanced Manufacturing Technology, 66(9), 1793-1803.

[86] Su, Y. R., Li, D., Liu, H.N., Chen, M.J., and Peng, H. (2013), Experiment research of polishing capability of magnetorheological finishing with a small permanent magnet ball-end tool, Key Engineering Materials, 589, 497-501.

[87] Judal, K.B., and Yadava, V. (2013), Modeling and simulation of cylindrical electro-chemical magnetic abrasive machining of AISI-420 magnetic steel, Journal of Materials Processing Technology, 213(12), 2089-2100.

[88] Singh, A.K., Jha, S., and Pandey, P.M. (2013), Mechanism of material removal in ball end magnetorheological finishing process. Wear, 302(1-2), 1180-1191.

[89] Sidpara, A., and Jain, V.K. (2013), Analysis of forces on the freeform surface in magnetorheological fluid based finishing process, International Journal of Machine Tools and Manufacture, 69, 1-10.

[90] Song, W.L., Choi, S.B., Cai, Q.C., Choi, J.Y., and Lee, C.H. (2013), Finishing performance of magneto-rheological fluid under magnetic field, Mechanics of Advanced Materials and Structures, 20(7), 529-535.

[91] Niranjan, M. S., and Jha, S. (2014), Flow behaviour of bidisperse MR polishing fluid and ball end MR finishing. Procedia materials science, 6, 798-804.

[92] Mishra, V., Goel, H., Mulik, R.S., and Pandey, P.M. (2014), Determining work-brush interface temperature in magnetic abrasive finishing process, Journal of Manufacturing Processes, 16(2), 248-256.

[93] Niranjan, M.S., and Jha, S. (2015), Experimental investigation into tool aging effect in ball end magnetorheological finishing, International Journal of Advanced Manufacturing Technology, 80(9), 1895-1902.

[94] Niranjan, M. S., and Jha, S. (2015), Optimum selection of machining parameters in ball end magnetorheological finishing process, International Journal of Precision Technology, 5(3-4), 217-228.

[95] Khan, D. A., Alam, Z., and Jha, S. (2016), Nano-finishing of copper using ball end magnetorheological finishing (BEMRF) process. *ASME* International mechanical engineering congress and exposition (https://doi.org/10.1115/IMECE2016-65974).

[96] Niranjan, M.S., Singh, K.P., and Murtaza, Q. (2017), Characterization of magnetic abrasive particles based Magnetorheological polishing fluid, Materials Today: Proceedings, 4(2), 752-757.

[97] Iqbal, F., Rammohan, R., Patel, H.A., and Jha, S. (2016), Design and development of automated work-piece cleaning system for ball end magneto-rheological finishing process, International Conference on Advances in Materials & Manufacturing,19(5), 289-295.

[98] Khan, D.A., Kumar, J., and Jha, S. (2016), Magneto-rheological nanofinishing of polycarbonate, International Journal of Precision Technology, 6(2), 89-100.

[99] Iqbal, F., and Jha, S. (2016). Nanofinishing of freeform surfaces using BEMRF. Nanofinishing science and technology, 1(1), 255-284, CRC press.

[100] Maan, S., Singh, G., and Singh, A.K. (2017), Nanosurface-finishing of permanent mold punch using magnetorheological fluid-based finishing processes, Journal of Materials and Manufacturing Processes, 32(9), 1004-1010.

[101] Skalski, P., and Kalita, K. (2017), Role of magnetorheological fluids and elastomers in today's world, Acta mechanica et automatica, 11(4), 267-274.

[102] Alam, Z., and Jha, S. (2017), Modeling of surface roughness in ball end magnetorheological finishing (BEMRF) process, Wear, 374, 54-62.

[103] Khurana, A., Singh, A.K., and Bedi, T.S. (2017), Spot nanofinishing using ball nose magnetorheological solid rotating core tool, International Journal of Advanced Manufacturing Technology, 92(1), 1173-1183

[104] Khan, D.A., and Jha, S. (2017), Selection of optimum polishing fluid composition for ball end magnetorheological finishing (BEMRF) of copper, International Journal of Advanced Manufacturing Technology, 100(5), 1093-1103.

[105] Barman, A., and Das, M. (2017), Simulation of magnetic field assisted finishing (MFAF) process utilizing smart MR polishing tool, Journal of The Institution of Engineers (India): Series C, 98(1), 75-82.

[106] Kumar, A., Alam, Z., Khan, D.A., and Jha, S. (2018), Nanofinishing of FDM-fabricated components using ball end magnetorheological finishing process, Journal of Materials and Manufacturing Processes, 34(2), 232-242.

[107] Nagdeve, L., Sidpara, A., Jain, V.K., and Ramkumar, J. (2018), On the effect of relative size of magnetic particles and abrasive particles in MR fluid-based finishing process, Journal of Machining Science and Technology, 22(3), 493-506.

[108] Alam, Z., Khan, D.A., and Jha, S. (2018), A study on the effect of polishing fluid volume in ball end magnetorheological finishing process, Journal of Materials and Manufacturing Processes, 33(11), 1197-1204.

[109] Khan, D.A., and Jha, S. (2018), Synthesis of polishing fluid and novel approach for nanofinishing of copper using ball-end magnetorheological finishing process, Journal of Materials and Manufacturing Processes, 33(11), 1150-1159.

[110] Alam, Z., Iqbal, F., Ganesan, S., and Jha, S. (2019), Nanofinishing of 3D surfaces by automated five-axis CNC ball end magnetorheological finishing machine using customized controller, International Journal of Advanced Manufacturing Technology, 100(5), 1031-1042.

[111] Liu, H., Cheng, J., Wang, T., and Chen, M. (2019), Magnetorheological finishing of an irregular-shaped small-bore complex component using a small ball-end

permanent-magnet polishing head, Nanotechnology and Precision Engineering, 2(3), 125-129.

[112] Ghosh, G., Sidpara, A., and Bandyopadhyay, P. P. (2021), Theoretical analysis of magnetorheological finishing of HVOF sprayed WC-Co coating, International Journal of Mechanical Sciences, vol 207, (1-12), 106629. https://doi.org/10.1016/j.ijmecsci.2021.106629

[113] Iqbal, F., Alam, Z., Khan, D.A., and Jha, S. (2022), Automated insular surface finishing by ball end magnetorheological finishing process, Journal of *Materials and Manufacturing Processes*, *37*(4), 437-447.

[114] Aggarwal, A., & Singh, A.K. (2022), Magnetorheological finishing of ball-cup surface using new tool to enhance ball-transfer-unit performance, Journal of Materials and Manufacturing Processes, 37(1), 1-17.

[115] Tian, J., Chen, M., Liu, H., Qin, B., Cheng, J., and Sun, Y. (2022), Study on mechanism of improving efficiency of permanent-magnet small ball-end magnetorheological polishing by increasing magnetorheological fluid temperature, Scientific Reports, 12(1), 1-13.

[116] Arora, K., Paswan, S. K., and Singh, A. K. (2022). Investigation of Surface Roughness in Novel Magnetorheological Finishing of the Internal Hemispherical-Shaped Acetabular Cup Work-pieces. Journal of Manufacturing Science and Engineering, 144(11), 111002.

[117] Horo, P. O., Kumar, P., Rathore, S. S., and Khan, D. A. (2022). Enhancement of Magnetic Flux Density Using a Novel Electromagnets Configurations in Belt-Type Magnetorheological Finishing Setup. *Proceedings of Recent Trends in Product Design and Intelligent Manufacturing Systems (IPDIMS)969-975. Singapore: Springer Nature Singapore.* https://doi.org/10.1007/978-981-19-4606-6_88.

[118] Kumar, M., Bhavani, T., Rawal, S., and Sidpara, A. (2022), Magnetorheological Finishing of Chemically Treated Electroless Nickel Plating, Magnetochemistry, 8(12), 184.

[119] Alam, Z., Khan, D. A., Iqbal, F., and Jha, S. (2022), Theoretical and Experimental Study on Forces in Ball End Magnetorheological Finishing Process, Advances in Forming, Machining and Automation,Proceedings of AIMTDR,391-401. https://doi.org/10.1007/978-981-19-3866-5_33.

[120] Sharma, A., & Niranjan, M. S. (2023). Chemical assisted ball end magnetorheological finishing of aluminium 7075 alloy. *Ain Shams Engineering Journal*, 102397.

[121] Derakhshan-Samani, M., & Rahimi, A. (2023). Improved CNC ball-end magnetorheological finishing process for borosilicate glass polishing. *Materials and Manufacturing Processes*, 1-12.

[122] Taira, S., Tanaka, K., and Yamasaki, T. (1978), A method of X-ray microbeam measurement of local stress and its application to fatigue crack growth problems, Journal of Japan Society of Materials Science, 27, 251-256.

[123] Sasaki and Hirose (1978), Trans. Jpn Soc. Mech. Eng. Part A, 61, 2288– 2295

[124] Mishra, A., and Prasad, T. (1985), Residual stresses due to a moving heat source, International Journal of Mechanical Sciences, 27(9), 571-581.

[125] Sugano, T., Takeuchi, K., Goto, T., and Yoshida, Y. (1988), Diamond Turning of an Aluminum Alloy for *Mirror, Mitsubishi Juko Giho, 25(2), 111-114.*

[126] Jang, D.Y., Watkins, T.R., Kozaczek, K.J., Hubbard, C.R., and Cavin, O.B. (1996), Surface residual stresses in machined austenitic stainless steel, Wear, 194(1-2), 168-173.

[127] Noyan, I.C., and Cohen, J.B. (2006), An X-ray diffraction study of the residual stress-strain distributions in shot-peened two-phase brass, Journal of Materials Science and Engineering, 75(1-2), 179-193.

[128] Brinksmeier, E.A. (2007), Model for the development of residual stresses in grinding, Advanced in Surface Treatments, Technology-Applications-Effects, 5, 173-189.

[129] Sasaki, Takahashi, Sasaki & Kobayashi (2009), Trans. Jpn Soc. Mech. Eng. Part A, 75, 219–227.

[130] Paul, A., and Akash, P.S. (2015), Residual Stress Analysis of Mild Steel ASTM A36 in Milling & Drilling, International Journal of Science and Research, 78(96), 1517-1521.

[131] Tanaka, K. (2018), X-ray measurement of tri-axial residual stress on machined surfaces by the cosα method using a two-dimensional detector, Journal of Applied Crystallography, 51(5), 1329-1338.

[132] Ali, P., Walia, R.S., Murtaza, Q., and Ranganath, M.S. (2020), Modeling and analysis of developed Thermal Additive Centrifugal Abrasive Flow Machining process, Surface Topography: Metrology and Properties, 8(3), 035013.

[133] Kumar, S., Grover, S., and Walia, R.S. (2018), Effect of hybrid wire EDM conditions on generation of residual stresses in machining of HCHCr D2 tool steel under ultrasonic vibration, International Journal on Interactive Design and Manufacturing, 12(3), 1119-1137.

[134] Rao, P.S., Ramji, K., and Satyanarayana, B. (2016), Effect of wire EDM conditions on generation of residual stresses in machining of aluminum 2014 T6 alloy, Journal of Alexandria Engineering, 55(2), 1077-1084.

[135] Ghosh, G., Sidpara, A., and Bandyopadhyay, P.P. (2021), Experimental and theoretical investigation into surface roughness and residual stress in magnetorheological finishing of OFHC copper, Journal of materials processing technology, vol 288 (31), 116899. https://doi.org/10.1016/j.jmatprotec.2020.116899.

[136] Sharma, A., and Niranjan, M. S. (2022), Experimental and theoretical investigation into surface roughness and residual stress using ball end magnetorheological finishing, Online First Article Journal of Engineering Research. https://doi.org/10.36909/jer.14281.

[137] Saraswathamma, K., Jha, S., & Rao, P. V. (2015). Experimental investigation into ball end magnetorheological finishing of silicon. *Precision Engineering*, *42*, 218-223.

List of Research Publications

International Journal

1. Himmat Singh, M. S. Niranjan and Reeta Wattal (2020), A Study for the Nanofinishing of an EN-31 Work-piece with Pulse DC Power Supply Using Ball-End Magnetorheological Finishing, Journal of Mechanical Engineering 66(7-8), 449-457.

2. Himmat Singh, M. S. Niranjan and Reeta Wattal (2021), Experimental Investigation into Residual Stress in Ball End Magnetorheological Finishing, Journal of Engineering Research (ICAPIE-2021) Special Issue, page 82-94 DOI:10.36909/jer.ICAPIE.15097.

International conference papers

1. Himmat Singh, M. S. Niranjan and Reeta Wattal**,** 'Magnetorheoloical Finishing: A Review, Proceedings of 2nd International Conference on Advanced Production and Industrial Engineering (ICAPIE 2017), Delhi Technological University, Oct. 6-7, 2017, Delhi, India.

2. Himmat Singh, M. S. Niranjan and Reeta Wattal**,** 'A study of active abrasive particles for mechanism of material removal in Pulsed ball end magnetorheological finishing process and a time based study for finishing of EN-31, Proceedings of 6th International Conference on Advanced Production and Industrial Engineering (ICAPIE 2021) Delhi Technological University, June18-19, 2021, Delhi, India

3. Himmat Singh, M. S. Niranjan and Reeta Wattal, 'Optimization of process parameters for finishing EN-24 with PBEMRF process using RSM technique, Proceedings of International conference on advanced technology, Sustainability and management (IATSM-2022), Sushant university Gurugram, July28-29, 2022, Gurugram, India.